Master's thesis

NTNU
Norwegian University of Science and Technology
Faculty of Medicine and Health Sciences
Department of Clinical and Molecular Medicine

Maria Kompatscher

Regulation of Toll-like receptors signaling by vesicle transport protein ZFYVE27

Master's thesis in Molecular Medicine
Supervisor: Mariia Yurchenko
June 2019

NTNU
Norwegian University of
Science and Technology

Maria Kompatscher

Regulation of Toll-like receptors signaling by vesicle transport protein ZFYVE27

Master's thesis in Molecular Medicine
Supervisor: Mariia Yurchenko
June 2019

Norwegian University of Science and Technology
Faculty of Medicine and Health Sciences
Department of Clinical and Molecular Medicine

NTNU
Norwegian University of
Science and Technology

Acknowledgements

At this point, I would like to take the opportunity to thank all those, who supported me on a professional and personal level during the elaboration of my Master Thesis.

First, I would like to thank my supervisor, Mariia Yurchenko for great supervision and motivating me throughout the work. She showed me with tireless enthusiasm the world of science by sharing her knowledge and fascination for research, teaching me as much as possible and answering all my question.

I would also like to thank Lene Melsæther Grøvdal for her supervision during the first time introducing me into the project, the lab and our lab group. Thanks to the trafficking group, especially my co-supervisor Harald Husebye for great input, suggestions and being open for discussions. A special thanks, I would like to say to Astrid Skjesol for being here to answer every kind of questions and support me whenever needed from my first to the last week of my project.

I want to thank Prof. Terje Espevik, the Director the Center of Molecular Inflammation Research (CEMIR) at St. Olavs University Hospital in Trondheim, Norway for providing the laboratory and equipment for the research. Thanks to all the people in the lab for their help, and nice and motivating chats during small incubation times. Additionally, thanks to CMIC for support with microscopy experiments.

An extraordinary thanks to my friends in Trondheim and friends and family in the distance for support, advice and being open for every kind of distractions.

A very special thanks goes to my parents and brothers for their support and encouragement in all my decisions, making it possible for me to explore different places and always being here for me.

Thank you!

Maria Kompatscher

Trondheim, 01.06.2019

Abstract

Toll like receptors (TLRs) represent members of the pattern recognition receptors and are responsible for discriminating self from non-self. In the human body, this function is executed by 11 specialized receptors present on the cell surface or in endosomal compartments of immune cells. These potent receptors, which induce secretion of inflammatory and anti-viral cytokines, need tight regulation to protect the host against systemic effects.

The LPS sensing TLR4 is present on the cell surface and in phagosomes of immune cells. ZFYVE27 is a membrane protein localized in the tubular endoplasmic reticulum required for protrusion outgrowth during neurite formation in neuronal cells. Preliminary data from our research group suggested an effect of the vesicle transport protein ZFYVE27 on TLR4-mediated signaling. *ZFYVE27* silencing was shown to impair TLR4-mediated signaling in human macrophages and macrophage-like THP-1 cells.

In this study we have narrowed down the effect of *ZFYVE27* silencing on TLR4-mediated signaling to intracellular TLR4 signaling and examined a possible effect of ZFYVE27 on phagocytosis of Gram-negative bacteria. *ZFYVE27* knockout cell lines were generated and tested in their LPS response to optimize the experimental conditions and generate a model cell line to expand the insight into the function of different protein domains of ZFYVE27. Moreover, pilot experiments on intracellular TLRs suggested a more general effect of ZFYVE27 on TLRs signaling. *ZFYVE27* silencing prolonged TLR8- and TLR9-mediated signaling (endosomal TLRs), and these results should be confirmed and examined further.

Detailed insight into the regulation network of TLRs can reveal additional targets for treatment strategies of different types of cancers, autoimmune and inflammatory disorders.

Abbreviations

AP-1	Activator protein 1
ATCC	American Type Culture Collection
BCA	Bicinchoninic acid
BSA	Bovine serum albumin
CC	Coiled coil
CD14	Cluster of differentiation 14
cDNA	Complementary DNA
CFU	Colony forming unit
CMP	Common myeloid progenitor
CRISPR	Clustered Regularly Interspaced Short Palindromic Repeats
crRNA	CRISPR RNA
CXCL10	C-X-C motif chemokine 10
DAMP	Damage associated molecular patterns
DD	Death domain
DMEM	Dulbecco's Modified Eagle Medium
ds	Double stranded
dT	Deoxythymidine
DTT	Dithiothreitol
E. coli	*Escherichia coli*
ER	Endoplasmic reticulum
ERC	Endocytic recycling compartment
FCS	Fetal calf serum
FFAT	Diphenylalanine in an acidic tract
FYCO1	FYVE and Coiled-Coil Domain Containing 1 protein
FYVE	Fab 1, YOTB, Vac 1, and EEA1
Gag	Group-specific antigen
GDP	Guanosine diphosphate
GDP	GDP dissociation inhibitor
gRNA	Guide RNA
GTP	Guanosine triphosphate
HDR	Homologous directed repair
HRP	Horseradish peroxidase
Hrs	Hepatocyte growth factor-regulated tyrosine kinase substrate
IFNβ	Interferon beta
IgG	Immunoglobulin G
IKK	IκB kinase
IM	Inner membrane
IRAK	Interleukin-1 receptor-associated kinase
IRF	Interferon regulatory factor
IκB	Inhibitor of kappa B
KIF5	Kinesin related protein 5
LBP	LPS-binding protein
LCR	Low complexity region
LDS	Lithium dodecyl sulfate

LPS	Lipopolysaccharide
LRR	Leucine rich repeat
MAL	MyD88-adaptor like
MAMP	Microbe associated molecular patterns
MAPK	Mitogen-activated protein kinase
M-CSF	Macrophage colony-stimulating factor
MD-2	Myeloid differentiation factor 2
MOPS	3-(N-morpholino)propane sulfonic acid
MyD88	Myeloid differentiation primary response protein 88
NCBI	National Center for Biotechnology Information
NEMO	NFκB essential modulator
NFκB	Nuclear factor 'kappa-light-chain-enhancer' of activated B-cells
NHEJ	Non-homologous end joining
OM	Outer membrane
P/S	Penicillin/Streptomycin
PAMP	Pattern associated molecular patterns
PAM	Protospacer adjacent motif
PBMC	Peripheral blood mononuclear cells
PBS	Phosphate-buffered saline
PI(3)P	Phosphatidylinositol-3-phosphat
$PI(4,5)P_2$	Phosphatidylinositol-4,5-bisphosphat
PMA	Phorbol myristate acetate
Pol	DNA polymerase
PRR	Pattern recognition receptor
pSTAT1	Phospho-STAT1
Rab11FIP	Rab11 family interacting protein
Rac1	Ras-related C3 botulinum toxin substrate 1
RBD11	Rab11-binding domain
RIP1	Receptor interacting protein 1
RIPA	Radioimmunoprecipitation assay buffer
RNAi	RNA interference
RT	Room temperature
RT-qPCR	Real time quantitative polymerase chain reaction
SDS-PAGE	Sodium dodecyl sulphate polyacrylamide gel electrophoresis
sgRNA	Single guide RNA
siRNA	Small/short interfering RNA
SLAMF1	Signaling Lymphocytic Activation Molecule Family Member 1
SNARE	Soluble N-ethylmaleimide-sensitive factor attachment protein receptors
SPG	Spastic paraplegia
ss	Single stranded
STAT1	Signal transducer and activator of transcription 1
TAB	TAK1-binding protein
TAG	TRAM adaptor with GOLD domain
TAK1	Transforming growth factor-β-activated kinase 1
TANK	TRAF family member associated NFκB activator
TBK1	TANK-binding kinase 1

TBP	TATA-binding protein
TBS-T	Tris-buffered saline with Tween20
TICAM	TIR domain-containing adapter molecule
TIR	Toll/Interleukin-1 receptor
TIRAP	TIR-domain containing adaptor protein
TLR	Toll-like receptor
TNF	Tumor necrosis factor
tracrRNA	Trans-activating CRISPR RNA
TRAF	TNF receptor associated factor
TRAM	TRIF-related adaptor molecule
TRIF	TIR-domain-containing adaptor protein inducing IFNβ
UNC93B1	Unc-93 homolog B1
VAP-A	Vesicle associated protein-A
VSV-G	Vesicular stomatitis virus G
WT	Wild type
ZFYVE27	Zinc finger FYVE domain containing protein 27

Index

List of Figures

List of Tables

1. Introduction

1.1 A brief insight into the immune system

The immune system is an effective defense mechanism against pathogens. Its key role consists in recognizing structural characteristics of pathogens or toxins which are distinct from them of host cells itself. This role is executed based on mechanisms provided by the innate and the adaptive immune system. Both subsystems collaborate to discriminate this so-called non-self. The innate immune system possesses the ability to react within short time by germline encoded receptors, while the specialized reaction of the adaptive immune system generates receptors recognizing individual and unique pathogen structures by somatic rearrangement. This highly complex system is regulated extensively to avoid self-harm[1].

1.2 Innate Immune system

The innate immune system has the ability to distinguish between pathogenic and beneficial microbes and to respond to its environmental threats[2]. It is classically described as a system lacking memory and being activated in a gradual manner by recognizing pathogens independent on previous pathogen invasions[3]. Innate immunity is a conserved defense feature of plants, invertebrates and mammals. Invasion by pathogens or tissue damage can be sensed by receptors of the innate immune system, the so-call pattern recognition receptors (PRRs). The response can either consist in a cell-dependent mechanism as phagocytosis or cytotoxicity, or in secretory factors[3,4].

1.3 Cells of the innate immune system

Innate immune cells are defined by the lack of somatic recombinant antigen-receptors and the lack of conventional immunological memory. They provide antimicrobial function and tissue protection[3].

These cells derive with one exception, the epithelial cells, from the hematopoietic stem cells. Hematopoietic stem cells reside and self-renew in the bone marrow, where they differentiate into lymphoid and myeloid progenitors giving rise to the immune cells[3]. The common myeloid progenitor (CMP) differentiates into erythroid cells and various leukocytes. Granulocytes, monocytes, macrophages and some dendritic cells belonging to leukocytes developed from CMP form most of the innate immune cells. Further, some cells derived from the lymphoid linage, the so-called innate lymphoid cells including the natural killer cells make part of the innate immune cells due to their lack of somatic recombinant immune receptors.

The functions of the innate immune cells consist in cellular mechanisms and secretion of cytokines[4]. Here in this study the focus is on the secretory and the phagocytotic function in macrophages.

1.3.1 Macrophages

Macrophages are cells of the innate immune system conducting different key functions in the first line of defense. These myeloid cells are the biggest population of phagocytotic cells in most normal tissues at homeostasis. They derive from either self-renewing cells in the tissue, which entered the tissue during embryonic development or from circulating monocytes entering the tissue during infection[4]. Both subsets of macrophages are armed with a variety of plasma membrane and intracellular receptors which enable them to sense their surroundings[3]. They phagocytose microbes as well as apoptotic cells and produce inflammatory cytokines. Further, they are involved in homeostasis and integrity maintenance in their resident tissue[3].

1.4 Pattern recognition receptors

Pattern recognition receptors (PRRs) are molecular receptors of the innate immune system and are localized in serum, on the cell surface, in endosomes and in cytoplasm. Such PRRs recognize pathogen associated molecular patterns (PAMPs) or microbe associated molecular patterns (MAMPs) which are expressed by pathogenic and non-pathogenic bacteria, viruses and fungi, but not by the host itself. Tissue damage like stress, infection, damage or

transformation are represented by the so-called damage associated molecular patterns (DAMPs) which also trigger activation of some PRRs[4,5].

PRRs can be classified into categories including Toll-like receptors (TLRs) among others. TLRs play a special role in determining the self- or non-self-origin of an antigen and so also in autoimmunity[5].

1.4.1 Toll-like receptors

The Toll-like receptor family is the most studied group of the PRRs[6]. After the investigation of *Toll* in *Drosophila melanogaster* as a protein involved in embryonic development for polarity and later for the antifungal immunity[1,2].

The TLRs are expressed by many cell types, including macrophages, dendritic cells, B cells, stromal cells and certain epithelial cells[4]. By recognizing endogenous DAMPs and exogenous PAMPs an inflammatory response is induced[5]. Pro-inflammatory and anti-viral signals help to eliminate the pathogens in the host[6].

In total, 11 TLRs are known in humans from which TLR1 to TLR10 are functional. In mice 13 TLRs are present and TLR10 is not functional. TLRs can be classified into three groups based on their ligands. TLR1, 2, 4 and 6 recognize lipids and lipopeptides, TLR5 and in mice TLR11 recognize proteins, like flagellin and profilin, and TLR3, 7, 8 and 9 sense nucleic acids. TLR10 is supposed to form heterodimers with TLR1 and 2 but their ligands are unknown[7]. Another system to classify the TLRs results in two groups based on their localization. Extracellular TLRs located on the cell surface include TLR1, 2, 4, 5, 6 and 10. The second group of TLRs is represented by TLR3, 7, 8, 9, 11, 12 and 13, which are found in endosomes[8].

1.4.1.1 TLRs structure

The members of the TLR family are proteins consisting in an extracellular, transmembrane and intracellular domain[2] belonging to the type I integral membrane glycoproteins[9].

Ligands are recognized by the extracellular domain which is build-up by leucine rich repeats (LRRs). The LRRs are consecutively assembled and form an arch-shaped or so-called horseshoe structure[2,9]. The concave surface of this arch is represented by tightly packed β-

sheets[2]. The high diversity in ligand recognition of lipids, proteins and nucleic acids evolved from different combinations in the number and sequence of LRR motifs[2]. A TLR spans the membrane with a single transmembrane domain composed of approximately 20 amino acids[2]. The intracellular domain of the receptors consists in the Toll/Interleukin-1 receptor (TIR) domain[9]. The TIR domain consists in approximately 200 amino acids providing three conserved boxes which play a crucial role in receptor signaling[9]. The structural composition of the TIR domain includes five alternating β-sheets and α-helices connected via loops resulting in a β-sheet core covered by α-helices[2,9].

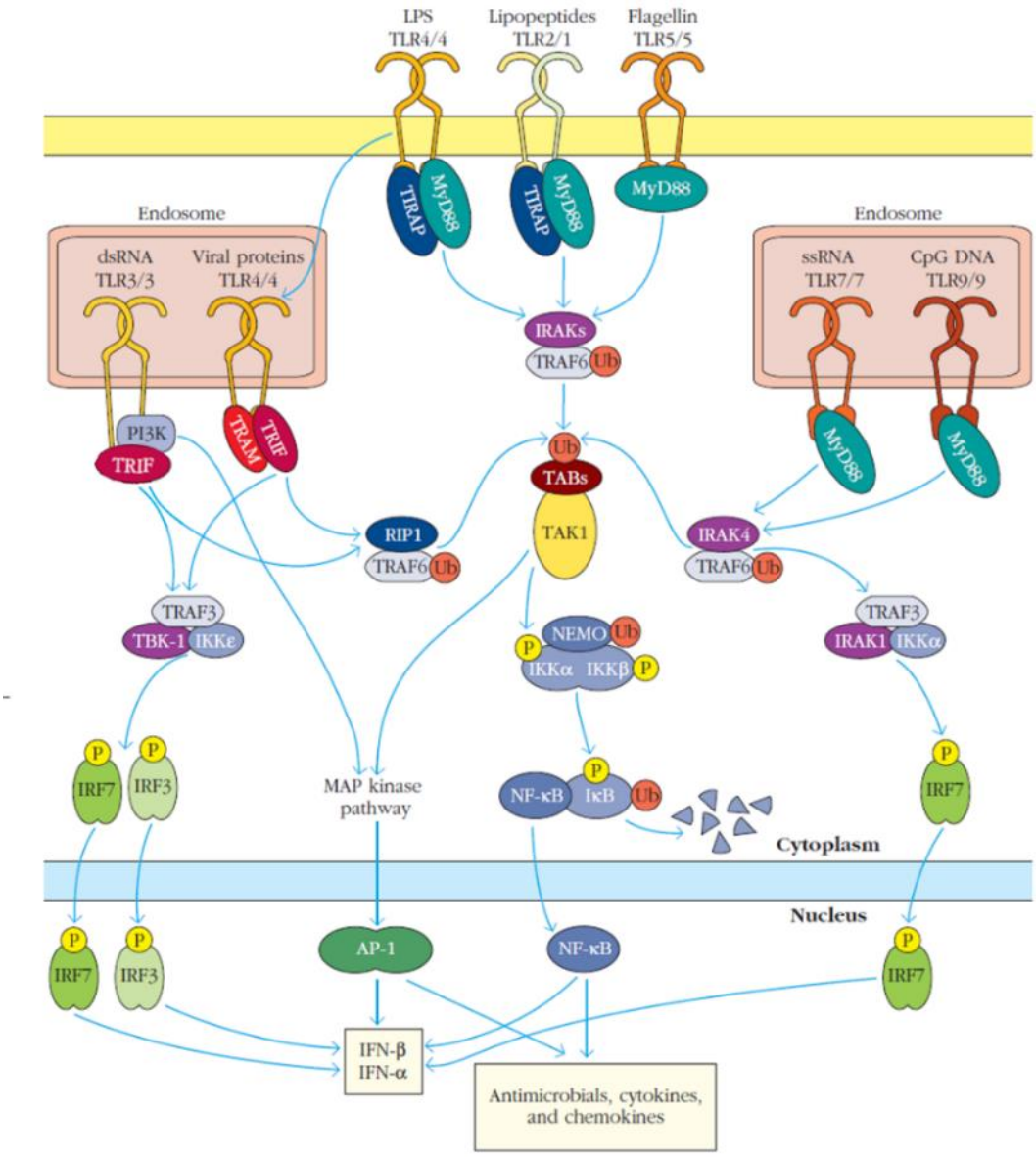

Figure 1.1. Schematic overview of Toll-like receptors localization, ligands and signaling pathways (adapted from Owen, 2009[10]).

1.4.1.2 TLRs signaling

TLRs signaling (Figure 1.1) is induced by ligand binding to the receptor. Ligand binding leads to receptor dimerization and conformational change which is required for the recruitment of downstream signaling molecules. The adaptor proteins linking the ligand-binding to the receptor to downstream signaling contain a TIR domain and interact so via TIR-TIR interaction with the TLR. The adaptor proteins are: myeloid differentiation primary response protein 88 (MyD88), TIR-domain containing adaptor protein (TIRAP or MAL), TIR-domain-containing adaptor protein inducing IFNβ (TRIF) and TRIF-related adaptor molecule (TRAM)[9].

The two main TLR signaling pathways are classified into MyD88-dependend and MyD88-independent signaling, since MyD88 is the universal adaptor protein used by all TLRs except for TLR3. The MyD88-independent pathway from TLR3 and TLR4 recruits TRIF as its adaptor protein[9]. The adaptor protein MAL is involved in the MyD88-dependent signaling downstream of TLR2 and TLR4. TLR4 uses in the MyD88-independent signaling pathway TRAM as a second adaptor molecule[7].

MyD88-dependent signaling pathway

MyD88 acts as an adaptor protein through its TIR domain and death domain (DD)[4]. After TLR dimerization and conformational change MyD88 interacts as a dimer via a TIR-TIR interaction with the TLR. The DD of MyD88 recruits the Interleukin-1 receptor-associated kinase (IRAK) 1 and IRAK4 via a DD-DD interaction. IRAK1 and IRAK4 are serine-threonine kinases which autoactivate. The tumor necrosis factor receptor-associated factor 6 (TRAF6) is a signal mediator and is indirectly linked to the TLR through IRAK by which it gets phosphorylated and thereby activated. TRAF6 acts as a E3 ubiquitin ligase and collaborates with an E2 ubiquitin ligase and a cofactor to generate a ubiquitin polymer. This polymer can act as a scaffold and recruits thereby transforming growth factor-β-activated kinase 1 (TAK1) by TAK1-binding protein 1 (TAB1) and TAB2. These two ubiquitin-binding proteins enable TAK1 activation by IRAK, by bringing them into proximity. TAK1 itself is also a serine-threonine kinase and activates certain MAPKs which activate the activator protein 1 (AP-1) family transcription factors leading to expression of cytokine genes. Further, TAK1 induces the NFκB pathway and so proinflammatory cytokine expression. TAK1 phosphorylates the IκB kinase (IKK) which phosphorylates and so induces

IκB degradation. This degradation releases NFκB and enables the transcription factor to translocate into the nucleus leading to expression of pro-inflammatory cytokines like TNF[4].

An additional pathway through MyD88-dependent signaling is induced by signaling through TLR7, TLR8 and TLR9. Thereby, MyD88-TRAF6-IRAK4 activates a complex consisting in TRAF3, IRAK1 and IKKα. This complex activates and induces dimerization of IRF7 which translocates to the nucleus where it induces type 1 interferon expression[4,10].

MyD88-independent signaling pathway

TRIF/TICAM1 is an adaptor protein containing TIR domains and mediates TLR3 and TLR4 signaling in an MyD88-independent manner. TLR4 needs a second adapter protein TRAM/TICAM2 for signaling through TRIF[9]. TRIF recruits the E3 ubiquitin ligase TRAF3. TRAF3 generates a polyubiquitin scaffold which recruits NEMO and TRAF family member associated NFκB activator (TANK). NEMO consist in three IκB kinases (IKKα, IKKβ, IKKγ). TANK and NEMO are associated with the TANK-binding kinase 1 (TBK1) and IKKε. TBK1 phosphorylate IRF3 which leads to the translocation of this transcription factor into the nucleus inducing type 1 interferon expression[4].

Further, TRIF recruits the protein kinase, receptor interacting protein 1 (RIP1) which activates TRAF6. Activation of TRAF6 induces the same following steps induced by the MyD88-dependent signaling[10].

1.4.2 Intracellular TLRs

Intracellular TLRs include TLR3, TLR7, TLR8 and TLR9. All these TLRs found in endosomal compartments are receptors for the recognition of nucleic acids. TLR3 recognizes double stranded (ds) RNA and was also found to sense single stranded (ss) RNA. The ligand for TLR7 is uridine- and guanosine-rich ssRNA. ssRNA can additionally be sensed in humans by TLR8. TLR9 was defined for a long time to sense unmethylated CpG which is a motif present in viral and bacterial DNA. This was although challenged and TLR9 is thought to detect dsDNA and ssDNA not based on their sequence, modification or species-origin but just based on the endolysosomal localitzation[11].

Endosomal TLRs are trafficked from the ER via the Golgi to endolysosomal compartments with the aid of Unc-93 homolog B1 (UNC93B1). UNC93B1 is an ER resident protein

interacting with TLRs to mediate their exit from the ER and further trafficking[12]. Activation of intracellular TLRs requires acidification of the endosomes. The maturation of endosomes contributes to the purification of the ligand upon microbe disassembly and plays a role in processing of TLRs. The ectodomain of the intracellular TLRs should be cleaved to induce signaling upon ligand binding. This might be an additional regulating step to restrict receptor signaling to specific endosomal compartments[11,12].

1.4.3 Toll-like receptor 4 (TLR4) and its accessory proteins

TLR4 is one of the cell surface located TLRs recognizing the lipopeptide, lipopolysaccharide (LPS). This member of the TLR family is dependent on accessory proteins for its correct trafficking to the plasma membrane as well as for ligand binding. The accessory protein myeloid differentiation factor 2 (MD-2) interacts with the central part of the extracellular receptor portion. MD-2 is required to mediate binding of LPS to TLR4. A second accessory protein, CD14 is located on the surface of macrophages, neutrophils, and dendritic cells or in a soluble form in plasma[13]. CD14 binds the ligand – LPS in complex with LPS-binding protein (LBP) present in blood and facilitates its interaction with TLR4-MD-2 complex[4,14]. Further, CD14 induces the relocation of the receptor complex to lipid rafts rich in Posphatidylinositol-4,5-bisphosphat ($PI(4,5)P_2$) where receptor dimerization occurs and TLR4 signaling starts[15].

1.4.3.1 TLR4 ligand: Gram-negative bacteria / LPS

LPS is expressed by gram negative bacteria, like *Escherichia coli* (*E. coli*). Gram negative bacteria are enveloped by two membranes limiting the periplasm. The periplasm includes an aqueous compartment containing a thin layer of peptidoglycan. The inner membrane (IM) is the plasma membrane of the bacteria cell and is a symmetric phospholipid bilayer. The outer membrane (OM) has an asymmetric architecture with a phospholipid inner leaflet and an LPS containing outer leaflet. The OM is to three quarters composed of LPS while the remaining quarter consists in proteins (Figure 1.2).

LPS is an endotoxin with medical importance. The term endotoxin describes a component of a bacterial structure which is not secreted and induces a cellular response with local and systemic effects[4]. LPS is an oligosaccharide consisting in non-repeating sugar residues

forming an inner and outer core. Optionally, this core can have a long polysaccharide chain attached on the outer core, the so-called O-antigen. This O-antigen has a protective function against phagocytosis and complement lysis and is not present in the K12 LPS used in our experiments. The inner core is connected to the most conserved part of LPS, the lipid A (Figure 1.2)[16].

LPS binds with five lipid chains to a hydrophobic pocket of MD-2. A sixth lipid chain of LPS stays thereby free and binds together with parts of the polysaccharide backbone to the convex part of a second TLR4 inducing dimerization. Binding of a second LPS molecule to the second TLR4 in the dimer leads to stabilization of the conformation. This dimerization caused by ligand binding activates intracellular signaling by bringing the intracellular TIR domains into proximity enabling interaction with other TIR domain containing adaptor molecules[4].

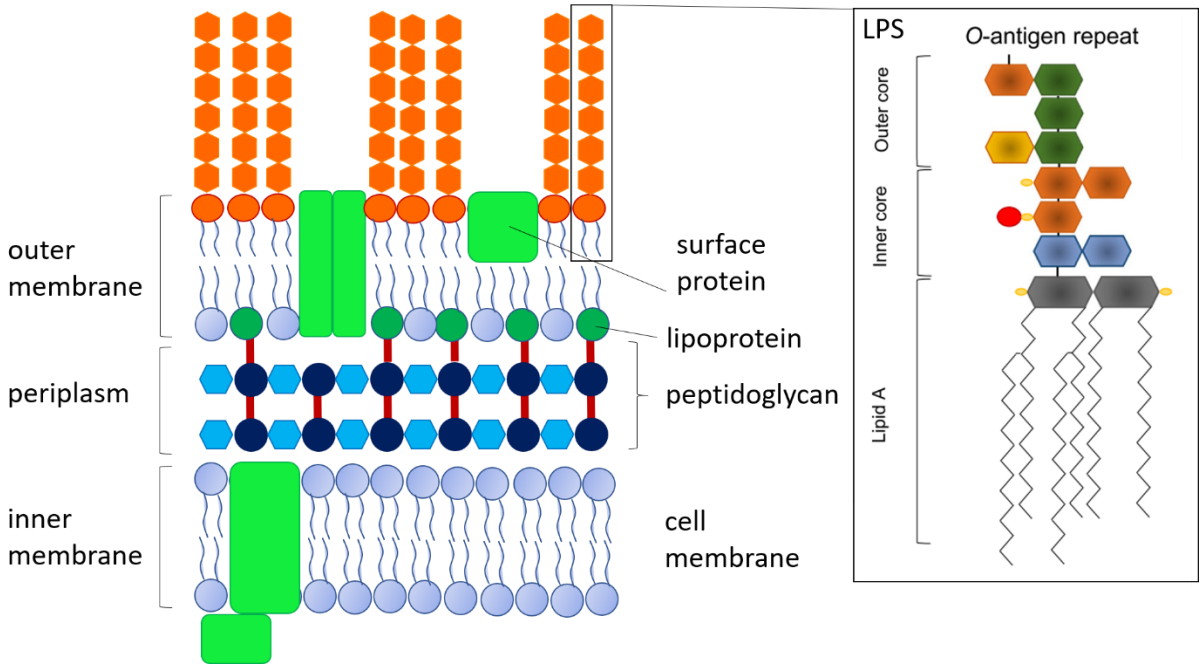

Figure 1.2. Schematic overview of the cell wall of Gram-negative bacteria on the left and of lipopolysaccharide (LPS) on the right (inspired by Murphey, 2017[17]; adapted from Sperandeo, et al., 2017[16]).

1.4.3.2 TLR4 signaling

TLR4 signaling occurs in two waves involving the MyD88-dependent pathway with the aid of MAL and signaling through TRIF mediated by TRAM. As TLR4 dimerizes upon stimulation, it relocates to the $PI(4,5)P_2$-rich lipid raft. MAL adaptor binds $PI(4,5)P_2$ and activates the MyD88-dependent pathway. This induces the first part of the TLR4 response. The second response is induced though signaling of the receptor complex from intracellular compartments after phagocytosis. TRIF signaling involving TRAM as a connecting adaptor makes the TLR4 response complete, as both signaling pathways are required to induce a full TLR4 response[15].

1.5 Phagocytosis

Phagocytosis describes a type of endocytosis[18] initiating the innate immune response, removing dead senescent cells and being involved in embryonic development and tissue remodeling. Phagocytosis is defined as uptake of >0.5 µm particles, and is executed by professional and facultative phagocytotic cells[19]. Professional phagocytes are cells deriving from the CMP, including monocytes, macrophages, neutrophils, eosinophils, dendritic cells and osteoclasts. The facultative or non-professional phagocytes are epithelial cells which can phagocyte during development and under pathogenic conditions[19].

Phagocytosis is initiated by receptor ligand interaction between specific cell surface receptors and their ligand represented by the surface of the particles[20]. Phagocytotic receptors are germ line encoded[21] and responsible for the recognition of altered self and non-self, represented by necrotic or apoptotic cells and microbes[19]. These receptors can be classified as opsonic and non-opsonic. Opsonic receptors include Fc receptors and complement receptors for the classical and the alternative lectin pathways[19]. The non-opsonic receptors include lectin-like recognition molecules, Dectin-1, C-type lectins and a group of scavenger receptors. TLRs are not classified as phagocytotic receptors, but are sensors and collaborate with non-opsonic receptors to contribute in the particle uptake[19]. The recognition of particles induces actin polymerization and actin-based uptake. The internalized phagosomes fuse with endosomes and lysosomes to achieve its maturation stage of a phagolysosome[20]. Maturation is characterized by acidification of the vesicles by a vacuolar ATPase and by vesicle trafficking towards the centrosome[19].

1.6 Vesicle trafficking and compartment identity

Eukaryotic cells with its characteristic compartments enclosed by membranes raise a challenge in content transfer between these compartmentalized structures. Vesicle trafficking is a specific and regulated mechanism addressing this content exchange challenge[22]. Secretion, protein presentation on certain membranes, endocytosis and several other cellular processes are dependent of on vesicular transport. In general, this cellular delivery system consists in vesicle budding from a donor membrane. The content of the vesicle, called cargo is selected involving the process of protein sorting. Vesicle targeting ensures subsequently transport of the vesicle towards its destination where vesicle fusion with the acceptor membrane takes place[23].

A regulating function in this context is executed by the small molecular switches, the Rab GTPases. The members of this large protein family are reversible associated to membranes giving identity and regulating trafficking. Rab GTPases are involved in cargo specific coat assembly during budding. Subsequently, they play a role in directional vesicle motility by direct or indirect motor protein recruitment. This motor proteins enable the transport of vesicles along intracellular filamentous structures, called actin filaments and microtubules. They can be compared to molecular cables acting as the roads for vesicle transport within the cell and mediate partly directionality and efficiency of vesicle motility[22]. Next step in vesicle trafficking is fusion of vesicles with acceptor membranes. Rab GTPases induce the recruitment of elongated tethering complexes, the SNARE proteins forming long distance contacts. These contacts mediate docking and fusion of vesicles with acceptor membranes[22].

The composition of Rab GTPases on a membrane gives identity and segregates vesicle populations. By recruiting other effector proteins Rab GTPases contribute themselves to the formation of membrane identity[22]. Phosphoinositides localized in a compartment specific manner recruit also specific complexes and support thereby the Rab GTPases in establishing membrane identity. The combination and crosstalk of Rab GTPases and phosphoinositides[22] results in a code which is compartment specific and enables effector protein recruitment with high affinity[24].

1.6.1 TLR4 trafficking upon ligand binding

TLR4 is localized on the plasma membrane[25] and to a larger extend in the endocytic recycling compartment (ERC) of macrophages. The ERC is a tubular endosome localized close to the centrioles and mediates receptor recycling[26]. The TLR4 ligand, LPS or *E. coli* is engulfed through receptor mediated endocytosis or phagocytosis into the cell[27]. Phagocytosis is required for a robust IFNβ response upon TLR4 signaling[27]. The NFκB activation was observed to be increased in cells inhibited in the endosomal pathway. This suggests that the endosomal pathway from the uptake of the receptor ligand complex up to lysosomal degradation has a desensitizing effect on the cell after TLR4 activation and so also a control function on the receptor response[25]. Recently, novel key players in the uptake of *E. coli* and TLR4 recruitment were investigated. These key players include, TRAM, Rab11 and the Rab11 family interacting protein 2 (FIP2)[28,29].

TRAM is known as adaptor protein involved in MyD88-independent signaling of TLR4. It is localized to the plasma membrane, diffusely throughout the cell and on small endosomal structures[30]. Further, it was also observed to have a regulating effect on phagocytosis and endosome maturation[28].

Rab11, the GTPase involved in recycling pathways, plays a role in controlling endocytosis and endosomal sorting by employing FIP2 as its effector protein[28]. More specific, the isoform Rab11a was previously described to localize TLR4 to its intracellular pool, the ERC and to control TLR4 and TRAM trafficking to *E. coli* phagosomes[27].

FIP2 is involved in phagocytosis and TLR4 and TRAM recruitment to *E. coli* phagosomes. Until recently Rab11a was thought to execute this role of localizing TLR4 and TRAM to the phagosomes, but Rab11a is indirectly involved by enhancing FIP2 binding to TRAM in a protein complex involving TRIF and itself[28].

Altogether, this reveals the importance of trafficking in the control of TLR4 signaling involving various proteins.

1.7 ZFYVE27

Zinc finger FYVE domain containing protein 27 (ZFYVE27), so called protrudin or spastic paraplegia protein 33 (SPG33) is encoded by the *ZFYVE27* gene[31]. To avoid confusions, we will call the protein throughout this thesis ZFYVE27.

Research on ZFYVE27 focused mainly on neurons. ZFYVE27 was found to be mutated in some patients with hereditary spastic paraplegias (SPGs). SPGs describe a group of neurodegenerative disorders. The pure SPG manifests by progressive weakness and spasticity of the lower extremities, while complex or complicated SPGs can involve further neurological or non-neurological symptoms[32]. These disorders are caused by mutations in proteins involved in maintenance of corticospinal tract axons[32]. The missense mutation in *ZFYVE27* was found in one family and was classified as a SPG causing gene mutation[33]. Later it was although challenged that this mutation is causative, since the mutated *ZFYVE27* did not show any impairment on its function compared to the wild type[34].

This protein consists of more than 400 amino acids and is classified as an oligomeric membrane protein localized in the tubular ER (Figure 1.3)[35]. ZFYVE27 is anchored in the ER membrane by 3 hydrophobic domains, two transmembrane and one intramembrane domain. The N- and C-terminus of the protein are cytosolic and a small loop connecting two hydrophobic transmembrane domains is located luminal[35]. The cytosolic part of the protein represents four different protein domains: the Rab11 binding domain (RBD11)[36], the diphenylalanine in an acidic tract (FFAT) domain[35], the low-complexity region (LCR)[37], the coiled-coil (CC) domain and the FYVE domain with a C-terminal $Zn^{2\pm}$ binding domain (Figure 1.3)[36]. The FYVE finger is a conserved double zinc-binding domain, which is assumed to be an essential structural element in proteins involved in endocytic or vacuolar membrane traffic. This domain binds PI(3)P[37], $PI(3,4)P_2$, $PI(4,5)P_2$ and $PI(3,4,5)P_3$[38]. Furthermore, ZFYVE27 interacts with kinesin-1 or more specifically with the kinesin-1 heavy chain dimer consisting of KIF5. Kinesin-1 is a motor protein moving unidirectionally towards the plus-end of the microtubules and mediating an anterograde transport of vesicles[39]. Interaction between KIF5A, the isoform which was shown to interact most efficiently with ZFYVE27, is mediated by the C-terminal region of ZFYVE27 and the N-terminal stalk region of KIF5[39]. The CC domain is together with the FFAT and the N-terminal part of the FYVE domain responsible for KIF5A binding[39]. An additional binding via the FFAT domain of ZFYVE27 is described with the vesicle associated protein-A (VAP-A)[40], an ER resident

protein. This interaction is assumed to play an important role in the ability of ZFYVE27 to induce neurite outgrowth[40]. Further, ZFYVE27 interacts with two small GTPases. The RBD11 of ZFYVE27 interacts preferentially with the guanosine diphosphate (GDP)-bound form of Rab11. The sequence of the RBD11 shows similarity to the GDP dissociation inhibitor (GDI)-α and the GDI-β. Both these GDIs interact with several GDP-bound Rab proteins[36]. A second GTPase interaction partner of ZFYVE27 is Rab7. It interacts in its GTP bound form with the LCR of ZFYVE27[37].

In literature the function of ZFYVE27 is described to play a role in the formation and stabilization of the ER and in vesicular transport in neurones[35] during neurite protrusion[39]. Additionally, it was also shown to induce neurite-like protrusions in nonneuronal cells. ZFYVE27 is suggested to be involved in polarized vesicular transport[39].

ZFYVE27 mediates plus-end directed microtubule-dependent trafficking of vesicles. Late endosomes, positive for Rab7 and PI(3)P interact with ZFYVE27. ZFYVE27 which also binds kinesin-1 loads this motor protein then onto FYVE and Coiled-Coil Domain containing protein 1 (FYCO1), located on the late endosomes. Thereby the transport of the vesicle towards the plasma membrane is enabled. It exists evidence that this process could be involved in the vesicle transport to the plasma membrane to allow expansion of the membrane during neurite outgrowth[41]. A further function of ZFYVE27 involves Rab11-GDP as interaction partner. Rab11 is a GTPase involved in the endocytic recycling pathway[22]. The association between ZFYVE27 and Rab11-GDP was observed to be required during process formation in neuronal cells[36,39].

A hypothesis to combine the function of ZFYVE27 with Rab7-GTP and Rab11-GDP was formulated by Raiborg and colleagues, 2016. They assume, since Rab11-GTP is involved in endocytic recycling that Rab11-GDP might inhibit recycling to prevent “dilution” of an optimal membrane composition for protrusion outgrowth[41]. Controversially, another hypothesis regarding Rab11 by Campa and colleagues, 2017 suggests, that Rab11 bound to GTP or GDP does not represent an active and inactive form, but might be a switch between trafficking directionality or between microtubule- or actin/myosin-dependent transport[42].

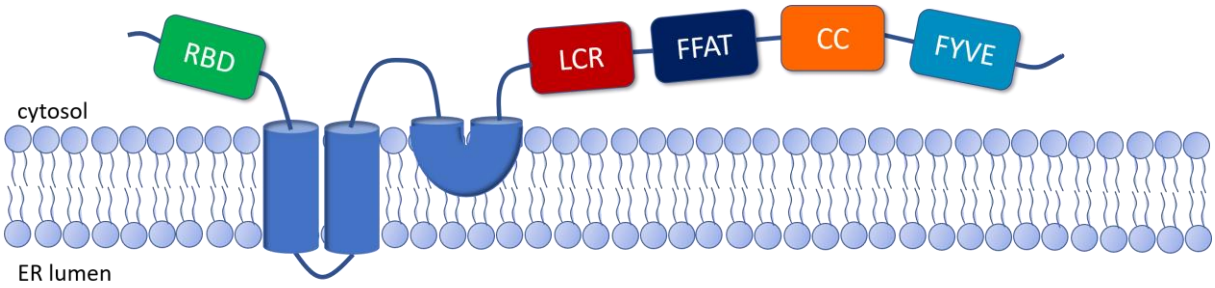

Figure 1.3. Schematic representation of the oligomeric protein ZFYVE27. RBD, Rab11 binding domain; LCR, low complexity region; FFAT, diphenylalanine in an acidic tract; CC, coiled coil domain; FYVE, is a zinc finger binding domain[35,37,43] (inspired by Chang, et al., 2013[43]).

1.8 Preliminary data on TLR4 and ZFYVE27 crosstalk

Observations showing a role for ZFYVE27 on TLRs-mediated signaling were made within our group. Dangol indicated in her Master Thesis (Dangol, 2015[44]) a positive effect of ZFYVE27 on TLR4-mediated signaling. Cytokine expression and secretion in primary macrophages upon LPS or *E. coli* stimulation was decreased in *ZFYVE27* silenced cells. The same observation was also made by Lindholm, 2017[45] in his Master Thesis on macrophage-like THP-1 cells. He showed that knockdown of *ZFYVE27* led to an impairment in secretion of TNF, IFNβ and in general a wide range of cytokines after LPS and *E. coli* stimulation. Moreover, a decrease of *TNF* and *IFNβ* mRNA levels was in line with observations made on secretion. As secretion of several cytokines was affected, an effect of *ZFYVE27* knockdown on viability of cells was addressed and excluded. Further, pilot experiments addressing TLR4 expression, phagocytosis, TLR4 and actin recruitment to *E. coli* phagosomes and phagosome maturation were performed.

At this point, further investigations were necessary to understand the underlying mechanisms causing the impairment of TLR4-mediated signaling in ZFYVE27 depleted cells. It was as well not known if ZFYVE27 might affect signaling via other TLRs.

2. Aim and perspectives of this study

The overall aim of this study was to investigate the role of the vesicle transport protein ZFYVE27 in TLRs signaling.

We planned to investigate the role of ZFYVE27 further in the context of TLR4 signaling and perform pilot screening of a possible ZFYVE27 involvement in regulation of signaling from endosomal TLRs.

Specific objectives to reach our goals:

- To examine the impact of *ZFYVE27* silencing on mRNA expression of the cytokines TNF and IFNβ in response to LPS stimulation.
- To investigate the uptake of *E. coli* particles, as well as TLR4 and actin recruitment to phagosomes and phagosome maturation in human macrophages and THP-1 cells silenced for *ZFYVE27*.
- To test the impact of ZFYVE27, TLR4 and proteins regulating TLR4 trafficking upon uptake of live *E. coli*.
- To generate *ZFYVE27* knockout sub cell lines and to screen for their responses to LPS treatment.
- To address the effect of *ZFYVE27* silencing on signaling via endosomal TLR8 and TLR9 in modified THP-1 cells.

3. Material and Methods

3.1 Cell culture

THP-1 (acute monocytic leukemia derived monocytic cell line, ATCC® TIB-202™) wild type (WT), THP-1 TLR8 pDest, THP-1 TLR9 mCherry and THP-1 CRISPR/Cas9 *ZFYVE27* knockout (KO) cells were used as macrophage model systems. Cells were cultured in RPMI-1640 (ATCC130–2001™) (Gibco) supplemented with 10% fetal calf serum (FCS) (Gibco), β-mercaptoethanol (0.05 mM) (Sigma-Aldrich), L-glutamine (700 µM) (Sigma-Aldrich) and penicillin-streptomycin (100 units - 100 µg/ml) (P/S) (Sigma-Aldrich) at +37°C, 5% CO_2. Medium was supplemented with 1 µg/ml puromycin (Sigma-Aldrich) for THP-1 TLR8 pDest and THP-1 CRISPR/Cas9 *ZFYVE27* KOs, and with 0.25 µg/ml for THP-1 TLR9 mCherry cells. Optimal culture conditions between $3x10^5$ to $1x10^6$ cells/ml were ensured by splitting every 2 to 3 days.

HEK293T cells (human embryonic kidney derived epithelial cell line, ATCC® CRL-3216™) were cultured in Dulbecco's Modified Eagle Medium (DMEM) (Lonza) supplemented with 10% FCS, L-glutamine (700 µM) and P/S (100 units – 100 µg/ml) at +37°C, 8% CO_2. Cells were split 1:30 every 3 to 4 days by applying Trypsin/EDTA (1X) (Lonza) and resuspending in growth medium. Cells were incubated at +37°C, 8% CO_2.

3.2 Primary macrophages

Blood from a buffy coat (Department of Immunology and Transfusion Medicine, St Olavs Hospital) was diluted in 80 ml of preheated PBS. 4x15 ml aliquots of Lymphoprep (Alere) were carefully overlaid by 30 ml of diluted blood. A centrifugation step at 700 x g for 25 min with minimum deceleration resulted in 4 phases. The peripheral blood mononuclear cells (PBMCs) were recovered and pooled in 2 fresh tubes. Pooled PBMCs were centrifuged at 800 x g for 10 min and supernatants were discarded by keeping 1 ml in the tube to resuspend the cells gently. Three washing steps were performed by resuspending cells in 20 ml of Hanks' Balanced Salt solution (Sigma-Aldrich), followed by one centrifugation at 200 x g for 8 min, and twice at 150 x g. After the third washing step, cells were pooled in 20 ml Hanks' and counted. Cell number was determined adding ZAP-OGLOBIN II lytic reagent (Beckman

Coulter Life Sciences) counting with the Z2 Coulter® Particle and size analyzer (Beckman Coulter Life Sciences). Cells were seeded in RPMI containing sterile filtered pooled 5% A^+ serum (Department of Immunology and Transfusion Medicine, St Olavs Hospital). $6x10^6$ cells were seeded in 35 mm microscopy dishes (MatTek Corporation) and in a well of a 6-well plate. After adhesion for 45-60 min at +37°C, 5% CO_2, cells were washed 3 times with Hanks' solution, and differentiated in RPMI supplemented with 10% A^+ serum, 700 µM L-glutamine, 20 µg/ml gentamicin (Sanofi-Aventis) and 50 ng/ml M-CSF (R&D Systems) at +37°C, 5% CO_2. Medium was changed on day 3 and 5 after cell isolation, whereby on day 5 to medium without gentamycin and M-CSF.

3.3 Generation of THP-1 CRISPR/Cas9 *ZFYVE27* knockout cells

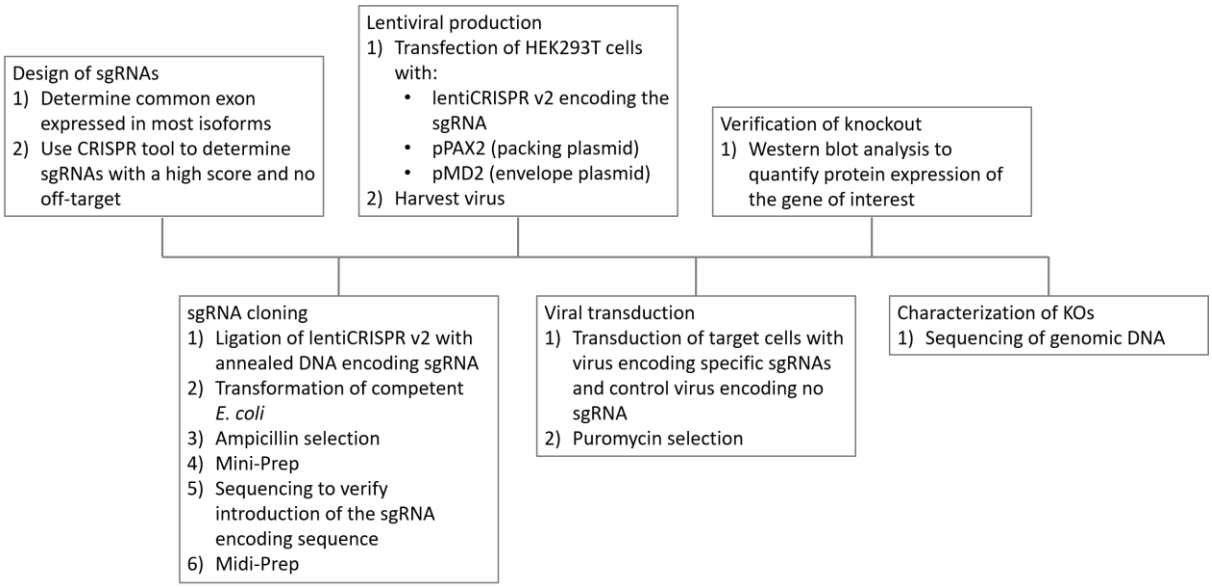

Figure 3.1. Schematic overview of steps during generation of a knockout cell line using the CRISPR/Cas9 technology.

3.3.1 General information of CRISPR/Cas9 technology

The CRISPR/Cas9 technology is developed based on the bacterial immunity against bacteriophages. Clustered Regularly Interspaced Short Palindromic Repeats (CRISPR) are DNA segments within the bacteria genome deriving from bacteriophage DNA. Bacteria have three types of CRISPR/Cas systems as defense mechanisms[46]. The type II system is employed

and optimized as an RNA-programmable genome editing tool[46], which was used here to generate a stable knockout in a human cell line.

The principle of this tool is an RNA guided endonuclease introducing a blunt end double strand break at a certain locus of a host genome resulting in random mutations or a precise gene modification[47].

Originally, the guide RNA (gRNA) is composed of two non-coding RNAs called CRISPR (cr)RNA and trans-activating crRNA (tracrRNA). The single guide RNA (sgRNA) applied here is a chimeric RNA, which combines the dual gRNA and simplifies the system[47].

The Cas9 endonuclease is targeted by the gRNA and dependent on a protospacer adjacent motif (PAM)[47]. The PAM consists in the nucleotide motif NGG (N can be any nucleotide, G is guanine) at the 3' end of the target sequence[46]. Cleavage by the endonuclease takes place upstream of the PAM. The double strand break gets repaired, which causes a knockout or a knock in by the non-homologous end joining (NHEJ) creating insertions or deletions (indels), or the homologous directed repair (HDR)[47].

To apply this technology a lentiviral vector could be used to deliver the required components into the cells destined for genome editing. A lentivirus is a ssRNA virus. Its RNA gets reverse transcribed into dsDNA and introduced into the host cell genome. Expression of the virus encoded sequences is performed then by the host cell transcription and translation machinery[48].

The lentiviral production to generate virus particles delivering the sequences of Cas9 and sgRNA is performed in HEK293T cells by applying the three-plasmid system. Thereby, one plasmid encodes structural proteins and enzymes called Gag, Pol, Rev and Tat, another plasmid encodes the viral envelope (VSV-G) and the third encodes Cas9, the sgRNA as well as a selection marker[49]. Cells performing lentiviral production get transfected with these plasmids. Harvested viruses enable then the transduction of the cells in which genome editing is desired. The RNA delivered by the virus particle gets reverse transcribed into DNA and introduced into the host cell genome[48]. Expression of Cas9 and the sgRNA leads then to the double strand break at the determined locus and introduces in most cases the shift in the reading frame or generates a preliminary stop codon[47].

3.3.2 Design of gRNAs for the ZFYVE27 gene

NCBI gene database (https://www.ncbi.nlm.nih.gov/gene) was used to determine common exons of multiple isoforms detected or predicted for the *ZFYVE27* (Gene ID: 118813) *Homo sapiens* (human) gene. Two exons, common for most of 32 splice *ZFYVE27* isoforms and located close to the 5' end of the gene, were chosen as targets for the gene knockout. The location of the targeted exons close to the 5' end is important to avoid expression of functional short proteins. The sgRNAs were designed using the CRISPR tool (http://crispr.med.edu). The sequences corresponding to exons 3 and 4 from Homo sapiens *ZFYVE27*, coding for transcript variant 1, mRNA (GI: 50557646) were used in this software to find sgRNAs without off targets in other genes. sgRNAs with the highest scores were chosen (Table 3.2). For cloning, if sg sequence did not have a 5' guanosine, one was added to the sequence. The reverse sequence was calculated, and the overhang AAAC was added to the 5' end of the reverse sequence and CACC - to the 5' end of the forward sequence (Table 3.1).

Table 3.1. Schematic overview for the generation of forward and reverse sequences with overhangs.

Forward	5' – CACCGXXXXXXXXXXXXXXXXXXX – 3'
Reverse	5' – XXXXXXXXXXXXXXXXXXXAAAC – 3'

Table 3.2. sgRNA sequences listed with their score, PAM and target exon.

	score	sequence	PAM	exon
#1	93	5' – AGGTCGCCTGTCTCGTCCCG – 3'	AGG	3
#2	92	5' – CTCCGCATCAGCTCGGAATC – 3'	AGG	3
#3	89	5' – GAAGTATCATAGCGTGAGGC– 3'	AGG	3
#4	89	5' – CGCCTACCGCGTGCTGCACT – 3'	GGG	4
#5	84	5' – CTCCCAGTGCAGCACGCGGT – 3'	AGG	4
#6	73	5' – ATGTGCAGCACAGGCGGCTC – 3'	AGG	4

3.3.3 sgRNA cloning

The plasmid lentiCRISPR v2 (Figure S 4) was a gift from Feng Zhang (Addgene plasmid # 52961; http://n2t.net/addgene:52961; RRID:Addgene_52961[50]) and was used for sgRNA cloning (Figure 3.2). LentiCRISPR v2 was incubated with the restriction enzyme BsmBI (NEB) and NEB2.1 buffer (NEB) as shown in Table 3.3 for 1 h at +55°C. Afterwards the restriction reaction was heat inactivated by +80°C for 20 min. Then dephosphorylation was enabled by incubation with 5.5 µl Antarctic phosphatase buffer (NEB) and 1 µl Antarctic phosphatase (NEB) for 30 min at +37°C. The plasmid was gel purified after dephosphorylation to obtain backbone ready for cloning.

Table 3.3. Restriction reaction of the plasmid.

LentiCRISPR_v2	5 µg
BsmBI	2 µl
NEB2.1	5 µl
Make final volume to 50µl with DD H_2O	

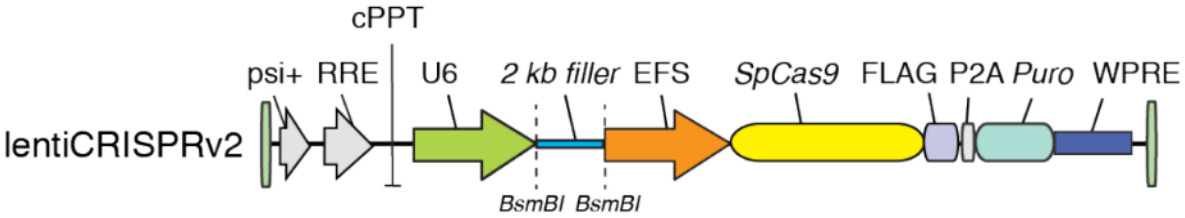

Figure 3.2. Part of the plasmid lentiCRISPR v2, which gets introduced into the host cell genome. The sgRNA gets introduced into the 2 kb filler region. (ZhangLab[51])

For this, the entire volume of the reaction was mixed with 6x loading buffer (Thermo Fisher) and loaded on a 0.8% agarose gel containing GelRed® Nucleic Acid Gel Stain (1:20000) (Biotium). Further, TrackIt™ 100 bp DNA Ladder (Thermo Fisher Schientific) was loaded and the gel was run for 1 h at 100 V giving two bands (plasmid and 2 kb filler, Figure 3.2). The upper band representing the restricted plasmid was cut and purified using the QIAquick gel extraction kit (Qiagen) by manufacturer protocol.

The complementary DNA oligos coding for sgRNAs were phosphorylated applying T4 PNK (NEB) (Table 3.4), by incubation at +37°C for 30 min, followed by adding 490 µl DD H_2O and a 5 min denaturation step at +95°C. After slowly cooling down tubes to +55°C to correctly anneal complementary oligos to each other, the phosphorylated annealed oligos were stored at -20°C before the ligation setup with the restricted target plasmid.

Table 3.4. Phosphorylation of sgRNAs.

10x T4 ligase buffer	1 µl
DD H_2O	6.5 µl
T4 PNK	0.5 µl
Oligo for sgRNA FWD (100 µM)	1 µl
Oligo for sgRNA REV (100 µM)	1 µl

Prepared DNA oligo pairs were ligated with purified lentiCRISPR v2 using T4 ligase (NEB) as presented in Table 3.5. Additionally, a control for plasmid self-annealing containing ultrapure MiliQ H_2O instead of oligos was prepared. For ligation, tubes were incubated overnight at +4°C, and ligation reactions were stored at -20°C before proceeding with bacterial transformation.

Table 3.5. Ligation of sgRNAs with the vector backbone.

Vector backbone (50 ng)	1 µl
10x T4 ligation buffer	2 µl
T4 ligase	1 µl
Annealed DNA oligos	1 µl
Add DD H_2O to 20 µl	

For transformation, competent *E. coli* DH5α were thawed on ice. 10 µl of the ligation reaction was added per 50 µl of competent bacteria and incubated for 30 min on ice. Heat shock was performed for 40 sec at +42°C, followed by 2 min on ice. Recovery of bacteria was enabled by adding 300 µl SOC medium (Table 3.6) per reaction and a 1 h incubation at +37°C and

250 rpm to ensure development of antibiotic resistance in successfully transformed bacteria. 30 µl of transformed and recovered bacteria were plated on agar plates (Table 3.6) containing 100 µg/ml of Carbenicillin (Ampicillin analogue, more stable) (Sigma-Aldrich) and incubated overnight at +30°C.

Table 3.6. Components of liquid and fixed LB medium, and SOC medium.

Liquid LB medium	**LB agar plates**	**SOC medium**
10g/L NaCl 10g/L trypton 5g/L yeast extract	10g/L NaCl 10g/L trypton 5g/L yeast extract 15g/L agar	20 g/L Tryptone 5 g/L Yeast Extract 4.8 g/L $MgSO_4$ 3.603 g/L dextrose 0.5g/L NaCl 0.186 g/L KCl

Two colonies per ligation reaction were picked and seeded in 3 ml liquid LB medium (Table 3.6) containing 100 µg/ml Ampicillin (Sigma-Aldrich) or Carbenicillin. Cultures were incubated overnight at +30°C and 250 rpm.

Plasmid isolation using the PureYield™ Plasmid Miniprep kit (Promega Corporation) was performed for the cultures, keeping 1 ml of culture stored at +4°C. Pre-mixed samples containing 5 µl of plasmids (100ng/ul) and 5 µl of sequencing primer (5 µM) U6_CRISPR_Seq3 5'-ATTTCTTGGGTAGTTTGCAG-3' were sent for sequencing to Eurofins Genomics (Germany) before proceeding further with plasmid midi preps production of viral particles.

Sequencing results were analyzed using nucleotide BLAST online database (https://blast.ncbi.nlm.nih.gov/Blast.cgi). The sequences were aligned to "Human genomic+transcript" database with program "Somewhat similar sequence" and checked for specificity against the *ZFYVE27* gene.

For correct clones, 50 µl of the cultures kept from mini preps were transferred to 50 ml of liquid LB medium with 100 µg/ml Ampicillin in 0.5-1L Erlenmeyer flasks. Cultures were incubated at least 12 h at +30°C and 250 rpm. Then, cultures were transferred to 50 ml tubes

and centrifuged for 15 min at 3300 rpm. Supernatants were discarded, and pellets were processed by ZymoPURE™ II Plasmid Midiprep Kit (Zymo Research).

3.3.4 Transfection of HEK293T cells and lentiviral production

HEK293T cells ($4x10^5$) were seeded in 6-well plates, 2 wells per virus with specific sgRNA. On the second day transfection was performed. Therefore, transfection mix (Table 3.7) containing Opti-Mem™ – Reduced Serum Medium, no phenol red (Gibco) and GeneJuice® Transfection Reagent (Sigma-Aldrich) was prepared. The mix was vortexed for 2 sec and incubated at RT, while preparing the mix containing the plasmids. For the plasmid mix (Table 3.7), a master mix containing the packaging (psPAX2 was a gift from Didier Trono (Addgene plasmid # 12260 ; http://n2t.net/addgene:12260; RRID:Addgene_12260) and envelope (pMD2.G was a gift from Didier Trono (Addgene plasmid # 12259 ; http://n2t.net/addgene:12259; RRID:Addgene_12259) plasmids was prepared. A lentiCRISPR v2 with the insert of a specific sgRNA coding sequence was added to the master mix. The transfection mix was blended carefully into the plasmid mix. 100 µl of the final mix was dispensed dropwise per well and incubated at +37°C and 8% CO_2 in the BSL-2 lab. 24 h later the medium was changed, and incubation continued under the same conditions. Again, in 24 h the supernatants were collected and centrifuged for 10 min at +4°C, 1000 x g to clear from cell debris. The supernatants with viral particles were aliquoted and stored at -80°C before use.

Table 3.7. Transfection mix and plasmid mix for the transfection of 2 wells.

Transfection mix	
Opti-Mem	200 µl
GeneJuice	8µl
Plasmid master mix	
psPAX2	2 µg
pMD2.G	1.34 µg
Add to master mix	
LentiCRISPR v2	2.66 µg

3.3.5 Viral transduction of THP-1 cells

8 wells containing 1x10^6 THP-1 WT cells with low passage number in 2 ml of medium were seeded in 6-well plates. Each well was treated with different virus. Each virus coded for one *ZFYVE27* specific sgRNA, 1 well was treated with a control virus coding for non-targeting sgRNA (Table 3.8), and 1 well was not treated by virus and was used as a control for effective puromycin selection. 500 µl of supernatant with viral particles and 8 µM protamine sulphate (Sigma-Aldrich) were added per well. The cells were incubated at +37°C at 5% CO_2 for 24 h. The next day, transduced cells were collected and centrifuged at 200 x g for 7 min to wash away viral particles. Pellets were resuspended in 4 ml of THP-1 medium containing 1 µg/ml puromycin to start selection for transduced cells. In 48 h cells were centrifuged at 100 x g for 5 min to remove dead cells. Pellets were resuspended in THP-1 medium containing 1 µg/ml puromycin and cultured as usual THP-1 cultures for 2 weeks.

Table 3.8. Forward and reverse sequences coding for 6 sgRNAs (#1-#6) and a non-targeting sgRNA (control).

#1	Fwd	5’ – CACCGAGGTCGCCTGTCTCGTCCCG – 3’
	Rev	5’ – AAACCGGGACGAGACAGGCGACCTC – 3’
#2	Fwd	5’ – CACCGCTCCGCATCAGCTCGGAATC – 3’
	Rev	5’ – AAACGATTCCGAGCTGATGCGGAGC – 3’
#3	Fwd	5’ – CACCGAAGTATCATAGCGTGAGGC – 3’
	Rev	5’ – AAACGCCTCACGCTATGATACTTC – 3’
#4	Fwd	5’ – CACCGCGCCTACCGCGTGCTGCACT – 3’
	Rev	5’ – AAACAGTGCAGCACGCGGTAGGCGC – 3’
#5	Fwd	5’ – CACCGCTCCCAGTGCAGCACGCGGT – 3’
	Rev	5’ – AAACACCGCGTGCTGCACTGGGAGC– 3’
#6	Fwd	5’ – CACCGATGTGCAGCACAGGCGGCTC – 3’
	Rev	5’ – AAACGAGCCGCCTGTGCTGCACATC – 3’
control	Fwd	5’ – CACCGTTTGTAATCGTCGATACCC – 3’
	Rev	5’ – AAACGGGTATCGACGATTACAAAC – 3’

3.4 Transient gene knockdown

3.4.1 General information

The transient gene knockdown is based on the principle of RNA interference (RNAi). Short interfering RNA (siRNA) is transfected into the cells. The siRNA unwinds and gets bound by assembly of a multicomponent complex, the RNA induced silencing complex (RISC). The RISC is guided by siRNA to mRNA with a complementary sequence. The targeted mRNA gets degraded by the catalytic component of the RISC complex. This degradation process takes place before mRNA translation causing gene silencing[52,53].

To deliver the siRNA into the cells, transfection is necessary. Lipofection is an approach to transfect cells with RNA or DNA. A mixture of lipids and siRNA enables the formation of liposomes. This liposomes containing the siRNA can then be taken up by cells through endocytosis or direct fusion of the liposome with the plasma membrane[54].

3.4.2 Silencing in THP-1 WT and THP-1 TLR8 pDest cells

To generate a transient knockdown, THP-1 cells were seeded in medium without antibiotics according to Table 3.9 and differentiated into macrophage-like cells by 40 or 60 ng/ml phorbol myristate acetate (PMA) (Sigma-Aldrich). In 24 h cells were transfected with 16 nM siRNA oligo using the transfection reagent Lipofectamine RNAiMax (Thermo Fisher Scientific). For wells with 2 ml of culture medium (per well of 6-well plate, for 2 wells of 24-well plate): mix 1 was prepared by adding 5 µl RNAiMax into 245 µl preheated Opti-Mem and incubated at RT for 5 min; mix 2 consisted of 248 µl of preheated Opti-Mem and 2 µl of 20 µM siRNA oligo (Table 3.10) and was carefully blended into mix 1 followed by incubation at RT for 20 min. After that 490 µl of prepared solution was dispensed dropwise to the cells. In 24 h medium was changed to PMA-free, antibiotic free THP-1 medium, and cells were additionally incubated for 48 h before proceeding with the experiments.

Table 3.9. Cell seeding for different experiments with a siRNA pre-treatment.

Type of experiment	**Cell type**	**Plate-format**	**Cells/well**	**Medium volume/well**
Stimulation	THP-1 WT cells / THP-1 TLR8 pDest cells	6-well plate	$400x10^3$	2 ml
	Primary macrophages		$6x10^6$	2 ml
Live *E. coli* uptake	THP-1 WT cells	24-well plate	$200x10^3$	1 ml
Confocal microscopy	THP-1 WT cells	24- well plate with glass bottom	$100x10^3$	1 ml
	Primary macrophages	35 mm dish with glass bottom	$6x10^6$	2 ml
Knockdown verification	THP-1 WT	12-well plate	$400x10^3$	1 ml

3.4.3 Silencing in THP-1 TLR9 mCherry cells

THP-1 TLR9 mCherry cells were transduced with siRNA in suspension using Lipofectamine™ 3000 Transfection Reagent (Thermo Fisher Scientific). For each silencing condition, 10 µl of Lipofectamine 3000 was mixed into 100 µl warm Opti-MEM (mix 1) by vortexing for 3 to 5 sec. After 5 min at RT, mix 2 containing 4 µl of siRNA oligo (Table 3.10) in 100 µl of Opti-Mem was added. The mix 2 was carefully blended into mix 1. The combined mix was incubated for 20 min at RT. In the meantime, $4.5x10^6$ THP-1 TLR9 mCherry cells per siRNA oligo were centrifuged at 200 x g for 7 min. Supernatant was discarded, and the cell pellet resuspended in 2 ml warm Opti-Mem and 1.8 ml transferred to a well of a 6-well plate. 200 µl of transfection reagent was added dropwise to the cells giving a concentration of 40 nM siRNA per well and cells were incubated for 2 h in an incubator at +37°C, 5%CO_2 After that cells were transferred to fresh T75-cell culture flasks and diluted by adding 8 ml fresh prewarmed THP-1 medium without antibiotics and incubated under normal THP-1 culture conditions for the next 24 h. Then the cells were centrifuged at 200 x g for 7 min, resuspended subsequently in 10 ml THP-1 medium without antibiotics containing 1 µg/ml doxycycline (Echelon Bioscience) to induce TLR9 expression from inducible promoter

and incubated again 24 h. Next, siRNA treatment was repeated. This second siRNA treatment was performed by increasing all the volumes 2 times. Incubation was continued until stimulation on the next day at +37°C, 5% CO_2 in medium containing 1 µg/ml doxycycline.

3.4.4 Silencing in primary macrophages

siRNA transfection in primary cells was performed on day 6 after isolation. Cells were cultured in concentration around $6x10^5$/well in 6-well plates, 2 ml of medium per well. For mix 1, 3 µl of Lipofectamine 3000 was added to 25 µl Opti-Mem per well, vortexed for 2-3 sec, and incubated at RT for 5 min. In the meantime, mix 2 was prepared by blending 3.3 µl siRNA oligo (Table 3.10) into 25 µl Opti-Mem. Mix 2 was carefully combined with mix 1 and incubated for 15 min at RT. 50 µl of combined mix was dropwise added per well giving a final concentration of 32 nM. In 24 h medium were changed, on day 8 siRNA transfection was repeated and on day 10 experiments were performed.

Table 3.10. List of siRNA oligos.

FlexiTube siRNA	**Cat. No.**	**Producer**
Control (AllStar)	SI03650318	Qiagen
RAB11A - 5	SI00301553	Qiagen
RAB11B - 6	SI02662695	Qiagen
RAB11FIP2 - 5	SI04305672	Qiagen
TLR4 - 2	SI00151011	Qiagen
ZFYVE27	SI00767795	Qiagen

3.5 Stimulation of cells by TLR ligands

Ultrapure K12 LPS (Invivogen) is a ligand of TLR4 and was used to stimulate THP-1 WT cells, THP-1 CRISPR/Cas9 *ZFYVE27* KO cells and primary macrophages with final concentration in culture medium 100 ng/ml. Prior to stimulation, stock solution of LPS (1

mg/ml) was vortexed for 45 sec, sonicated at program 6 for 1 min at RT in the ultrasound cleaning bath - USC1200TH and vortexed again for 45 sec before usage.

CL075 (Invivogen) is a synthetic thiazoloquinoline compound and a ligand for TLR8. It was used to stimulated THP-1 TLR8 pDest cells at final concentration in medium 1 µg/ml.

CpG ODN 2006 (2016 batch) (TIB MOLBIOL) is a synthetic oligonucleotide containing unmethylated CpG dinucleotides. It was used to stimulate THP-1 TLR9 mCherry cells at final concentration in medium of 10 µM.

3.6 Collection of supernatants and cell lysis for RNA/protein isolation

Stimulation was stopped by placing plates with cells on ice. 500 µl of the supernatant from stimulated PMA differentiated cells was collected and stored at -80°C. Supernatants of cells in suspension were collected after centrifugation for 5 min at 400 x g and +4°C in 1.5 ml Eppendorf tubes.

Cells were washed with 1 ml ice-cold PBS followed by addition of 500 µl QIAzol lysis reagent (Qiagen) per well. QIAzol lysates were collected, and samples were processed immediately or stored on -80°C.

For lysis in RIPA buffer, cells were washed 3 times with 1 ml cold PBS. Suspension cells were centrifuged for 5 min at 400 x g and +4°C. Supernatants were removed, and cells lysed in 150 µl RIPA buffer with protease and phosphatase inhibitors (cOmplete™, Mini, EDTA-free Protease Inhibitor Cocktail (Roche); PhosSTOP™, phosphatase inhibitor tablets (Roche)). Lysates were incubated at the shaker or in the rotation module at +4°C for 20 min, collected to 1.5 ml tubes and stored at -20°C. RIPA lysates were processed by thawing and centrifuging for 15 min at +4°C, 15000 x g. 120 µl supernatants were transferred into fresh tubes. 4x LDS buffer was added to the cleared lysates resulting in a 1x solution. Subsequently, lysates were put on +80°C for 5 min, before storing at -20°C.

Table 3.11. Composition of RIPA buffer.

2x RIPA lysis buffer	**Producer**
300 mM NaCl	Merck
10 mM EDTA	Sigma-Aldrich
2% Triton X100	Sigma-Aldrich
100 mM Tris HCl pH 7.5	Trizma base, Sigma

3.7 Simultaneous isolation of RNA/protein from QIAzol lysates

3.7.1 RNA isolation

100 µl of Chloroform was added per 500 µl QIAzol lysate, and tubes were shaken vigorously for 15 sec. In order to separate the aqueous phase from the organic phase a centrifugation step of 15 min at +4°C and 11600 x g was performed. The upper aqueous phase contains RNA, the interphase DNA and the lower organic phase the proteins. The upper RNA containing phase was recovered carefully and transferred into a fresh 1.5 ml Eppendorf tube. Half of the volume of absolute ethanol was added and mixed by inverting. These mixtures were transferred onto RNeasy spin columns in RNAeasy ® Mini Kit (Qiagen) and processed for RNA isolation as suggested by manufacturer. A DNase treatment step using the RNase-Free DNase Set (Qiagen) was included to prevent genomic DNA contamination of the RNA isolates. The purity and concentration of the RNA was measured by NanoDrop ND-1000 (Thermo Fisher Scientific).

Tubes with the lower organic phase were supplemented with 160 µl of absolute ethanol and stored at -80°C before proceeding with protein extraction.

3.7.2 Protein extraction

Samples with lower organic phase prepared during RNA isolation were thawed and centrifuged for 5 min at 2000 x g at +4°C to clear protein fraction from genomic DNA. Supernatants were transferred to 750 µl isopropanol for precipitation of proteins, and samples

were incubated for 10 min at RT, followed by centrifugation at 12000 x g at +4°C for 10 min. The supernatants were discarded. The protein pellet was washed 3 times by adding 1 ml of 0.3 M guanidine hydrochloride in 95% ethanol and incubating pellets for 10 min at RT. Pellets were centrifugated for 5 min at 7500 x g at +4°C between washing steps. After the third wash 1 ml absolute ethanol per sample was added, pellet were incubated for 20 min at RT and centrifugated for 5 min at 7500 x g at +4°C. Afterwards, the supernatant was discarded, pellets were air dried for 5 min, and dissolved in 50-200 µl of buffer containing 1% SDS and 4 M urea. NuPAGE™ LDS Sample Buffer (4X) (Thermo Fisher Scientific) with 0.1 M DTT (AmpliChem) was added to get 1x solution (one third of protein solution volume). The samples were boiled for 10 min at +95°C before storing at -20°C.

3.8 Gene expression analysis

3.8.1 General information

Gene expression analysis determines changes in mRNA expression level of certain genes by using the two-step reverse transcription quantitative polymerase chain reaction (RT-qPCR). Two-step RT-qPCR is the procedure in which isolated RNA gets reversely transcribed into complementary DNA (cDNA) during the first step. Reverse transcription is performed by using an oligo $(dT)_{18}$ and/or random hexamer primers. The second step consists in the actual PCR, during which the product amplification gets quantified simultaneously. The TaqMan chemistry finds application here in this study. Specific TaqMan primer-probe mixes contain oligonucleotide probes with a 5' end fluorescent reporter dye and a 3' end quencher. The TaqMan polymerase with its 5' nuclease activity releases the fluorescent reporter dye from the quencher during amplification and allows detectable emission. The amplification consists in the exponential, the linear and the plateau phase (Figure 3.3). During the exponential phase the concentration can be determined most accurately. The C_T value determines the timepoint at which the fluorescent intensity is above background. This value is the cycle number at which the threshold was reached and is therefore a smaller value the higher the starting concentration[55].

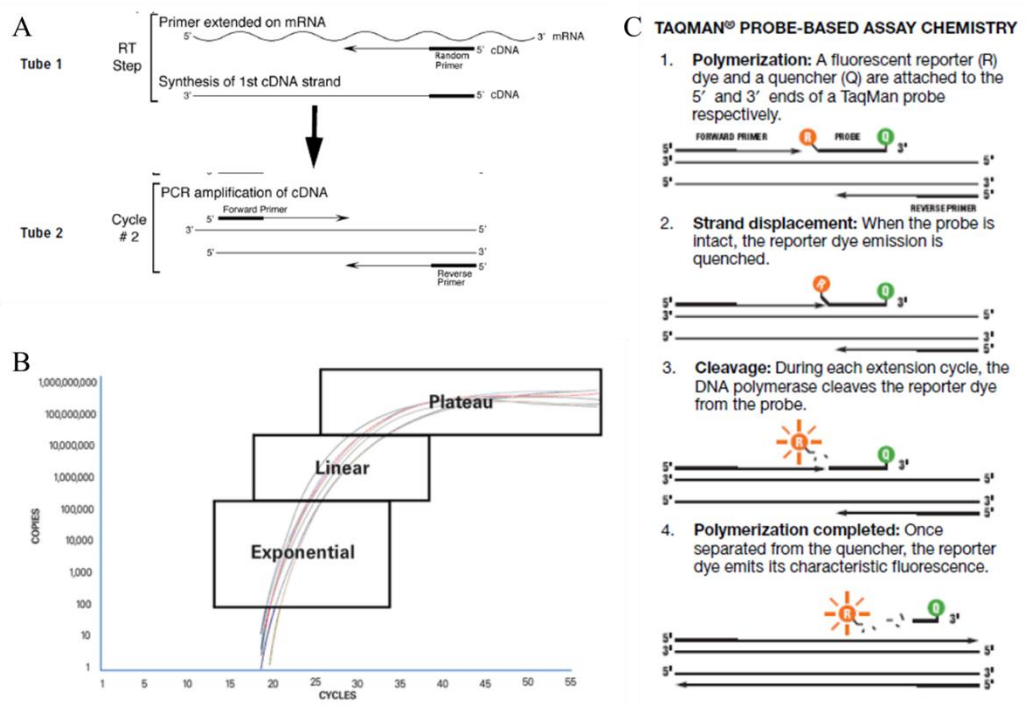

Figure 3.3. Two-step reverse transcription quantitative polymerase chain reaction (RT-qPCR) consists in the synthesis of complementary DNA in the first step (A) and the second step during which the concentration of a certain gene transcript is quantified (C). The amplification of the PCR products follows an exponential curve (B) with three phases: the exponential, the linear and the plateau phase. Within the exponential phase the C_T is determined which represents the cycle number in which the threshold of fluorescent intensity exceeds the background level. (adapted from Applied Biosystems[55]).

3.8.2 RT-qPCR

500 ng RNA was used to synthetize cDNA with the Maxima First Strand cDNA Synthesis Kits for RT-qPCR (Thermo Fisher Scientific) in a C1000™ Thermal Cycler. After synthesis, the cDNA was diluted 1:5 in nuclease free water. 5 µl of the diluted cDNA was used per RT-qPCR sample of a total volume of 20 µl containing PerfeCTa qPCR FastMix UNG (Quantabio), nuclease free water and specific Applied Biosystems™ TaqMan® Assays containing probe and primers (Table 3.12). Duplicates of each reaction were mixed in MicroAmp Fast Optical 96-Well Reaction Plate with Barcode (Applied Biosystems). The plate was sealed with MicroAmp™ Optical Adhesive Film (Applied Biosystems) and centrifuged for 2 min at +4°C and 1500 x g. Reaction was run in the StepOnePlus Real time PCR System (Applied Biosystems).

The expression level of the TATA-binding protein (TBP), a housekeeping gene, was detected for every sample. TBP levels were used to normalize the data to enable expression level comparison of certain target genes between samples. Other TaqMan assays used for sample analysis are listed in Table 3.12.

Table 3.12. List of TaqMan® probes produced Applied Biosystems™.

RT-qPCR target	**Applied Biosystems™ TaqMan® Assays**	**Cat. No.**
CXCL10	Hs01124251_g1	4331182
IFNβ	Hs01077958_si	4351370
Rab11a	Hs00900539_m1	4351370
Rab11b	Hs00188448_m1	4331182
Rab11FIP2	Hs00914191_m1	4351372
TBP	Hs00427620_m1	4351368
TLR4	Hs00152939_m1	4351370
TNF	Hs00174128_m1	4351368
ZFYVE27	Hs00990279_m1	4351372

3.8.3 RT-qPCR data analysis

To analyze and determine relative quantification the $2^{-(\Delta\Delta CT)}$ method was used. Fold changes in gene expression of treated and control cells at certain timepoints, normalized to endogenous control gene expression levels and values for untreated control sample was calculated. Therefore, the ΔC_T values were generated by calculating the difference of the C_T value of a timepoint (x) to the C_T value of the control treated, timepoint (0) represented by the not treated, medium control sample (T(0); C(0)). The fold change of the ΔC_T value of the target gene relative to the ΔC_T of the endogenous control gene was generated. Results indicate the change in target gene expression in control cells and treated cells at different timepoints[56].

$$2^{-(C_{T,T(x)}-C_{T,T(0)})-(C_{T,C(x)}-C_{T,C(0)})} = 2^{-(\Delta\Delta C_T)}$$

3.9 Western blotting

3.9.1 General information

Western blotting is a method used for identification, quantification or molecular weight determination of a specific protein. Protein extracts are separated according to their molecular weight. A sodium dodecyl sulphate polyacrylamide gel electrophoresis (SDS-PAGE) can be used for protein separation. Thereby, the proteins get denatured and negatively charged enabling the separation according to molecular weight. In the next step, the proteins get transferred onto a nitrocellulose membrane by electroblotting. The following blocking step masks epitopes which could cause unspecific antibody binding during incubation with a primary antibody specific for the target protein. The secondary antibody carrying a horseradish peroxidase enables subsequently the band visualization. A proportional amount of chemiluminescent agent to the protein is cleaved resulting in luminescence. Membranes can be stripped, which means clearing from antibodies, and reprobed after blocking with a specific primary antibody. By reprobing a membrane for a housekeeping protein, quantification of the protein bands enables relative comparison of expression levels between samples[57].

3.9.2 SDS-PAGE

Protein extracts were thawed and boiled for 3 to 5 min at +95°C, centrifuged and resuspended before loading. 10 to 20 µl sample from protein extracts or 25 µl from RIPA lysates were loaded per well into a Mini or Midi NuPAGE™ 4-12% Bis-Tris Protein Gel (Life Technologies). Gels were run in 1x NuPAGE™ MOPS SDS Running Buffer (Life Technologies) for 20 min at 100 V followed by 1 to 2 h at 185 V.

3.9.3 Blotting

After electrophoresis, the gel was rinsed in distilled water and the proteins were transferred to the membrane by dry blotting using iBlot® 2 NC Regular/Mini Stacks (Life Technologies) in the iBlot 2 Dry Blotting System (Life Technologies).

After protein transfer the membrane was rinsed in TBS-T (Table 3.13) before blocking for 1 h in 5% non-fat milk in TBS-T. Membrane was rinsed once again in TBS-T before overnight

incubation with primary antibody at +4°C on a shaker. The following day the membrane was washed 4 times for 3 min in TBS-T at RT at the shaker. Subsequently, membranes which have been incubated with ZFYVE27 antibodies were incubated with swine anti-rabbit polyclonal antibody HRP in 1% milk (1:4000) for 1 h on the shaker at RT. Meanwhile, membranes previously incubated with pSTAT1 antibodies were incubated for 2 h with the primary antibody solution targeting β-tubulin. These membranes were washed 4 times in TBS-T and subsequently incubated with the swine anti-rabbit secondary antibody solution for 1 h. Information about antibodies could be found in Table 3.14.

After secondary antibody incubation, membranes were washed 4 times in TBS-T and incubated for 4 min with HRP substrate solution. SuperSignal™ West Femto Maximum Sensitivity Substrate (Thermo Fisher Scientific). Images were taken using Odyssey® Fc (LI-CORE).

3.9.4 Stripping and reprobing

Due to the similar molecular weight of ZFYVE27 and β-tubulin, membranes had to be stripped from ZFYVE27 antibody to apply staining for control protein β-tubulin. For this, membranes were rinsed with water and incubated for 1 h on the water bath with shaker at +60°C in stripping buffer (62.5 M Tris pH 6.8, 2% SDS) containing 100 mM β-mercaptoethanol. The membrane was washed for at least 1 h in TBS-T on the shaker at RT, before the 1-h blocking step and overnight incubation with primary antibody. Following procedure until imaging was performed as described previously.

Table 3.13. Composition of TBS-T.

TBS-T	**Producer**
0.05 M Tris HCl pH 7.5	Trizma base, Sigma
0.15 M NaCl	Merck
0.1 % Tween-20	Sigma-Aldrich
Distilled H_2O	

Table 3.14. List of antibodies for Western blotting.

Protein of interest	**Primary antibody**	**Dilution**	**Diluted in**	**Cat. no.**	**Supplier**
B-tubulin	Rabbit monoclonal [EPR16778] to beta I Tubulin	1:25000	2% BSA-TBS-T	ab7921	Abcam
pSTAT1 (Y701)	Phospho-Stat1 (Tyr701) (D4A7) Rabbit mAb	1:1500	2% BSA-TBS-T	#7649	Cell signaling
ZFYVE27	ZFYVE27 Antibody Rabbit Polyclonal	1:1300	2% milk-TBS-T	12680-1-AP	Proteintech Europe
	Secondary antibody	**Dilution**	**Diluted in**	**Cat. no.**	**Supplier**
	Swine Anti-Rabbit Immunoglobulins/HRP	1:4000	1% milk-TBS-T	P0399	Dako

3.10 Live bacteria uptake

$2x10^5$ THP-1 WT cells were seeded in 1 ml medium without antibiotics per well in 24-well plates, PMA-differentiated and siRNA treated.

On the day of the experiment, an overnight culture *E. coli* DH5α was diluted 1:50 in LB medium and grown to an optical density of 0.36 to 0.45 at 600 nm, and 20 ml of culture were distributed into two 15 ml tubes and centrifuged for 15 min at +4°C at maximum speed. Supernatants were discarded, and *E. coli* pellets were washed in 1 ml cold PBS each by resuspending and centrifuging at +4°C maximum speed for 5 min. This washing step was repeated to a total of 3 times, before combining the two pellets into a total volume of 1 ml PBS.

A dose of 10 to 50 bacteria per cell in 10% FCS-RPMI was added to 4 to 5 replicates. By centrifugation for 7 min at 750 x g at +4°C contact of the bacteria with the macrophage monolayer was ensured. Plates were warmed for 15 min to +37°C in a water bath. Then, the plates were quickly transferred onto ice and washed 3 times with ice-cold PBS. After this washing step, warm 10% FCS-RPMI containing 100 µg/ml gentamycin was added to remove

extracellular bacteria. Cells were immediately incubated at +37°C for 30 min. Plates were again put onto ice and washed 3 times with ice-cold PBS. Phagocytosed bacteria were released by lysis of the cells in 1 ml sterile water. Lysates were diluted 200-to 1000-fold and 10 µl of dilutions were plated in triplicates on LB agar plates. To determine the number of phagocytosed bacteria per cell, the colony forming unit (CFU) was counted. To determine total protein concentrations of cell lysates Pierce™ BCA Protein Assay Kit (Thermo Fisher Scientific) was performed to normalize the cell number per well. Efficient gene knockdown was confirmed by RT-qPCR of replicate wells, which were seeded and siRNA treated simultaneously.

3.10.1 Bicinchoninic acid (BCA) protein assay

3.10.1.1 General information

Bicinchoninic acid (BCA) protein assay bases on the principle of the biuret reaction (Figure 3.4). This reaction describes the chelate formation with Cu^{2+} by peptides consisting in at least three amino acid residues. The cupric ion forms together with 4 to 6 peptide bonds a blue-colored complex, whereby the color intensity is proportional to the number of peptide bonds involved. During this first step, Cu^{+} gets formed, which subsequently reacts with a BCA reagent. This reagent is a sensitive and specific colorimetric detection reagent. Two BCA reagent molecules form a chelate with a cupric cation and have a linear absorbance at 562 nm with increasing protein concentration[58].

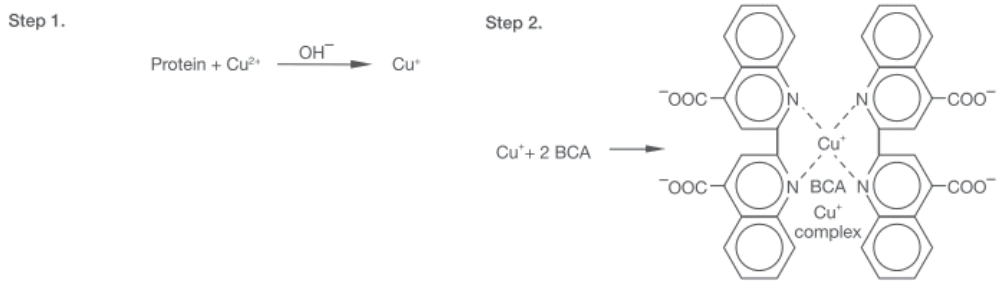

Figure 3.4. Principle of the bicinchoninic acid (BCA) protein concentration assay. Step 1: describes the reaction by which chelation of peptides with Cu^{2+} results in the formation of Cu^{+}. Step 2: shows two BCA molecules chelating with the in step 1 formed cupric cation. (adapted from invitrogen[58])

3.10.1.2 BCA protein assay

Protein concentrations of one replicate per siRNA treatment used in the live bacteria uptake assay were assessed using the Pierce™ BCA Protein Assay Kit (Thermo Fisher Scientific). The RIPA lysates were cleared by a 10 min centrifugation step at maximum speed (15000 rpm) and +4°C. The assay was performed according to manufacture protocol using 25 µl of standard and supernatant from the cleared lysates, in replicates. After 30 min incubation at +37°C in an incubator the absorbance at 570 nm was measured on iMark™ Microplate Absorbance Reader (Bio-Rad) and concentration determined by the Microplate Manager Software 6.

3.11 pHrodo *E. coli* bioparticles uptake and confocal microscopy

$1x10^5$ THP-1 WT cells were seeded per well in a Glass Bottom 24-Well Plates No. 1.5 uncoated γ-irradiated – P24G-1.5-13-F (MatTek Corporation), or $6x10^6$ primary macrophages per 35 mm dish No. 1.5 – P35G-1.5-10-C (MatTek Corporation). For the phagocytosis assay pHrodo™ Red *E. coli* BioParticles™ Conjugate for Phagocytosis (Invitrogen) were vortexed for 45 sec, sonicated at program 6 in the ultrasound cleaning bath - USC1200TH for 1 min at RT and vortexed again for 45 sec. The bioparticles were opsonized for 5 min in 10% sterile filtered A+ serum in PBS. Doses in a range from 1 to 15 *E. coli* BioParticles™ per cell were used. Cells were incubated with the bacteria particles for 15 min in 10% FCS-RPMI. Then solution was replaced with fresh 10% FCS-RPMI and incubated for additional 30 min.

3.11.1 Fixation

E. coli bioparticles uptake was stopped on ice. Then medium was removed, and samples washed with ice-cold PBS. Methanol-Acetone (1:1) was added to wells, and plates/dishes were stored at -20°C until proceeding with staining.

3.11.2 Immunolabelling and staining

Rehydration of the samples was performed after discarding methanol-acetone, addition of PBS and incubation at RT for 1 h followed by blocking for 30 min with 20% sterile filtered A^+ in PBS. Samples were rinsed once with 2% A^+ in PBS before applying the 1:100 TLR4 (C-18) goat polyclonal IgG (Santa Cruz Biotechnology) in 2% A^+ in PBS and incubating in a wet-chamber overnight at +4°C. On the next day, samples were washed 3 times for 5 min with PBS, rinsed once with 2% A^+ and incubated with 1:2000 Alexa 647 Donkey anti-Goat (Thermo Fisher Scientific) in 2% A^+ for 30 min at RT, covering plates/dishes from light by foil. Samples washed 2 times, 5 min and incubated for 10 min in PBS with diluted 1:40 Alexa 488 Phalloidin (Thermo Fisher Scientific). Samples were washed again 2 times for 5 min and stored at +4°C, covered from light, until imaging.

3.11.3 Confocal microscopy

3.11.3.1 General information

Fluorescence microscopy uses the property of exciting fluorophores by a certain wavelength and the detection of an emitted longer wavelength. Excitation of fluorophores by a certain wavelength causes an energy transfer by a photon onto the fluorophore. This extra energy causes the elevation of the fluorophore into a higher energy level by pushing an electron into a different orbital. During vibrational relaxation and internal conversion energy gets lost which is called the Stokes shift and leads to the emission of a photon with a longer wavelength. The Stokes shift enables the filtration and detection of the emitted light[59]. Secondary fluorescence is avoided by applying a confocal microscope which enables the optical slicing of the specimen. Two pinholes, one in front of the excitation source and the second in front of the detector, restrict detection of out-of-focus light and increase axial (z-axis) and lateral (x- and y-axis) resolution (Figure 3.5)[60].

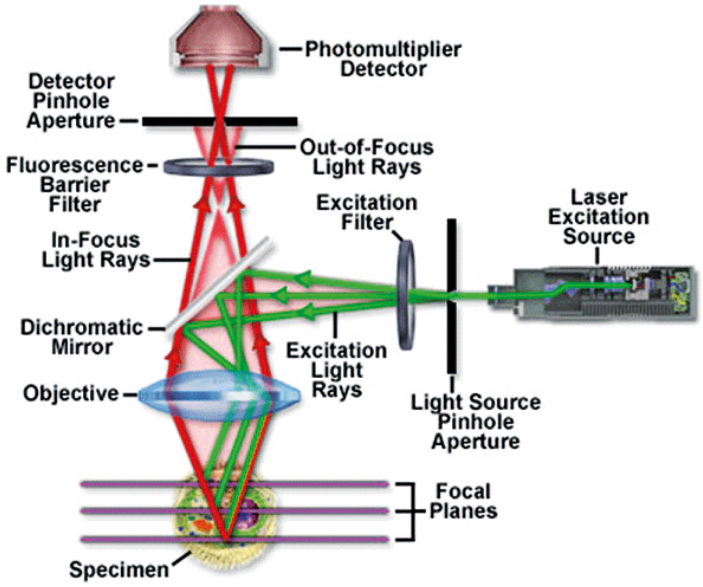

Figure 3.5. Schematic overview of the principle of a confocal microscope. The laser excitation light passes one of the two pinholes and an excitation filter. The light rays of the excitation light get reflected and pass the objective reaching the specimen. The light ray excites fluorophores at a certain location in the x-, y- and z- axis of the specimen. Emitted light from the fluorophores is of longer wavelength and can pass the dichromatic mirror after the objective. Passing a fluorescence barrier filter and the second pinhole in front of the detector leads to detection of fluorescence excluding out-of-focus light (adapted from Fellers, 2012[60])

3.11.3.2 Imaging

Confocal imaging was performed using HC plan-apochromat 63×/1.4 CS2 oil-immersion objective and the LAS X software at the Leica TCS SP8 (Leica Microsystems). Z-stacks imaging of Alexa 488, Alexa 647 and pHrodo™ Red *E. coli* BioParticles™ was performed by estimating the stack size dependent on the distribution of the particles throughout the cells in order to capture all of them.

3.11.3.3 Image analysis

The Bitplane-IMARIS 8.4.2 software was used to detect particles of 1 µm diameter in size in the channel imaging the pHrodo *E. coli* bioparticles. These 1 µm voxels are represented in the software as spheres, which were quantified per cell. Extracellular spheres were removed and information of the intensities of each channel within the detected voxels exported.

3.12 Statistical analysis

Statistical analysis was performed using the GraphPad Prism version 8.00 for Windows, GraphPad Software, La Jolla California USA, www.graphpad.com".

3.13 Bioinformatical analysis

For bioinformatical analysis following online databases were used:

- NCBI Gene (https://www.ncbi.nlm.nih.gov/gene/)
- NCBI Protein (https://www.ncbi.nlm.nih.gov/protein/)
- UniProt (https://www.uniprot.org/)[61]
- Clustal Omega (https://www.ebi.ac.uk/Tools/msa/clustalo/)[62]

4. Results

4.1 Effect of *ZFYVE27* silencing on TLR4 signaling outcome

4.1.1 mRNA expression of TLR4 and TLR4-induced cytokines after LPS stimulation

Trafficking of TLR4 and its adaptor proteins was shown to be crucial in the regulation of TLR4-mediated response[27,28]. Here, we investigate a link between the vesicle transport protein ZFYVE27 and the LPS sensing PRR, TLR4. Preliminary data had shown that silencing of *ZFYVE27* could have inhibitory effect on TLR4-mediated signaling. Decreased TNF and IFNβ secretion and mRNA expression was observed (Master thesis by Lindholm, 2017[45]). To confirm these results, we used RT-qPCR to measure changes in mRNA expression of *TLR4*, *TNF* and *IFNβ* upon silencing of *ZFYVE27* in macrophages-like THP-1 cells or primary human macrophages. Cells were treated with a non-silencing control and *ZFYVE27* targeting siRNA oligo, followed by LPS stimulation for different time points. PMA differentiated THP-1 cells were stimulated in three independent experiments with 2 biological replicates for one of them. Results from THP-1 experiments were pooled (Figure 4.1A) for statistical analysis, and independent results for each experiment are shown in the supplementary (Figure S 1). The same experiment addressing less timepoints was also performed once in human primary macrophages (Figure 4.1B).

We found that *ZFYVE27* silencing in THP-1 cells resulted in the significant decrease of TLR4-mediated *IFNβ* mRNA expression in 2 h of LPS stimulation. A trend for the decreased *IFNβ* mRNA levels was also seen at early and late stimulation time points (Figure 4.1A). The negative effect of *ZFYVE27* silencing on IFNβ protein secretion was supported by the same trend of *CXCL10* mRNA expression (Figure 4.1A), which is an IFNβ inducible gene[9]. Primary macrophages show the decrease in LPS-induced *IFNβ* mRNA only after 2 h of LPS stimulation, while it was increased after 1 h in comparison to cells treated with control oligos (Figure 4.1B). As to the TNF, we found no significant effect of *ZFYVE27* silencing on *TNF* mRNA expression in THP-1 cells or primary macrophages (Figure 4.1).

Regulation of TLR4 expression could be a possible explanation for the effect of ZFYVE27 on TLR4-mediated expression levels of cytokines. However, there was no effect on *TLR4* mRNA expression in THP-1 cells or macrophages (Figure 4.1). At the same time, we reached 60% of

ZFYVE27 silencing efficacy in THP-1 cells and at least 40% efficacy in macrophages (Figure 4.1).

Overall, we confirmed previous findings that ZFYVE27 could be involved in regulation of *IFNβ* mRNA expression and secretion and excluded the hypothesis that this effect is mediated by alterations in *TLR4* mRNA expression levels. Unaffected *TNF* mRNA expression suggests that only intracellular TLR4-TRAM-TRIF-mediated signaling was affected by *ZFYVE27* knockdown, but not TLR4-MAL-MyD88-mediated signaling.

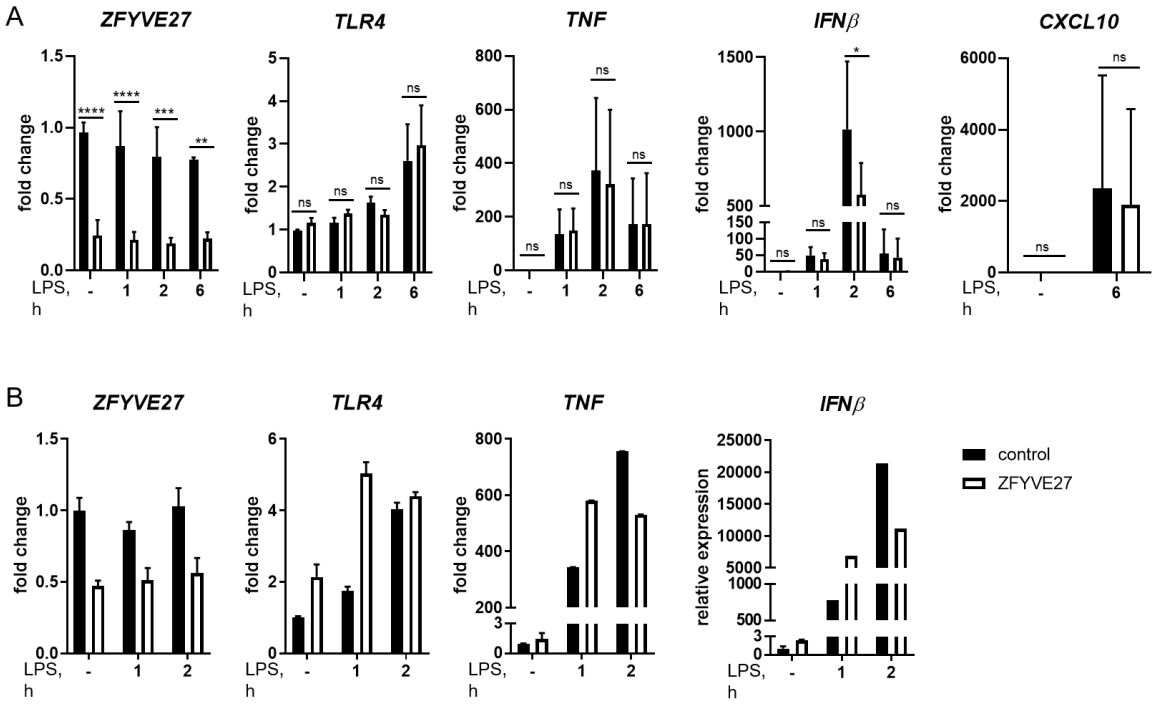

Figure 4.1. Knockdown of *ZFYVE27* impaired TLR4-TRAM-TRIF-mediated signaling in THP-1 cells and primary human macrophages. qPCR analysis of *ZFYVE27*, *TLR4*, *TNF, IFNβ*, *CXCL10* mRNA expression in differentiated THP-1 cells (A) and primary macrophages (B) stimulated with ultrapure K12 LPS (100 ng/ml), pre-treated by control siRNA oligo (black bars) or *ZFYVE27* specific siRNA oligo (white bars). Statistical analysis was performed as described: (A) means of three experiments with 2 to 4 biological replicates, error bars indicate the standard deviations (SDs), statistical significance evaluated using Sidak's multiple comparisons test to compare *ZFYVE27* silenced cells to control cells for each timepoint - 0.1234 (ns), 0.0332 (*), 0.0021 (**), 0.0002 (***), <0.0001 (****); (B) data for one donor, error bars indicate SDs between technical duplicates.

4.1.2 ZFYVE27 protein levels and LPS-induced STAT1 phosphorylation in ZFYVE27 silenced THP-1 cells

In our silencing experiments we observed quite high variation of cytokines expression levels (Figure 4.1, Figure S 1) and suggested that it could be mediated by inefficient decrease of ZFYVE27 protein levels in silenced cells. Then the explanation for such high variations could be in different protein levels of ZFYVE27 from experiment to experiment. Therefore, we performed Western blotting of protein extracts from cell lysates simultaneously purified with RNA samples analyzed by qPCR (Figure 4.1). We have chosen an experiment with two biological replicates as it demonstrated most variable results (Figure S 1C). ZFYVE27 protein levels were not depleted as effectively (Figure 4.2) as indicated by mRNA levels of *ZFYVE27* (Figure S 1C). This could explain why the qPCR results of this experiment did not show the decreased *IFNβ* mRNA expression as clearly as observed in the other experiments (Figure S 1). Most efficient depletion of ZFYVE27 was detected for 2 h of LPS stimulation time point (Figure 4.2). This is the timepoint at which we were able to see the significant effect of *ZFYVE27* silencing on *IFNβ* mRNA expression (Figure 4.1). Thus, this might be an indication that ZFYVE27 depletion on protein level should be controlled along with mRNA levels for obtaining reliable data.

To address if *ZFYVE27* silencing would affect IFNβ secretion on protein level, we decided to examine the phosphorylation of STAT1 transcriptional factor in silenced cells. STAT1 Tyr701 is phosphorylated upon IFNβ binding to interferon α/β receptor (IFNAR)[63], and which could be used as a readout for the relative levels of secreted IFNβ (control cells *vs. ZFYVE27* silenced cells).

Level of phospho-Tyr701 STAT1 (pSTAT1) was slightly decreased in *ZFYVE27* silenced cells after 6 h of stimulation (Figure 4.2). This result confirms that ZFYVE27 depletion could alter IFNβ protein secretion in response to TLR4 signaling, but pSTAT1 analysis should be repeated as it was addressed just once. Moreover, in this particular experiment ZFYVE27 depletion on protein level was not very efficient (Figure 4.2), suggesting it could result in stronger inhibition of pSTAT1 levels when silencing would be increased.

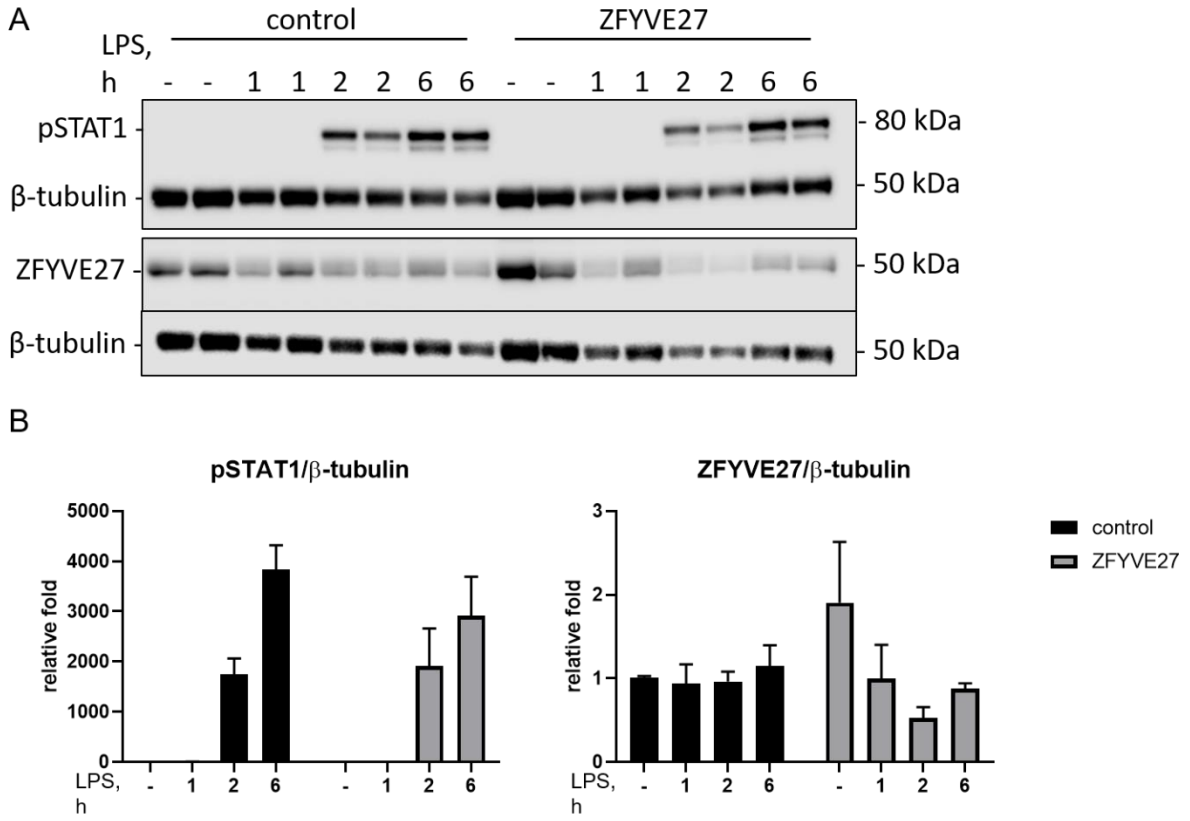

Figure 4.2. **Analysis of ZFYVE27 and pSTAT1 Tyr701 in THP-1 cells silenced for *ZFYVE27* and stimulated by LPS.** Western blots (A) of protein extracts from differentiated THP-1 cells treated with control and *ZFYVE27* siRNA oligos, showing ZFYVE27 and phospho-Tyr701 STAT1 levels. ZFYVE27 and pSTAT1 expression were normalized to endogenous control protein β-tubulin. Bars in (B) show the means of the biological duplicates quantified by LiCOR Odyssey software, SD indicated by error bars.

4.1.3 Uptake of pHrodo E. coli bioparticles by ZFYVE27 silenced cells investigated by confocal microscopy

We observed that *ZFYVE27* silencing affects TLR4-TRAM-TRIF-mediated signaling with *IFNβ* and *CXCL10* expression as readout. Therefore, we wanted to investigate, if this effect of ZFYVE27 could be linked to alterations of LPS or bacterial uptake as soon as only phagocytosed LPS or bacteria would induce TLR4-mediated IFNβ expression.

A pilot experiment, in which cells were treated with *E.coli* pHrodo bioparticles, fixed and analyzed by confocal microscopy (Master Thesis by Lindholm, 2017[45]), was repeated in the current study to evaluate if ZFYVE27 influences uptake of *E. coli*, phagosome maturation or TLR4 or actin recruitment to the phagosomes.

Primary macrophages and macrophage-like THP-1 cells were incubated with fluorescent *E. coli* bioparticles. After pulse-chase incubation for 15+30 min, cells were washed and fixed. Subsequently, samples were stained with TLR4 antibodies and phalloidin. Confocal xyz images of *ZFYVE27* silenced and control treated cells (Figure S 2) were analyzed by detecting *E. coli* bioparticles by an imaging software (Figure 4.3A). The detected *E. coli* were shown as spheres. These spheres indicate a voxel of 1 µm in size and represent a phagosome.

Phagosomes per cell were counted and plotted on a scatter plot. A significant decrease in *E. coli* bioparticles per cell was observed in *ZFYVE27* silenced primary macrophages (Figure 4.3B) as well as macrophage-like THP-1 cells (Figure 4.3C). These results were in line with the preliminary results by Lindholm, 2017 (Master Thesis)[45].

To get an insight into recruitment of TLR4 and actin to phagosomes, and maturation of phagosomes, the median voxel intensities for TLR4, actin and *E. coli* bioparticles were extracted and plotted to compare the *ZFYVE27* silenced cells to control cells (Figure 4.3B, C).

A decrease in TLR4 recruitment would be a possible explanation for the observed impairment in IFNβ expression. In fact, preliminary results had shown a significant decrease in TLR4 recruitment upon *ZFYVE27* silencing. Our results showed a significant decrease of TLR4 recruitment to the phagosomes in the primary macrophages, but there was no significant difference detectable in the THP-1 cells (Figure 4.3B, C). However, results shown by Lindholm, 2017[45] and in the current study are not directly comparable, because of different time points for stimulation – 15+15 vs. 15+30.

Moreover, we also observed different results to the preliminary data regarding actin recruitment which was shown to be significantly decreased in *ZFYVE27* silenced cells by Lindholm, 2017[45]. We have not detected any changes in actin recruitment to phagosomes neither in primary cells nor in THP-1 cells (Figure 4.3B, C).

The increased intensities of the phagosomes indicate a more acidic environment of the *E. coli* bioparticle as the fluorescent dye linked to the *E. coli* bioparticle is pH-sensitive and increases in intensity with decreasing pH[64]. Our data here indicates decreased maturation of phagosomes by *ZFYVE27* silencing (Figure 4.3B), while Lindholm, 2017 had observed the opposite. This might be caused by the different timepoints and cells addressed. Phagosome maturation is shown here just for primary macrophages (Figure 4.3B), because intensities from THP-1 cells were oversaturated and therefore could not be quantified.

To draw a conclusion this experiment should be repeated several times in THP-1 cells as wells as primary macrophages. Addressing several timepoint would give the possibility to compare dynamics of receptor and actin recruitment as well as phagosome maturation. Analyzing just one timepoint might not be representative as it is just a snapshot, which cannot represent such dynamic processes.

Furthermore, the efficiency in *ZFYVE27* silencing might vary between biological replicates and from cell to cell. Therefore, it would be necessary to quantify *ZFYVE27* expression by simultaneous staining for ZFYVE27. Altogether this experimental set-up requires optimization regarding the assessment of ZFYVE27 depletion and addressing several timepoints.

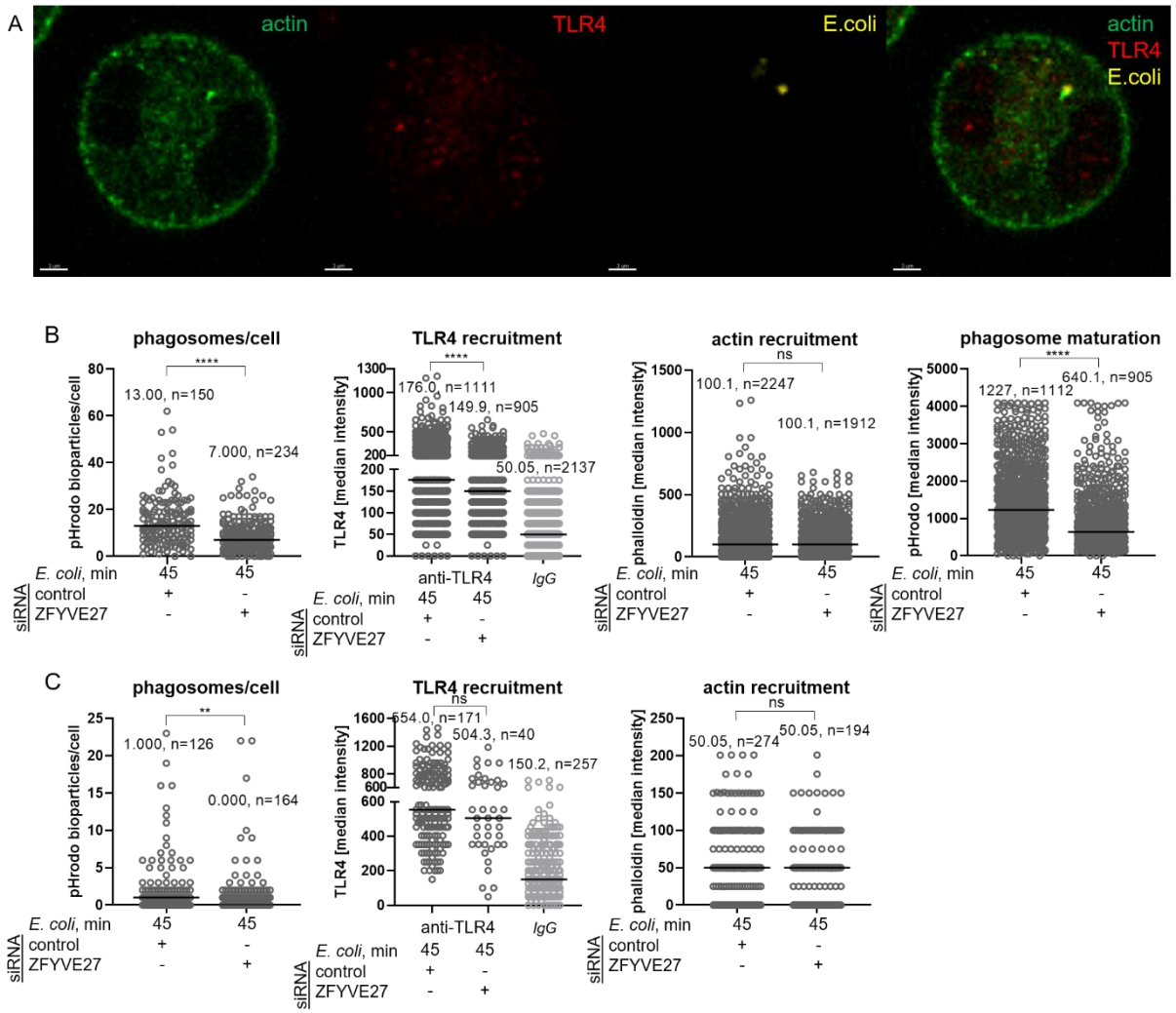

Figure 4.3. Uptake of *E. coli* bioparticles, TLR4 recruitment to phagosomes and phagosome maturation are decreased in *ZFYVE27* silenced cells, while actin recruitment is unaffected. Uptake of *E. coli* bioparticles, TLR4 and actin recruitment to phagosomes and phagosome maturation after 15+30 min pulse-chase with *E. coli* bioparticles in differentiated THP-1 cells (B) and primary macrophages (C) pretreated with control or *ZFYVE27* targeting siRNA oligo is shown. Each dot in graphs showing phagosomes/cell represent one cell, while each dot in graphs representing TLR4 or actin recruitment or phagosome maturation represents a phagosome. Horizontal lines indicate the medians of one experiment and is stated as number above together with number of dots (n). Statistical significance was calculated by the Mann-Whitney test comparing the *ZFYVE27* silenced cells to control - 0.1234 (ns), 0.0332 (*), 0.0021 (**), 0.0002 (***), <0.0001 (****). A confocal image (A) of a primary macrophage treated with *ZFYVE27* targeting siRNA oligo, stimulated with *E. coli* bioparticles and stained for TLR4 and actin is presented.

4.1.4 Uptake of live E. coli DH5α by ZFYVE27, Rab11a/b, TLR4 and Rab11FIP2 silenced cells

Confocal microscopy indicated that *ZFYVE27* silencing might have an impact on uptake of *E. coli*. Next, we wanted to confirm this observation, by determining the effect on uptake of live *E. coli*.

Uptake of live *E. coli* DH5α by macrophage-like THP-1 cells was assessed by a synchronized pulse-chase incubation. During chase incubation extracellular bacteria were killed by antibiotics. Subsequently, cells were washed and lysed. Cell lysate dilutions were plated on agar and colony forming units were counted to calculate *E. coli* phagocytosed per cell. For normalization of bacteria counts to THP-1 cell number in wells treated by different siRNA oligos, we quantified protein concentration in cell lysates from simultaneously treated wells (Figure S 3F).

In this assay we addressed the effect of *ZFYVE27, Rab11a/b, TLR4* and *Rab11FIP2 (FIP2)* silencing on uptake of the live laboratory strain *E. coli* DH5α. Silencing levels were controlled by RNA isolation and respective qPCR for simultaneously treated cells (Figure S 3A-E). *TLR4* silencing was investigated to observe a direct connection between *E. coli* recognition and uptake. Rab11a/b is a GTPase known to be involved in TLR4 and TRAM trafficking[27] and an interaction partner for ZFYVE27[41]. A second trafficking protein involved in TLR4 and TRAM trafficking is FIP2, which links TRAM to Rab11a/b[28]. Furthermore, silencing of *FIP2* was shown to significantly decrease *E. coli* uptake in human primary macrophages and THP-1 cells[28]. Thus, *FIP2* silencing was a positive control for this assay.

ZFYVE27, *Rab11a/b* and *TLR4* silencing did not show a significant effect on uptake of *E. coli*, but *FIP2* silenced THP-1 cells showed a decrease in uptake as expected (Figure 4.4). In general, a big variation in uptake between biological replicates was observed. A possible explanation for the high variability within one treatment condition could be in the protocol for pre-incubation of the *E. coli* DH5α with THP-1 cells. It was observed previously by our group that opsonization of the bacteria by co-incubating with 10% FCS medium increases variability within conditions. Therefore, these experiments should be repeated with optimized serum-free conditions.

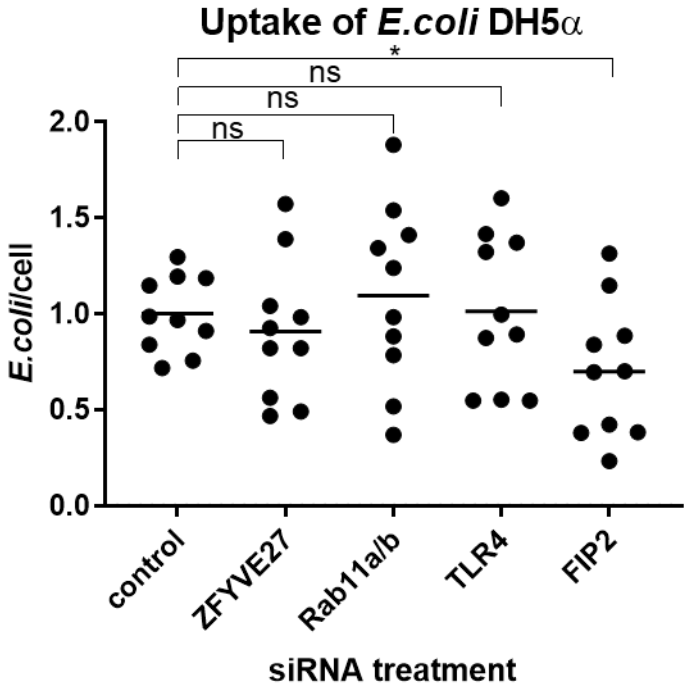

Figure 4.4. Uptake of *E. coli* DH5α by THP-1 cells is not affected by silencing of *ZFYVE27, Rab11a/b* and *TLR4,* with some decrease for *Rab11FIP2* silenced cells. PMA differentiated THP-1 cells were treated with control or *ZFYVE27, Rab11a* and *Rab11b, TLR4* or *Rab11FIP2* specific siRNA oligo. Uptake was synchronized by adding *E. coli* DH5α on ice and centrifugation at +4°C before 15 min incubation at +37°C in a water bath. Graph represents data collected for three independent experiments, two with three and one with four biological replicates per condition. Each dot in the graph represents bacteria count for one biological replicate, horizontal line indicates mean of *E. coli*/cell taken up per condition. Values for each biological replicate were calculated from three technical replicates and normalized to protein concentrations assessed by BCA assay. Mann Whitney test was used to compare each treatment to the control - 0.1234 (ns), 0.0332 (*), 0.0021 (**), 0.0002 (***), <0.0001 (****).

4.2 Generation of THP-1 *ZFYVE27* knockout cell lines and screening for TLR4-mediated response

4.2.1 Generation and verification of knockouts

In previously described experiments ZFYVE27 was depleted by siRNA. But protein levels could not correlate with the mRNA levels, which was shown by evaluation of ZFYVE27 protein expression by Western blotting in one of the experiments (Figure 4.2). Therefore, a stable knockout cell line would be beneficial to investigate the role of ZFYVE27 in TLR4 signaling and possibly other pathways. Moreover, a stable *ZFYVE27* knockout cell line would be a step towards the development of different mutants to get a better insight into the function of single protein domains. A *ZFYVE27* knockout cell line would be also a useful tool to optimize the uptake experiments, as ZFYVE27 depletion upon silencing can vary in between cells and replicate samples.

In this study, the CRISPR/Cas9 technology was used to generate a *ZFYVE27* knockout in THP-1 cells. We designed 6 different sgRNAs, targeting exon 3 and exon 4 by using the exon sequence of the transcript variant 1 (detailed information in Table S 1).

To integrate the sgRNA encoding sequence into the vector backbone cloning was required. The vector backbone was restricted and dephosphorylated. Efficiently restricted plasmids were separated on a DNA gel (Figure 4.5). Afterwards, gel purified restricted vectors were ligated with the annealed DNA pairs encoding an sgRNA.

After transformation of competent *E. coli*, two clones per sgRNA were chosen and isolated plasmids were sequenced. Sequencing results showed successful ligation of the sgRNA encoding sequence into 11 out of 12 sequenced plasmids. One virus per sgRNA was produced resulting in six different viruses encoding sgRNAs, three targeting exon 3 and three for exon 4. After puromycin selection of THP-1 cells transduced with these six viruses or a control virus, successful knockout was verified. For the verification the six sublines, the control transduced subline and THP-1 WT cells were lysed in RIPA buffer with or without PMA differentiation. Cell lysates were analyzed by Western blot to assess ZFYVE27 protein expression (Figure 4.6). Three out of the six sublines showed effective depletion of ZFYVE27 before and after differentiation. One of these three sublines was generated by targeting exon 3 (#3) and two others were generated by applying an exon 4 targeting sgRNA (#5 and #6).

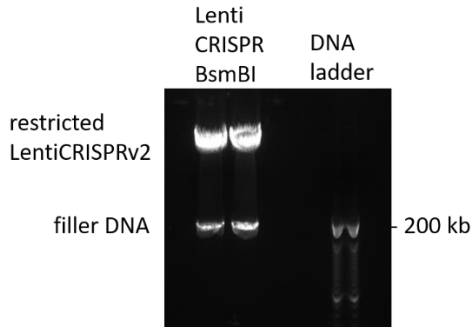

Figure 4.5. 0.8% agarose gel containing GelRed® to separate restricted lentiCRISPR v2. Reactions (25-30 µl) of lentiCRISPR v2 restricted with the restriction enzyme BsmBI were loaded into 2 wells to separate the restricted linearized vector backbone (upper bands) from the unrestricted vector and filler DNA (lower band), with DNA ladder in the right lane for fragment size reference. The gel was run for 1 h at 100 V.

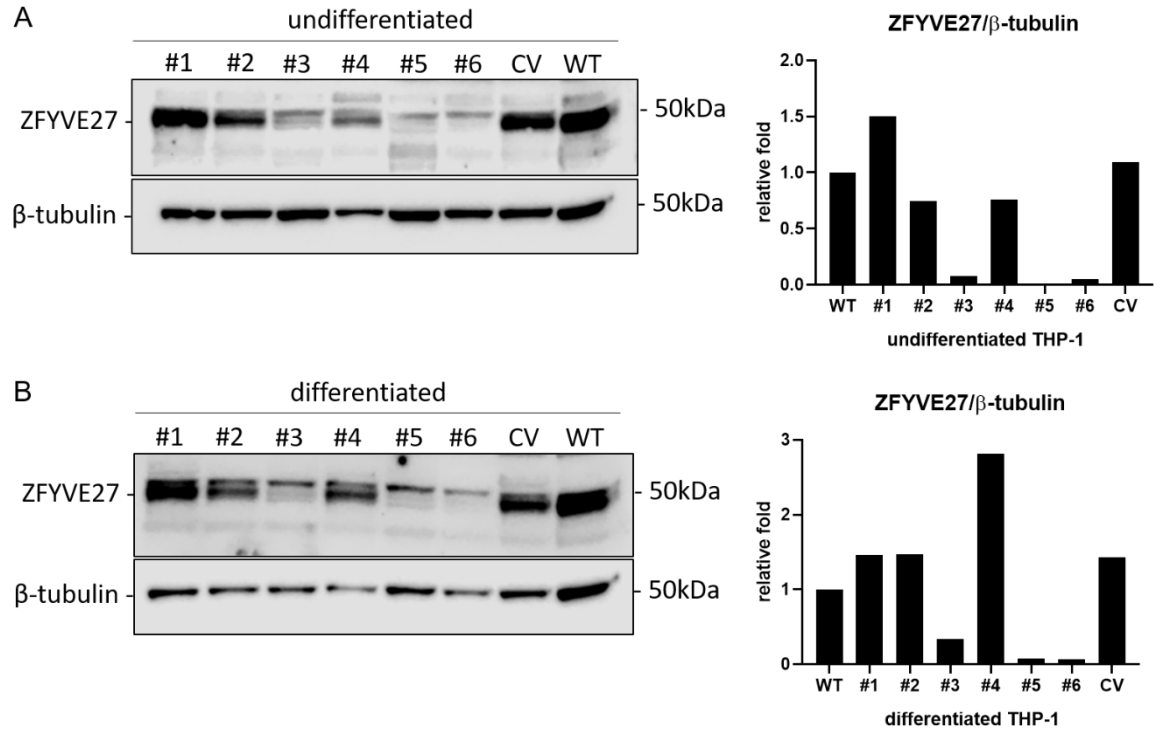

Figure 4.6. Efficient depletion of ZFYVE27 in three CRISPR/Cas9 generated THP-1 sublines. Western blots of cell lysates from undifferentiated (A) and differentiated (B) THP-1 CRISPR/Cas9 *ZFYVE27* KOs, control treated THP-1 and THP-1 WT cells show ZFYVE27 protein levels. ZFYVE27 expression was normalized to the endogenous control protein β-tubulin. Bars (on the right) show normalized protein levels quantified by LiCOR Odyssey software.

4.2.2 TLR4-mediated signaling in stable ZFYVE27 knockout cells

After, verification of the *ZFYVE27* knockout in three sublines, these three sublines (#3, #5, #6) and control cells were PMA differentiated and stimulated by LPS. ZFYVE27 protein levels were assessed by Western blot and were detectable only in small amounts in all the verified sublines (Figure 4.8).

mRNA expression of TLR4-induced cytokines was analyzed by RT-qPCR (Figure 4.7, Figure S 5). Expression of *TNF* and *IFNβ* mRNA was slightly altered in two out of three KO sublines in comparison to the control cells. A significant change could only be detected for *IFNβ* mRNA expression at 2 h of LPS stimulation for the sublines #5 and #6. Phosphorylation of STAT1 was unexpectedly high in the subline #6 (Figure 4.7). Thus, the Western blots should be performed for all the experiments analyzed by RT-qPCR to get a better insight on pSTAT1 levels. In general, a similar trend can be observed for the sublines #5 and #6, while results from #3 showed a different pattern.

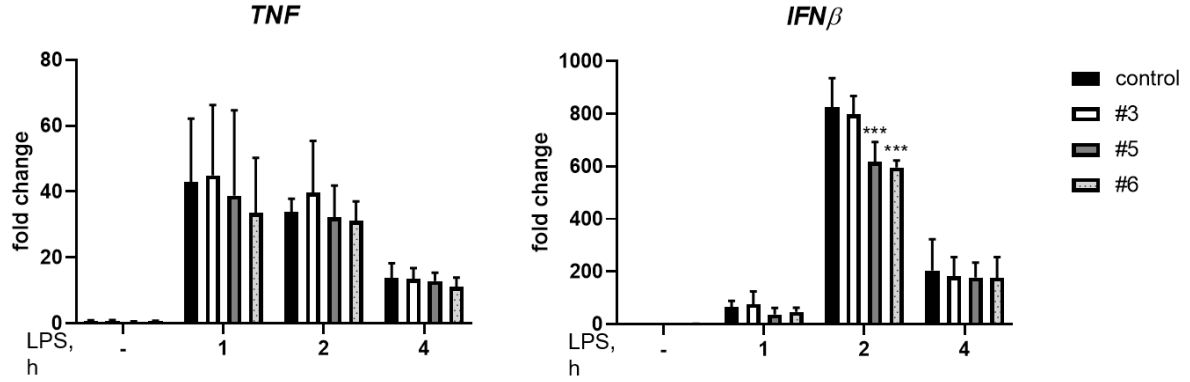

Figure 4.7. Effect of *ZFYVE27* knockout on TLR4-mediated signaling. *TNF* and *IFNβ* mRNA expression in differentiated THP-1 CRISPR/Cas9 *ZFYVE27* KO sublines (#3, #5, #6) and THP-1 CRISPR/Cas9 control cells stimulated with ultrapure K12 LPS (100 ng/ml) was analyzed by qPCR. Bars show means of three experiments with standard deviations as error bars. Significance calculated by Dunnett's multiple comparisons test to compare each subline (#3, #5, #6) to the control for each timepoint - 0.1234 (ns), 0.0332 (*), 0.0021 (**), 0.0002 (***), <0.0001 (****).

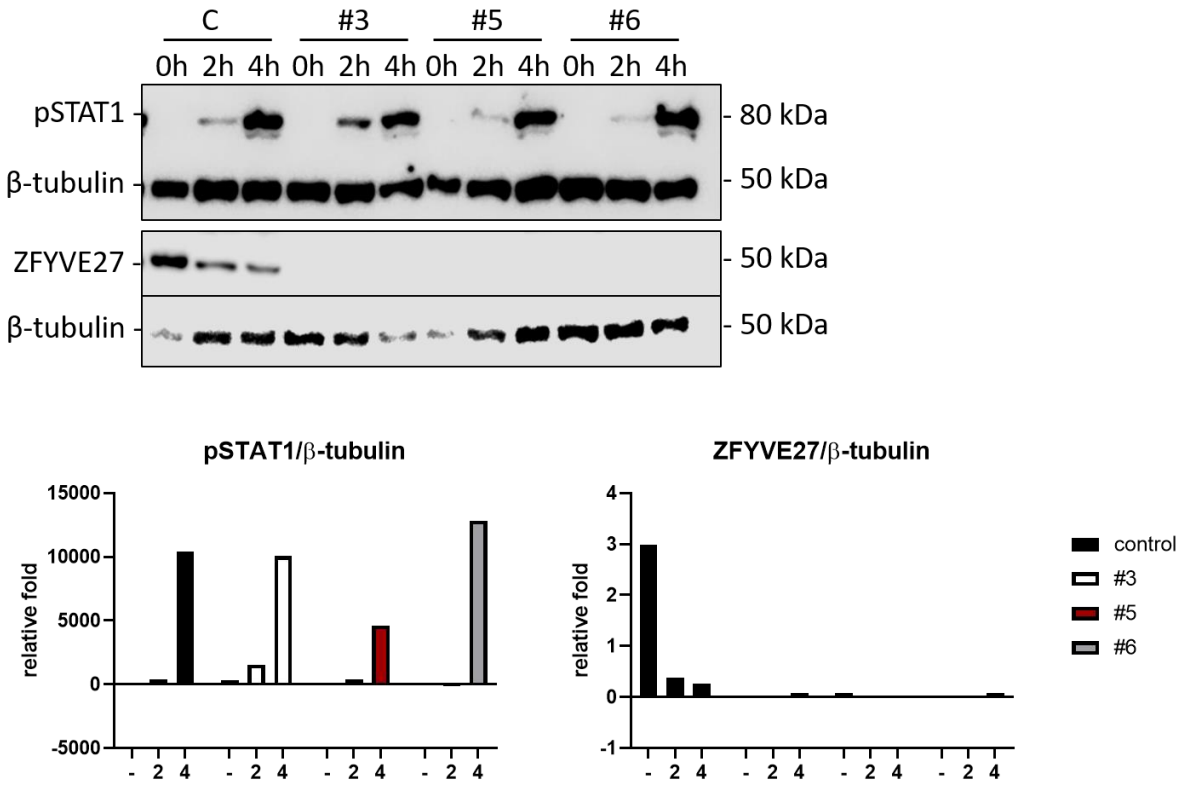

Figure 4.8. Phosphorylation of STAT1 Tyr701 varies after LPS stimulation in ZFYVE27 depleted THP-1 CRISPR/Cas9 *ZFYVE27* KO between sublines in comparison to control cells. Western blots (A) for ZFYVE27 and pSTAT1 in protein extracts from THP-1 CRISPR/Cas9 *ZFYVE27* sublines. (B) Normalized levels of ZFYVE27 and pSTAT1 to the endogenous protein β-tubulin quantified by LiCOR Odyssey software.

4.2.3 Bioinformatic analysis of ZFYVE27 transcript variants targeted by different sgRNAs in exons 3 and 4

The observation of similar responses to LPS stimulation for two of the three verified KO sublines suggested that the different effect could be mediated by specific features of applied sgRNAs. The sublines #5 and #6 were generated by targeting exon 4, while #3 by targeting exon 3. This led us to have a closer look for the presence of targeted sequences in the transcript variants coding for different splice isoforms of *ZFYVE27*. Alternative splicing could be an explanation for the varying response between sublines.

Targeted transcript variants were determined by running a megablast using nucleotide Blast (https://blast.ncbi.nlm.nih.gov/Blast.cgi) to align the sgRNA sequences to "highly similar sequences (megablast)" in "Human genomic plus transcript (Human G+T)". The comparison of the targeted transcript variants by #3, #5 and #6 showed that the two exon 4-targeting sgRNAs #5 and #6 were targeting six additional transcript variants, which were not covered by sgRNA used to generate subline #3 (Table S 2).

Next, we addressed the protein domains present in proteins encoded by these six transcript variants in comparison to full size transcript variant 1. The online software Clustal Omega (https://www.ebi.ac.uk/Tools/msa/clustalo/)[62] was used to align the protein sequences of the six transcript variants to the reference transcript variant 1. Information from ZFYVE27 protein topology from the online software UniProt (https://www.uniprot.org/)[61] was used to determine which parts of the transcript variants were lacking in comparison to the reference sequence (Table S 3).

In all these transcript variants an 86 amino acid long part close to the N-terminus was detected to be missing and one amino acid upstream of the missing part is exchanged from arginine to serine. This part of the protein sequence represents two transmembrane helices connected by a luminal loop and a part of the cytoplasmic loop connecting the transmembrane to the intramembrane domain. Further, the transcript variant 5 was lacking two sequence parts (consisting in 5 or 7 amino acids) in the C-terminal cytoplasmic tail. The predicted transcript variants X13, X14, X15, X23 and X26 were lacking either no or one of the two small pieces in the cytosolic C-terminal tail (Figure 4.9).

We hypothesize that the difference in LPS induced TLR4-mediated response between sublines could be explained by a different set of intact/not targeted by CRISPR/Cas9 splice isoforms. In total, there are at least 32 *ZFYVE27* splice isoforms with possibly redundant

function for TLR4-mediated signaling, and better coverage by the knockout could results in a more dramatic effect on TLR-mediated signaling.

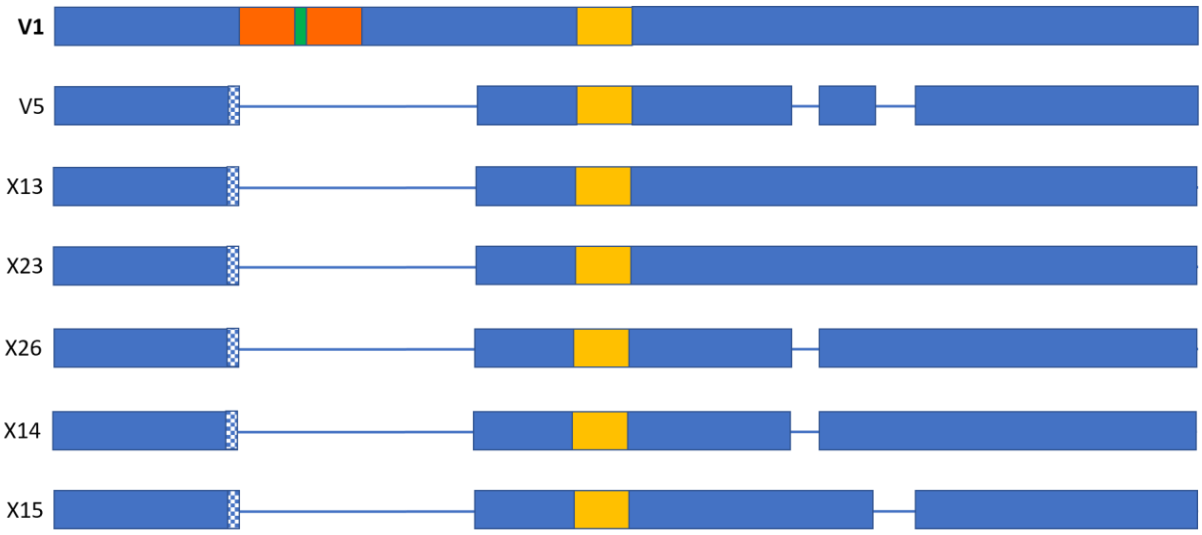

Figure 4.9. Schematic overview of proteins encoded by transcript variants that were not altered by the sgRNA (#3) used to generate CRISPR/Cas9 knockouts. Blue boxes indicate cytosolic domains, orange boxes transmembrane domains, yellow box intramembrane domain, green box is a luminal amino acid and the white-blue squared box indicates an amino acid exchange from arginine to serine. Lines between the boxes indicate missing parts of the protein in comparison to the reference, consisting in 86, 5 or 7 amino acids.

4.3 Effect of *ZFYVE27* silencing on signaling of endosomal TLRs

The focus of all previously described experiments was on TLR4, but Lindholm, 2017[45] indicated already in his Master Thesis that cytokine secretion was also impaired in *ZFYVE27* silenced cells stimulated with TLR2 ligand FSL-1. To investigate if ZFYVE27 could play a role in regulation of signaling by other TLRs, we addressed signaling via two other members of the TLR family. Since cytokine expression in our hands was impaired from the intracellular TLR4 signaling complex, the focus was set onto intracellular/endosomal TLRs like TLR8 and TLR9.

4.3.1 TLR8-mediated response in ZFYVE27 silenced cells

An impact of *ZFYVE27* silencing on the TLR8-mediated response was addressed in THP-1 TLR8 pDest cells (overexpression of TLR8) by stimulating cells with the synthetic ligand thiazoloquinoline compound CL075.

RT-qPCR was performed to quantify *TNF* and *IFNβ* mRNA expression in control and *ZFYVE27* silenced cells (Figure 4.10). Further, Western blotting was performed to assess the efficiency of depleting ZFYVE27 on protein level and to evaluate the effect of secreted IFNβ on the phosphorylation state of STAT1 (Figure 4.11).

The mRNA expression levels of the cytokines, *TNF* and *IFNβ,* were both affected by *ZFYVE27* silencing (Figure 4.10) in TLR8 overexpressing cells. Additionally, the increase of STAT1 phosphorylation assessed by Western blot indicated the positive effect of *ZFYVE27* silencing on TLR8-mediated signaling on protein level (Figure 4.11), and supported the observations made on mRNA level. To investigate the effect of ZFYVE27 on TLR8 signaling further, this experiment should be repeated several times by addressing later time points.

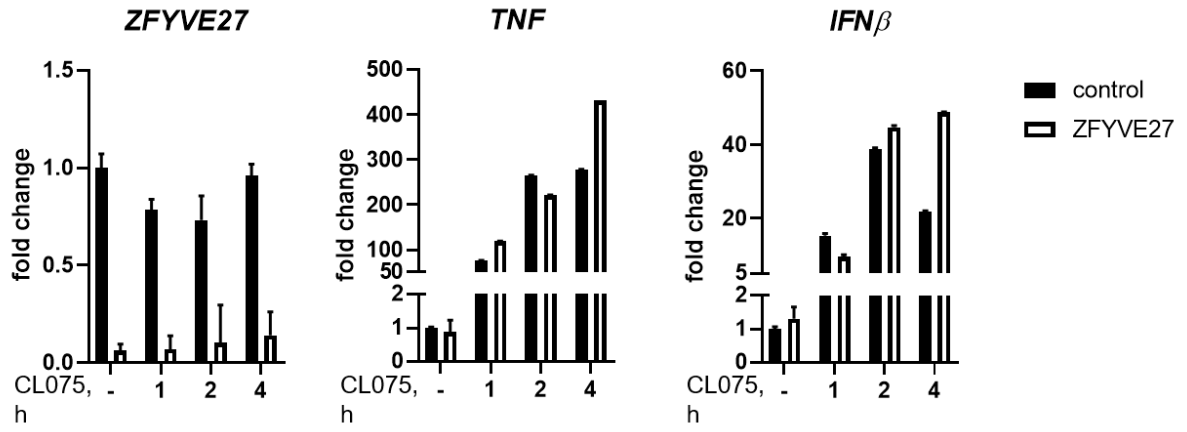

Figure 4.10. TLR8-mediated *TNF* and *IFNβ* mRNA expression is increased upon *ZFYVE27* silencing in THP-1 TLR8 pDest cells. qPCR analysis of *ZFYVE27*, *IFNβ* and *TNF* in PMA differentiated THP-1 TLR8 pDest cells treated with control siRNA and *ZFYVE27* targeting siRNA and stimulated by CL075 (1 µg/ml). Bars represent means between technical duplicates; error bars indicate standard deviations.

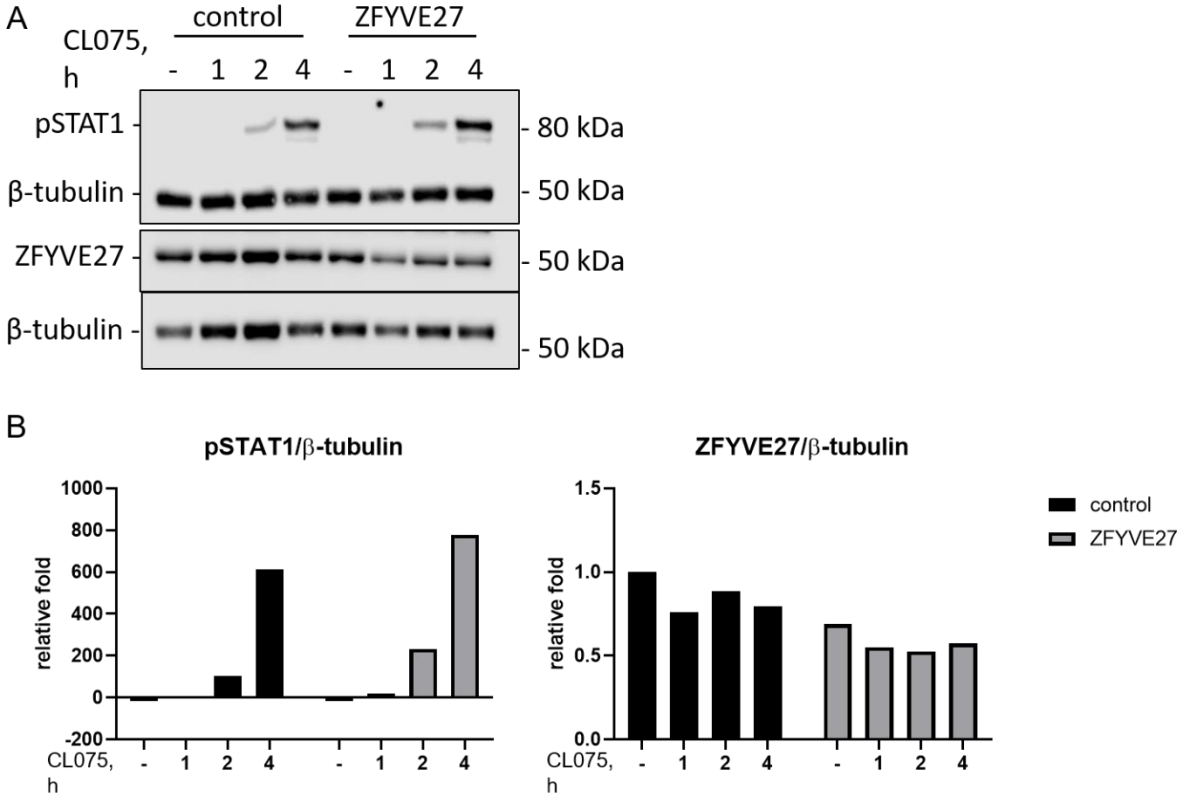

Figure 4.11. **Slightly decreased ZFYVE27 in THP-1 TLR8 pDest cells resulted in some increase of phospho-Tyr701 STAT1 upon CL075 stimulation.** (A) Western blots of protein extracts from differentiated *ZFYVE27* silenced and control treated THP-1 TLR8 pDest cells after CL075 stimulation. (B) Graphs show protein levels of ZFYVE27 and pSTAT1 normalized to the endogenous control, β-tubulin.

4.3.2 TLR9-mediated response in ZFYVE27 or Rab11a/b silenced cells on mRNA level

To investigate, if *ZFYVE27* silencing has an effect of on TLR9-mediated signaling, we used THP-1 TLR9 mCherry cells (inducible overexpression of TLR9), which were stimulated by the synthetic TLR9 ligand CpG 2006 (10 µg/ml). IFNβ expression in response to CpG was induced only in cells that were not treated by PMA (cells in suspension) as shown by Cemalovic, 2019[65] (Master Thesis). Thus, transient transfection of siRNA into these cells was not much efficient due to the necessity to perform silencing in suspension cells. Therefore, we performed in parallel *Rab11a/b* silencing as a control, because it was previously observed to be a highly efficient siRNA oligo. Furthermore, Rab11a/b is a ZFYVE27 interacting protein, and was of interest to investigate in parallel with ZFYVE27.

mRNA expression levels of *ZFYVE27*, *Rab11a/b*, *TNF* and *IFNβ* after CpG stimulation were quantified by RT-qPCR (Figure 4.12). Silencing of *Rab11a/b* caused a consistent decrease of *Rab11a/b* mRNA expression below 40%, while *ZFYVE27* silencing efficiency was below 50% in unstimulated cells and mRNA levels increased proportionally to the stimulation time. The mRNA expression levels of the addressed cytokines were slightly increased both by *Rab11a/b* and *ZFYVE27* silencing. These results here, generated in a pilot experiment, might indicate a role of ZFYVE27 and/or Rab11a/b in a TLR9-mediated response (Figure 4.12). Nonetheless, this experiment should be repeated several times and requires optimization regarding stimulation and silencing to draw a conclusion.

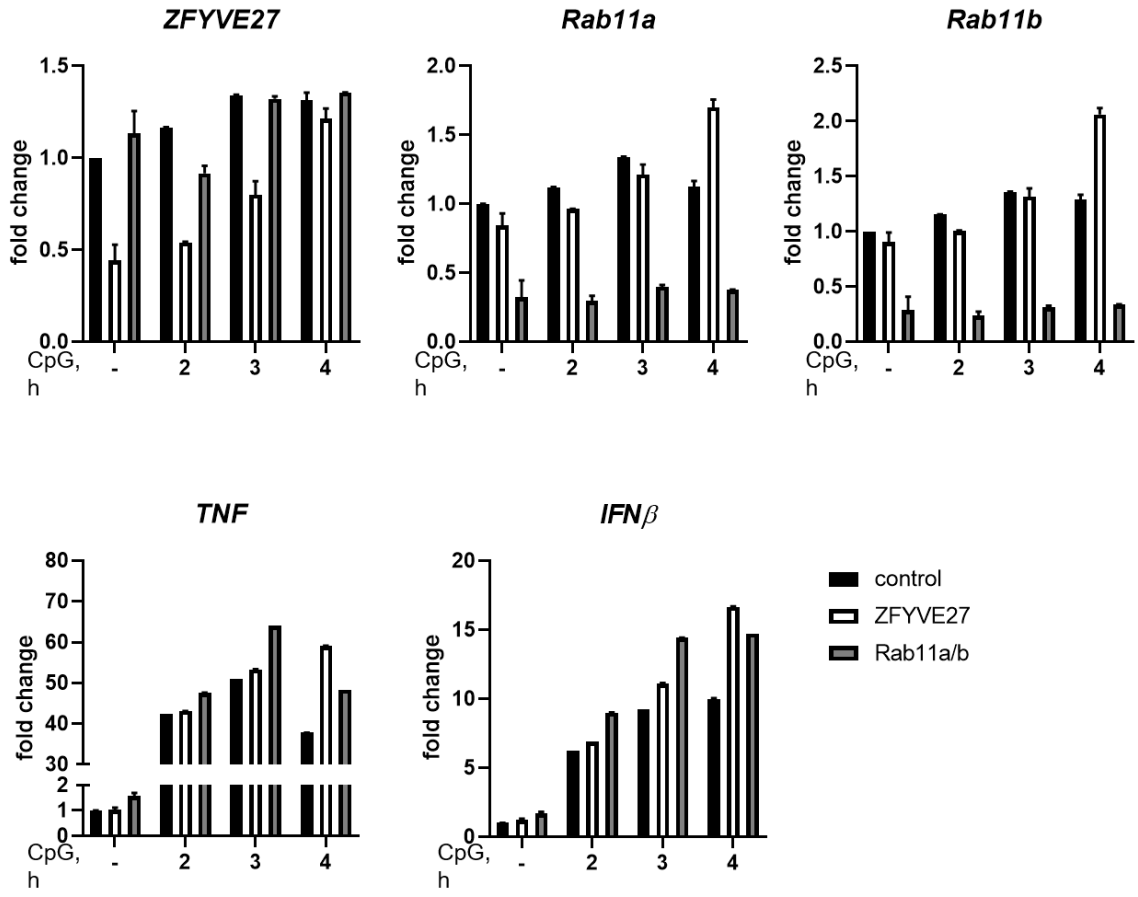

Figure 4.12. TLR9-mediated *TNF* and *IFNβ* mRNA expression is increased in *ZFYVE27* or *Rab11a/b* silenced THP-1 TLR9 mCherry cells stimulated by CpG. *ZFYVE27*, *Rab11a*, *Rab11b*, *TNF* and *IFNβ* mRNA expression was analyzed by qPCR in THP-1 TLR9 mCherry cells treated with control siRNA, *ZFYVE27* or *Rab11a+Rab11b* targeting oligos and stimulated with CpG 2006 (10 µg/ml). Bars represent means of technical replicates; error bars indicate standard deviations.

5. Discussion

ZFYVE27 was identified as a protein involved in protrusion outgrowth in cells by inducing directional vesicle transport. In general, directed trafficking of proteins in cells is crucial for cellular homeostasis and survival in different conditions, including encountering pathogens. TLRs are responsible for recognition and elimination of pathogens. Thus, their trafficking was shown to be very important for the effective immune response to infections[66]. In our group a novel link between ZFYVE27 and TLR4-mediated signaling was observed.

Previously, it was shown that ZFYVE27 regulates cytokines mRNA expression and secretion in macrophages-like THP-1 cells upon LPS or *E. coli* stimulation (Master thesis by Lindholm 2017[45]). In the present study we observed a significant negative impact of *ZFYVE27* silencing on *IFNβ* expression on mRNA and protein level in a TLR4-mediated response by THP-1 cells, supported by the data from primary macrophages. The fact that we did not observe changes in *TNF* mRNA expression leads to the assumption that ZFYVE27 functions in the regulation of TLR4-TRAM-TRIF signaling from the intracellular endosomal compartment. Type 1 interferon expression induced though TLR4-TRAM-TRIF signaling was shown to be dependent on TLR4 internalization[67] and on TLR4 recruitment from the ERC to the LPS or *E. coli* containing phagosomes[27]. This made it possible to narrow the effect of ZFYVE27 down to either involvement in regulation of LPS/bacterial uptake or in other intracellular events like recruitment of TLR4 to bacterial phagosomes.

Impaired TLR4-TRAM-TRIF-mediated signaling in *ZFYVE27* silenced cells could possibly be explained by a decreased uptake of TLR4-ligand complexes. Inhibition experiments by Husebye and colleagues showed that the dynamin inhibitor dynasore decreased IFNβ expression by blocking endocytosis[27].

Addressing the question if ZFYVE27 affects TLR4 signaling due to regulation of phagocytosis was investigated by confocal microscopy. Uptake of *E. coli* bioparticles seemed to be significantly decreased in *ZFYVE27* silenced cells. The attempt to confirm this finding by another phagocytotic assay with live *E. coli* did not show a significant difference. However, the data generated for the uptake of live bacteria showed a high spread between biological replicates. This high variation could although be explained by methodological issues. The fact that cells were co-cultured with the laboratory strain of bacteria *E. coli* DH5α in the presence of FCS in the uptake experiments could be a possible explanation. We used heat inactivated serum with inactivated complement factors, but serum proteins might still

opsonize and contribute to phagocytic mechanisms which might not be regulated by ZFYVE27 and cause thereby high variation that covers the effect of *ZFYVE27* silencing.

The uptake study with bacterial pHrodo bioparticles which showed us a decrease in uptake was further used to assess TLR4 recruitment to the phagosomes. TLR4 was shown to be localized on the plasma membrane and to a higher extent present in the ERC[27]. Further, downregulated expression of IFNβ and IFNβ-dependent genes was observed upon impaired recruitment of TLR4 and TRAM from the ERC to phagosomes[28]. This raises a further possible scene for ZFYVE27 to act in TLR4 signaling. Indeed, TLR4 recruitment to *E. coli* phagosomes was decreased significantly in primary macrophages but showed just the same tendency without significance in THP-1 cells upon 45 min of *E. coli* bioparticle stimulation. The pilot experiment presented in the Master Thesis by Lindholm, 2017[45] showed a significant decrease in TLR4 recruitment in THP-1 cells after 30 min stimulation with *E. coli* bioparticles.

It is theoretically reasonable that ZFYVE27 would be involved in regulation of TLR4 recruitment to phagosomes, because the ZFYVE27 interacting partner Rab11 GTPase was determined as a key player in this context[27]. Rab11-GTP promotes FIP2 in the recruitment of TLR4 and TRAM to the phagosomes[28]. Interesting here is that Rab11 as interaction partner for ZFYVE27 was observed to be GDP bound. Based on this observation, it was suspected that the traditional view on active and inactive GTPases might possibly not be an apt description for Rab11. Rab11 might instead be a molecular switch between the directionality of microtubular transport or the transport types such as microtubules or actin/myosin dependent transport[42,68]. ZFYVE27 interacting with Rab11-GDP could possibly support FIP2 in the function inducing TLR4 and TRAM recruitment to the phagosomes. ZFYVE27 could transport thereby vesicles by a microtubular-based plus-end directed transport. FIP2 is an adaptor for the motor protein myosin Vb and mediates plus-end directed transport on actin filaments[68].

Actin is a cytoskeletal filament and its polymerization was determined to be another important event in internalizing bacteria and in TLR4 recruitment to phagosomes[27]. We did not observe an impact of ZFYVE27 on actin recruitment to phagosomes in our experiments, while Lindholm 2017[45] showed a decreased actin recruitment to the phagosomes. However, these experiments performed by us and by Lindholm, 2017[45], addressed each only one timepoint, which is with 45 or 30 min bioparticle stimulation late for detecting actin

polymerization. Actin polymerization building foci surrounding *E. coli* during phagocytosis were observed at early timepoints[28]. Nonetheless, actin does not disassemble immediately after internalization of particles into the cells during phagocytosis. It was assumed that disassembly of actin from phagosomes allows fusion with early endosomes leading to vesicle maturation. This view was although challenged and actin recruitment to phagosomes was shown[69].

Maturation of the phagosomes would be interesting as it destines TLR4 to lysosomes and is together with endosomal sorting required for TLR4 degradation[25]. We observed decreased phagosome maturation in *ZFYVE27* silenced primary macrophages, while Lindholm, 2017[45] showed an increased maturation state in *ZFYVE27* silenced THP-1 cells. It would be interesting to determine the state of phagosome maturation at several timepoints to investigate the dynamics. An accelerating effect of *ZFYVE27* silencing on phagosome maturation could explain a decreased TLR4-TRAM-TRIF signaling as phagosome maturation determines TLR4 to lysosomal degradation and limits TLR4 signaling[30].

Taking together these results from the bioparticles uptake experiments, we should admit that these findings should be treated with caution. These results might explain to a certain extent the impairment in TLR4-TRAM-TRIF signaling in *ZFYVE27* silenced cells, but there are some methodological limitations, which should be solved. First, we addressed here just one timepoint, which does not give an insight into dynamics as recruitment processes or pH gradients. This might also be a possible explanation for different results shown here compared to preliminary data of our group where an earlier timepoint was addressed (Master Thesis by Lindholm, 2017[45]). Therefore, it would be necessary to address more timepoints to draw final conclusions. Second, ZFYVE27 was depleted by siRNA and its expression was verified for all experiments by RT-qPCR. Variability between mRNA abundance and protein levels are although common, as post-transcriptional processes and protein stability play roles in this context[70]. Our data showed that *ZFYVE27* mRNA levels did not correlate with protein levels detected by Western blot. Based on this observation we assume that although knockdown was verified on mRNA levels variable findings could be explained by different ZFYVE27 protein abundance in the cells. As protein levels might vary between biological replicates or also between cells, it makes it very important to determine protein levels of ZFYVE27 in all experiments rather than rely solely on qPCR data. Regarding the bioparticles uptake experiment, this could be addressed by simultaneous co-staining of the cells with a ZFYVE27 antibody to be able to correlate ZFYVE27 protein expression levels with bacterial uptake,

recruitment of TLR4 or actin, phagosome maturation, etc. However, so far, we have not had access to ZFYVE27 specific antibodies suitable for fluorescent microscopy. Additionally, thinking of the live bacteria uptake assay, it would be impossible to find a solution to check protein levels for each biological replicate, but it would be possible to use KO cells without any remaining ZFYVE27 protein, which we have generated and verified in this study.

Thus, we decided to tackle this particular limitation by the generation of stable *ZFYVE27* knockout cell lines by lentiviral transduction of CRISPR/Cas9 and guiding RNA. We have not performed subsequent isolation of single cell clones, but rather used pooled cell cultures. The reason for this is that THP-1 cells are easily modified by long-term incubation in culture (ATCC recommendations). Thus, their features after long-term single cell cloning could attribute to their modification in culture, but not to the effect of the particular gene knockout. Moreover, this cell line is highly sensitive to culture conditions regarding cell density. Immortalized cell lines such as THP-1 cells are altered in different cell checkpoint genes, like tumor suppressor genes or genes involved in telomere maintenance. These alterations are often related to mutations and increasing genomic instability during subculturing. This accumulating changes can be described as passage-dependent effects summarizing changes in morphology, responsiveness to stimuli, protein expression patterns and growth[71]. These limitations regarding THP-1 cells reasoned the decision not to select single cell clones. Nonetheless, we showed an effective *ZFYVE27* knockout by determining protein levels with Western blots. Further genomic analysis could be performed to estimate the percentage of cells with genomic alterations induced by CRISPR/Cas9 in the targeted exon.

Within this project we verified *ZFYVE27* full size knockout in three THP-1 CRISPR/Cas9 *ZFYVE27* KO sublines and tested them in their response to LPS. Interestingly, we observed differential response patterns between the sublines which correlated with the CRISPR/Cas9 sgRNA targeted exon. Transcription from the *ZFYVE27* gene results in multiple splice isoforms (over 30) and in fact some are not targeted by the sgRNA used to introduce the knockout. Alternative splicing is the mechanism explaining the big mismatch between the number of human protein coding genes and the number of proteins[72]. Isoforms generated by alternative splicing can be highly different in their function and interaction with other proteins. Some splice isoforms were also investigated to be as different to each other as to a protein encoded by another gene[73].

We were able to determine six splice variants which were not targeted by the sgRNA in exon 3. Most of them are bioinformatically predicted, but the expression of at least one splice isoform (transcript variant 5) was confirmed (NM_001174120.1). Indeed, sgRNA targeting exon 3 in one of the sublines theoretically was not able to alter the protein encoded by transcript variant 5, and we have not observed any decrease in TLR4-mediated *IFNβ* mRNA expression in these cells. It is important to point out that all used sgRNAs were designed to target full size *ZFYVE27* transcript variant 1. This indicates that it could be another splice isoform, which is differentially targeted by sgRNAs, that is responsible for the regulation of TLR4-mediated signaling in macrophages. Further investigations regarding these splice isoforms should be performed to determined weather different ZFYVE27 splice isoforms have different functions and expression levels in macrophages.

Our preliminary data suggest that ZFYVE27 as a trafficking protein with its multidomain structure may be involved in the regulation of signaling via different TLRs. Data from pilot experiments addressing TLR8 and TLR9 signaling indicates a delayed and prolonged cytokine mRNA expression upon stimulation of *ZFYVE27* silenced THP-1 cells by the respective ligand. Delayed and prolonged signaling though endosomal TLRs could be explained by retarded phagosome maturation. TLR8 and TLR9-mediated signaling requires cleavage of their ectodomain. Processing of these receptors is dependent on their localization and occurs in specific endosomes which makes endosomal TLR signaling dependent on phagosome maturation[11]. ZFYVE27 could play a role in the maturation state and luminal pH of phagosomes as it was investigated that positioning of lysosomes within the cell correlates with their luminal pH[74].

In future studies, ELISAs for IFNβ or CXCL10 could be performed with supernatants from the knockout sublines, as well as from the TLR8 and TLR9 pilot experiments. Within this project the time was not enough to address protein secretion, but supernatants were collected and could be tested. Moreover, the knockout sublines could be tested in the live bacteria uptake assays and could be used as starting point to generate *ZFYVE27* mutants to investigate which domains or splice isoforms are crucial for the observed effect on TLRs signaling.

Furthermore, it would be of interest to check if *ZFYVE27* silencing would have an impact on TLR3-mediated signaling, because this intracellular TLR signals through the TRIF adapter protein as TLR4 from the phagosomes.

Investigating the novel link between the vesicle transport protein ZFYVE27 and TLRs singling could contribute to the understanding of intracellular trafficking and connected events.

6. Conclusion

In summary, the focus of this study was on investigating the role of ZFYVE27 in TLRs signaling.

- By silencing *ZFYVE27* in macrophage-like THP-1 cells and primary macrophages we found that ZFYVE27 positively regulates TLR4-TRAM-TRIF-mediated signaling without affecting TLR4 expression.
- ZFYVE27 was important for efficient upregulation of IFNβ and subsequent *CXCL10* mRNA expression as well as STAT1 phosphorylation in response to LPS.
- *ZFYVE27* silencing affected *E. coli* bioparticle uptake in primary macrophages, while indicating the same trend in THP-1 cells.
- No effect was observed for ZFYVE27, TLR4 or TLR4 trafficking proteins Rab11a and Rab11b on live bacteria uptake in THP-1 cells.
- *ZFYVE27* silencing affected TLR4 recruitment to *E. coli* bioparticle phagosomes in primary macrophages and THP-1 cells, without effect on actin recruitment.
- Phagosome maturation in *ZFYVE27* silenced primary macrophages was decreased.
- Three verified *ZFYVE27* knockout THP-1 sublines were generated.
- Responsiveness to LPS of THP-1 CRISPR/Cas9 *ZFYVE27* KO sublines correlated with their sgRNA targeted exon indicating differential functions of splice isoforms.
- Pilot experiments suggested that *ZFYVE27* silencing prolonged and enhanced signaling via TLR8 and TLR9 receptors.

Understanding the impact of the vesicle transport protein ZFYVE27 on TLRs signaling could possibly provide further targets in the development of drugs for TLR involved disorders. Moreover, it could contribute to the general understanding of intracellular trafficking and the functions of the ZFYVE27 protein.

7. References

1 Chaplin, D. D. Overview of the immune response. *The Journal of allergy and clinical immunology* **125**, S3-23, doi:10.1016/j.jaci.2009.12.980 (2010).

2 Voogdt, C. G. P. & van Putten, J. P. M. in *The Evolution of the Immune System* (ed Davide Malagoli) 311-330 (Academic Press, 2016).

3 Gasteiger, G. *et al.* Cellular Innate Immunity: An Old Game with New Players. *Journal of innate immunity* **9**, 111-125, doi:10.1159/000453397 (2017).

4 Murphy, K. & Weaver, C. (ed Garland Science/Taylor & Francis) Ch. Chapter 2: Innate Immunity: The First Lines of Defense; Chapter 3: The induced Responses of Innate Immunity, (2017).

5 Vidya, M. K. *et al.* Toll-like receptors: Significance, ligands, signaling pathways, and functions in mammals. *International Reviews of Immunology* **37**, 20-36, doi:10.1080/08830185.2017.1380200 (2018).

6 Pradere, J. P., Dapito, D. H. & Schwabe, R. F. The Yin and Yang of Toll-like receptors in cancer. *Oncogene* **33**, 3485-3495, doi:10.1038/onc.2013.302 (2014).

7 Kawai, T. & Akira, S. TLR signaling. *Semin Immunol* **19**, 24-32, doi:10.1016/j.smim.2006.12.004 (2007).

8 Kawasaki, T. & Kawai, T. Toll-like receptor signaling pathways. *Frontiers in Immunology* **5**, 461-461, doi:10.3389/fimmu.2014.00461 (2014).

9 Akira, S. & Takeda, K. Toll-like receptor signalling. *Nature Reviews Immunology* **4**, 499, doi:10.1038/nri1391 (2004).

10 Owen, J. A., Punt, J. & Stranford, S. A. *Kuby Immunology*. Vol. 7th Edition (W. H. Freeman and Company, 2009).

11 Blasius, A. L. & Beutler, B. Intracellular toll-like receptors. *Immunity* **32**, 305-315, doi:10.1016/j.immuni.2010.03.012 (2010).

12 Lee, B. L. & Barton, G. M. Trafficking of endosomal Toll-like receptors. *Trends in cell biology* **24**, 360-369, doi:10.1016/j.tcb.2013.12.002 (2014).

13 Pahwa, R., Devaraj, S. & Jialal, I. The effect of the accessory proteins, soluble CD14 and lipopolysaccharide-binding protein on Toll-like receptor 4 activity in human monocytes and adipocytes. *International Journal Of Obesity* **40**, 907, doi:10.1038/ijo.2016.32

https://www.nature.com/articles/ijo201632#supplementary-information (2016).

14 Park, B. S. & Lee, J.-O. Recognition of lipopolysaccharide pattern by TLR4 complexes. *Experimental &Amp; Molecular Medicine* **45**, e66, doi:10.1038/emm.2013.97 (2013).

15 Marongiu, L., Gornati, L., Artuso, I., Zanoni, I. & Granucci, F. Below the surface: The inner lives of TLR4 and TLR9. *Journal of leukocyte biology*, doi:10.1002/jlb.3mir1218-483rr (2019).

16 Sperandeo, P., Martorana, A. M. & Polissi, A. Lipopolysaccharide biogenesis and transport at the outer membrane of Gram-negative bacteria. *Biochimica et biophysica acta. Molecular and cell biology of lipids* **1862**, 1451-1460, doi:10.1016/j.bbalip.2016.10.006 (2017).

17 Murphy, K. & Weaver, C. *Janeway's immunobiology*. 9th edn, 85-87; 111-113 (Garland Science, Taylor & Francis Group, 2017).

18 Casem, M. L. in *Case Studies in Cell Biology* (ed Merri Lynn Casem) 217-240 (Academic Press, 2016).

19 Gordon, S. Phagocytosis: An Immunobiologic Process. *Immunity* **44**, 463-475, doi:https://doi.org/10.1016/j.immuni.2016.02.026 (2016).

20 Aderem, A. & Underhill, D. M. Mechanisms of phagocytosis in macrophages. *Annual review of immunology* **17**, 593-623, doi:10.1146/annurev.immunol.17.1.593 (1999).
21 Aderem, A. Phagocytosis and the Inflammatory Response. *The Journal of Infectious Diseases* **187**, S340-345, doi:10.1086/374747 (2003).
22 Stenmark, H. Rab GTPases as coordinators of vesicle traffic. *Nature reviews. Molecular cell biology* **10**, 513-525, doi:10.1038/nrm2728 (2009).
23 Bonifacino, J. S. & Glick, B. S. The mechanisms of vesicle budding and fusion. *Cell* **116**, 153-166 (2004).
24 Mayinger, P. Phosphoinositides and vesicular membrane traffic. *Biochimica et biophysica acta* **1821**, 1104-1113, doi:10.1016/j.bbalip.2012.01.002 (2012).
25 Husebye, H. *et al.* Endocytic pathways regulate Toll-like receptor 4 signaling and link innate and adaptive immunity. *The EMBO journal* **25**, 683-692, doi:10.1038/sj.emboj.7600991 (2006).
26 Ullrich, O., Reinsch, S., Urbe, S., Zerial, M. & Parton, R. G. Rab11 regulates recycling through the pericentriolar recycling endosome. *The Journal of cell biology* **135**, 913-924, doi:10.1083/jcb.135.4.913 (1996).
27 Husebye, H. *et al.* The Rab11a GTPase controls Toll-like receptor 4-induced activation of interferon regulatory factor-3 on phagosomes. *Immunity* **33**, 583-596, doi:10.1016/j.immuni.2010.09.010 (2010).
28 Skjesol, A. *et al.* The TLR4 adaptor TRAM controls the phagocytosis of Gram-negative bacteria by interacting with the Rab11-family interacting protein 2. *PLOS Pathogens* **15**, e1007684, doi:10.1371/journal.ppat.1007684 (2019).
29 Yurchenko, M. *et al.* SLAMF1 is required for TLR4-mediated TRAM-TRIF-dependent signaling in human macrophages. *The Journal of cell biology* **217**, 1411-1429, doi:10.1083/jcb.201707027 (2018).
30 Palsson-McDermott, E. M. *et al.* TAG, a splice variant of the adaptor TRAM, negatively regulates the adaptor MyD88-independent TLR4 pathway. *Nature immunology* **10**, 579-586, doi:10.1038/ni.1727 (2009).
31 Baggiolini, M. Chemokines in pathology and medicine. *Journal of internal medicine* **250**, 91-104 (2001).
32 Finsterer, J. *et al.* Hereditary spastic paraplegias with autosomal dominant, recessive, X-linked, or maternal trait of inheritance. *Journal of the Neurological Sciences* **318**, 1-18, doi:https://doi.org/10.1016/j.jns.2012.03.025 (2012).
33 Mannan, A. U. *et al.* ZFYVE27 (SPG33), a novel spastin-binding protein, is mutated in hereditary spastic paraplegia. *American journal of human genetics* **79**, 351-357, doi:10.1086/504927 (2006).
34 Martignoni, M., Riano, E. & Rugarli, E. I. The role of ZFYVE27/protrudin in hereditary spastic paraplegia. *American journal of human genetics* **83**, 127-128; author reply 128-130, doi:10.1016/j.ajhg.2008.05.014 (2008).
35 Hashimoto, Y. *et al.* Protrudin regulates endoplasmic reticulum morphology and function associated with the pathogenesis of hereditary spastic paraplegia. *The Journal of biological chemistry* **289**, 12946-12961, doi:10.1074/jbc.M113.528687 (2014).
36 Shirane, M. & Nakayama, K. I. Protrudin Induces Neurite Formation by Directional Membrane Trafficking. *Science* **314**, 818-821, doi:10.1126/science.1134027 (2006).
37 Raiborg, C. *et al.* Repeated ER–endosome contacts promote endosome translocation and neurite outgrowth. *Nature* **520**, 234, doi:10.1038/nature14359

https://www.nature.com/articles/nature14359#supplementary-information (2015).
38 Gil, J. E. *et al.* Phosphoinositides differentially regulate protrudin localization through the FYVE domain. *The Journal of biological chemistry* **287**, 41268-41276, doi:10.1074/jbc.M112.419127 (2012).

39 Matsuzaki, F., Shirane, M., Matsumoto, M. & Nakayama, K. I. Protrudin serves as an adaptor molecule that connects KIF5 and its cargoes in vesicular transport during process formation. *Molecular biology of the cell* **22**, 4602-4620, doi:10.1091/mbc.E11-01-0068 (2011).
40 Saita, S., Shirane, M., Natume, T., Iemura, S. & Nakayama, K. I. Promotion of neurite extension by protrudin requires its interaction with vesicle-associated membrane protein-associated protein. *The Journal of biological chemistry* **284**, 13766-13777, doi:10.1074/jbc.M807938200 (2009).
41 Raiborg, C., Wenzel, E. M., Pedersen, N. M. & Stenmark, H. ER-endosome contact sites in endosome positioning and protrusion outgrowth. *Biochemical Society transactions* **44**, 441-446, doi:10.1042/bst20150246 (2016).
42 Campa, C. C. & Hirsch, E. Rab11 and phosphoinositides: A synergy of signal transducers in the control of vesicular trafficking. *Advances in biological regulation* **63**, 132-139, doi:10.1016/j.jbior.2016.09.002 (2017).
43 Chang, J., Lee, S. & Blackstone, C. Protrudin binds atlastins and endoplasmic reticulum-shaping proteins and regulates network formation. *Proceedings of the National Academy of Sciences of the United States of America* **110**, 14954-14959, doi:10.1073/pnas.1307391110 (2013).
44 Dangol, S. *Role of an ER-endosome contact protein in TLR signaling* Master thesis, Norwegian University of Science and Technology, (2015).
45 Lindholm, H. T. *The Vesicle Transport Protein Protrudin Affects Toll-Like Receptor 4 Signaling* Master thesis, Norwegian University of Science and Technology, (2017).
46 O'Brien, S. J., Ekman, M. B., Manek, S. & Galandiuk, S. CRISPR-mediated gene editing for the surgeon scientist. *Surgery*, doi:10.1016/j.surg.2019.01.030 (2019).
47 Jiang, F. & Doudna, J. A. CRISPR-Cas9 Structures and Mechanisms. *Annual review of biophysics* **46**, 505-529, doi:10.1146/annurev-biophys-062215-010822 (2017).
48 Acheampong, E., Rosario-Otero, M., Dornburg, R. & Pomerantz, R. J. Replication of lentiviruses. *Frontiers in bioscience : a journal and virtual library* **8**, s156-174 (2003).
49 Merten, O.-W., Hebben, M. & Bovolenta, C. Production of lentiviral vectors. *Molecular therapy. Methods & clinical development* **3**, 16017-16017, doi:10.1038/mtm.2016.17 (2016).
50 Sanjana, N. E., Shalem, O. & Zhang, F. Improved vectors and genome-wide libraries for CRISPR screening. *Nature methods* **11**, 783-784, doi:10.1038/nmeth.3047 (2014).
51 ZhangLab. (ed GeCKO - Genome Scale CRISPR Knock-out).
52 Dana, H. *et al.* Molecular Mechanisms and Biological Functions of siRNA. *International journal of biomedical science : IJBS* **13**, 48-57 (2017).
53 Qiagen. Flexible RNAi Technologies You Can Rely On. *www.qiagen.com* (2010).
54 Carter, M. & Shieh, J. in *Guide to Research Techniques in Neuroscience (Second Edition)* (eds Matt Carter & Jennifer Shieh) 239-252 (Academic Press, 2015).
55 AppliedBiosystems. Introduction to Gene Expression Getting Started Guide. (2010).
56 Livak, K. J. & Schmittgen, T. D. Analysis of Relative Gene Expression Data Using Real-Time Quantitative PCR and the 2−ΔΔCT Method. *Methods* **25**, 402-408, doi:https://doi.org/10.1006/meth.2001.1262 (2001).
57 Jensen, E. C. The basics of western blotting. *Anatomical record (Hoboken, N.J. : 2007)* **295**, 369-371, doi:10.1002/ar.22424 (2012).
58 invitrogen, p. b.-t. s.-. *Protein assay technical handbook*. (Thermo Fisher Scientific, 2017).
59 Lichtman, J. W. & Conchello, J. A. Fluorescence microscopy. *Nature methods* **2**, 910-919, doi:10.1038/nmeth817 (2005).

60 Fellers, T. J. D., Michael W. *Introduction to Confocal Microscopy*, <http://olympus.magnet.fsu.edu/primer/techniques/confocal/confocalintro.html> (2012).
61 Consortium, T. U. UniProt: a worldwide hub of protein knowledge. *Nucleic acids research* **47**, D506-D515, doi:10.1093/nar/gky1049 (2018).
62 Sievers, F. *et al.* Fast, scalable generation of high-quality protein multiple sequence alignments using Clustal Omega. *Molecular Systems Biology* **7**, 539, doi:10.1038/msb.2011.75 (2011).
63 Ivashkiv, L. B. & Donlin, L. T. Regulation of type I interferon responses. *Nature reviews. Immunology* **14**, 36-49, doi:10.1038/nri3581 (2014).
64 Technologies, L. pHrodo™ Red and Green BioParticles® Conjugates for Phagocytosis - Manual. (2013).
65 Cemalovic, E. *TLR9 trafficking and signaling* Master thesis, Norwegian University of Science and Technology, (2019).
66 Tan, Y. & Kagan, J. C. Microbe-inducible trafficking pathways that control Toll-like receptor signaling. *Traffic (Copenhagen, Denmark)* **18**, 6-17, doi:10.1111/tra.12454 (2017).
67 Kagan, J. C. *et al.* TRAM couples endocytosis of Toll-like receptor 4 to the induction of interferon-beta. *Nature immunology* **9**, 361-368, doi:10.1038/ni1569 (2008).
68 Welz, T., Wellbourne-Wood, J. & Kerkhoff, E. Orchestration of cell surface proteins by Rab11. *Trends in cell biology* **24**, 407-415, doi:10.1016/j.tcb.2014.02.004 (2014).
69 May, R. C. & Machesky, L. M. Phagocytosis and the actin cytoskeleton. *Journal of cell science* **114**, 1061-1077 (2001).
70 Greenbaum, D., Colangelo, C., Williams, K. & Gerstein, M. *Greenbaum D, Colangelo C, Williams K, Gerstein M. Comparing protein abundance and mRNA expression levels on a genomic scale. Genome Biol 4: 117*. Vol. 4 (2003).
71 ATCC. Passage Number Effects In Cell Lines. *The Essentials of Life Science Research Globally Delivered* (2010).
72 Wang, Y. *et al.* Mechanism of alternative splicing and its regulation. *Biomedical reports* **3**, 152-158, doi:10.3892/br.2014.407 (2015).
73 Yang, X. *et al.* Widespread Expansion of Protein Interaction Capabilities by Alternative Splicing. *Cell* **164**, 805-817, doi:10.1016/j.cell.2016.01.029 (2016).
74 Johnson, D. E., Ostrowski, P., Jaumouillé, V. & Grinstein, S. The position of lysosomes within the cell determines their luminal pH. *The Journal of cell biology* **212**, 677-692, doi:10.1083/jcb.201507112 (2016).

8. Supplemental material

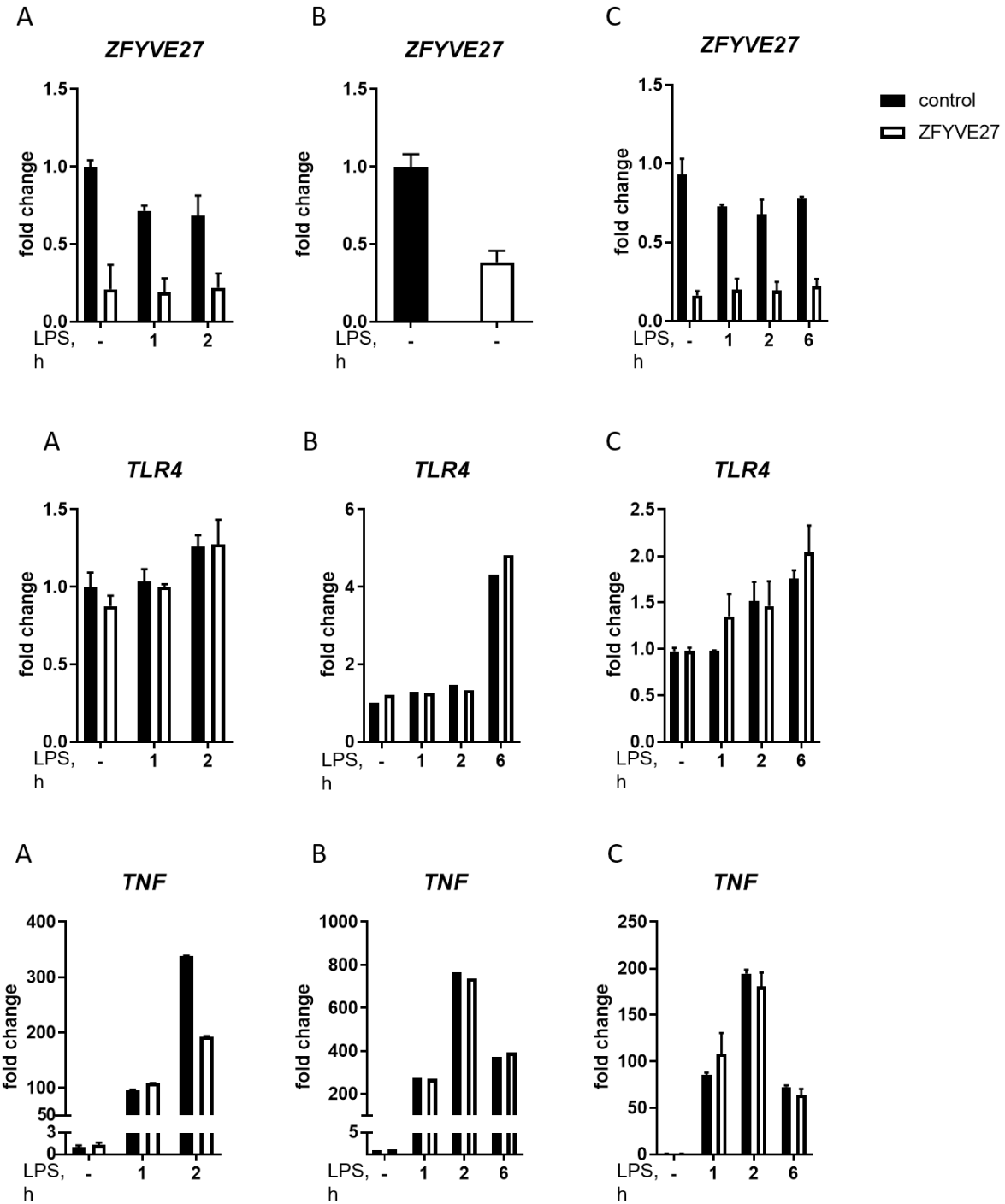

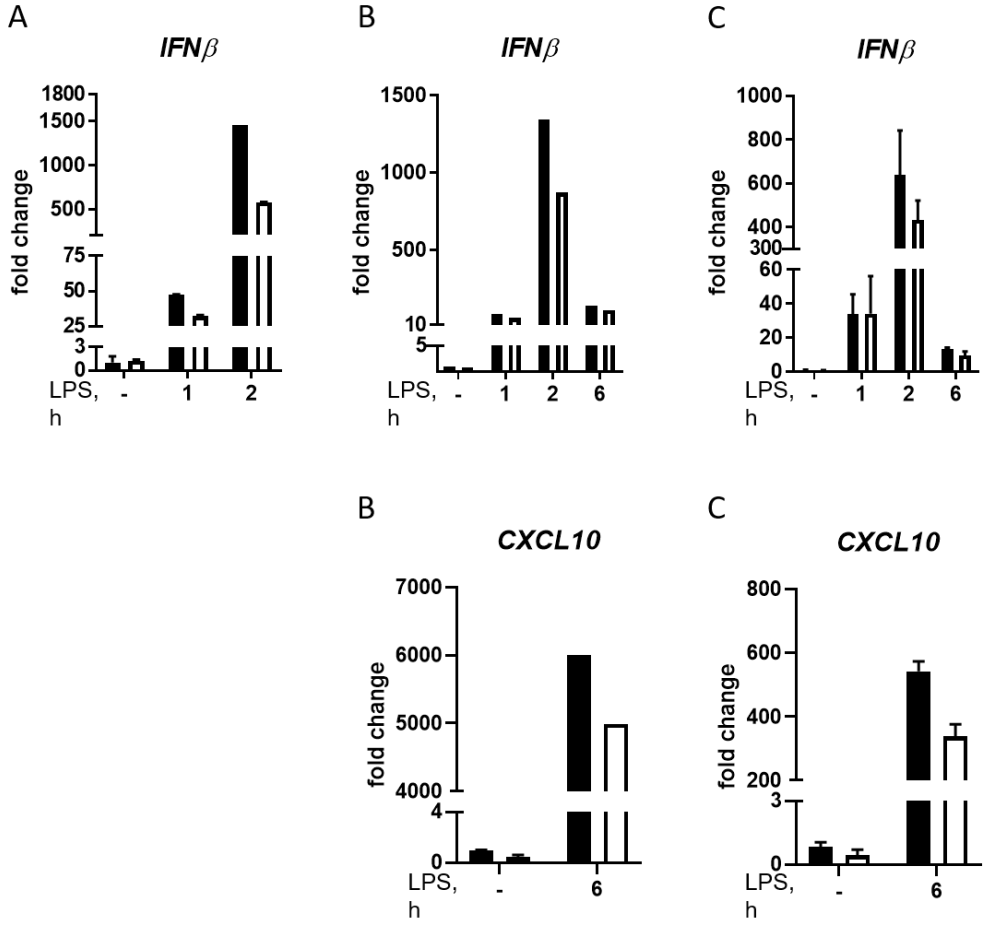

Figure S 1. TLR4-TRAM-TRIF-mediated signaling in THP-1 cells is affected by silencing of *ZFYVE27*, without affecting TLR4 mRNA expression levels. qPCR data from *ZFYVE27*, *TLR4, TNF, IFNβ* and *CXCL10* of *ZFYVE27* silenced and control treated differentiated THP-1 cells after stimulation with ultrapure K12 LPS (100 ng/ml). Graphs show data from three independent experiments (A, B, C). Bars in (A) and (B) indicate means of technical replicates with standard deviations as error bars. In (C), bars represent the mean and error bars the standard deviation of two biological replicates.

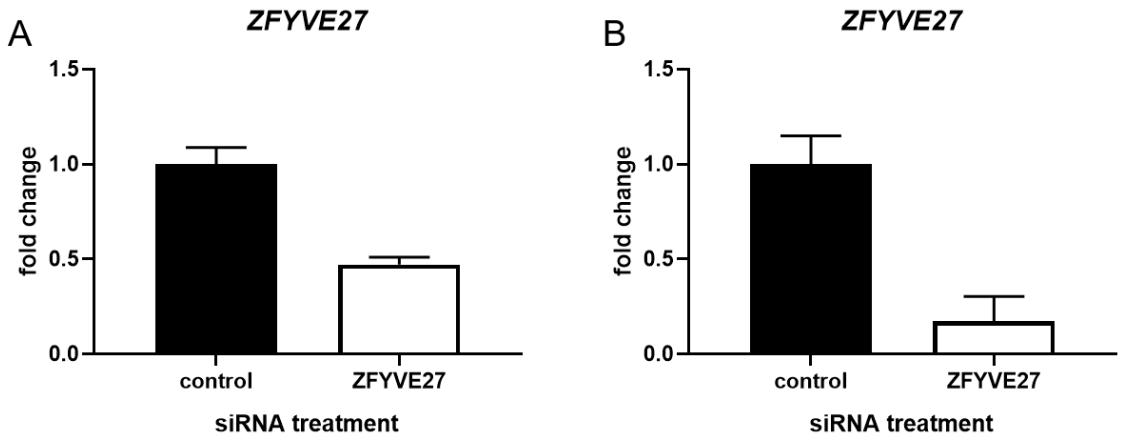

Figure S 2. *ZFYVE27* knockdown verification for pHrodo *E. coli* bioparticle uptake. *ZFYVE27* mRNA expression measured by qPCR in (A) primary macrophages and (B) in PMA differentiated THP-1 cells after siRNA treatment with a control or a *ZFYVE27* targeting siRNA oligo. Bars indicate means of technical duplicated; error bars indicate standard deviations.

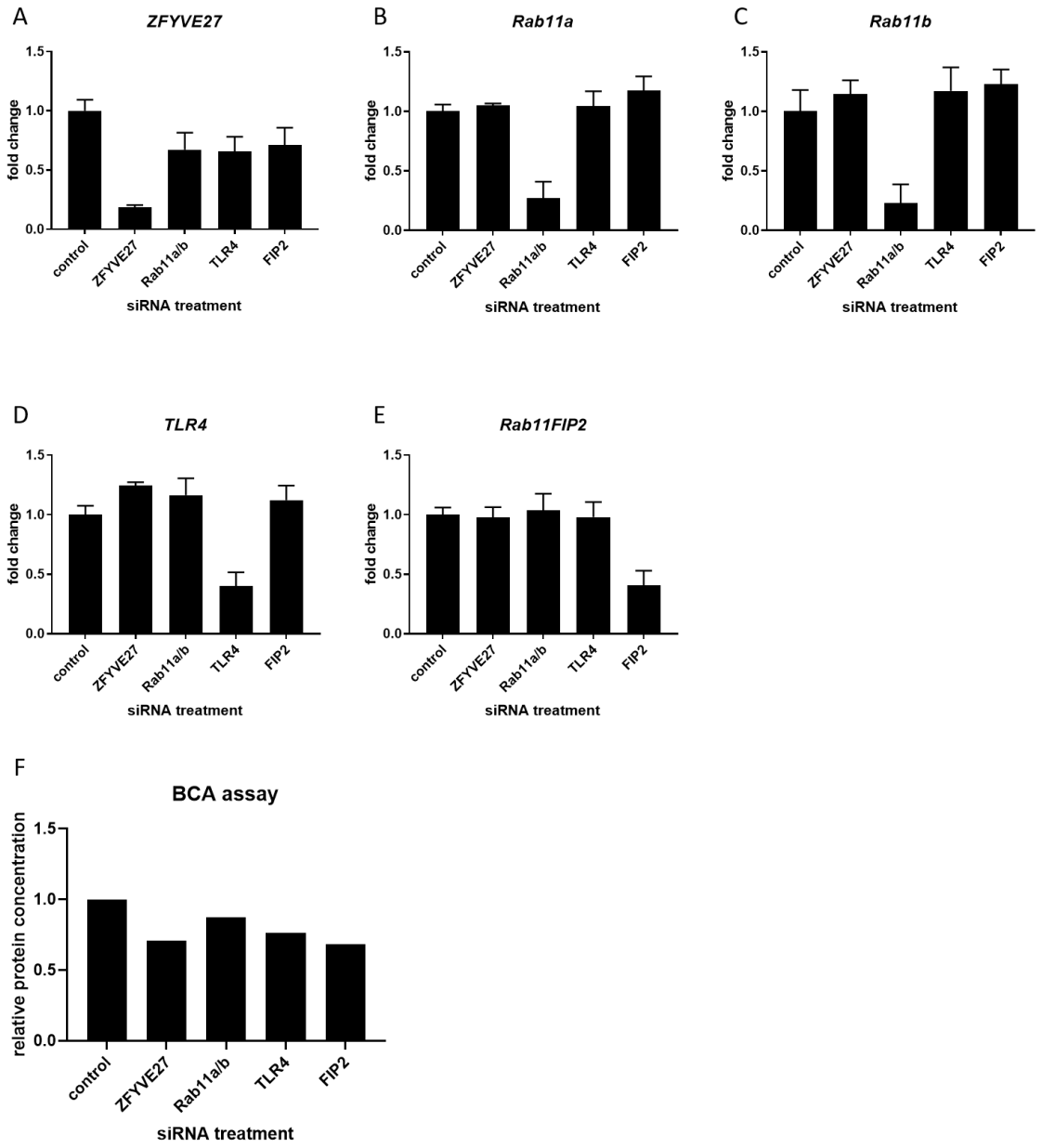

Figure S 3. Knockdown verification of *ZFYVE27*, *Rab11a* and *Rab11b*, *TLR4* and *Rab11FIP2* (*FIP2*) in THP-1 cells and protein concentrations of silenced cells after incubation with *E. coli* DH5α. A representative qPCR analysis of *ZFYVE27*(A), *Rab11a* (B), *Rab11b* (C), *TLR4* (D) and *FIP2* (E) mRNA expression in differentiated THP-1 cells treated with specific gene targeting siRNA oligos or a control siRNA oligo. In (F) a representative relative protein concentration analysis of siRNA treated differentiated THP-1 cells after incubation with *E. coli* DH5α assessed by BCA assay is shown.

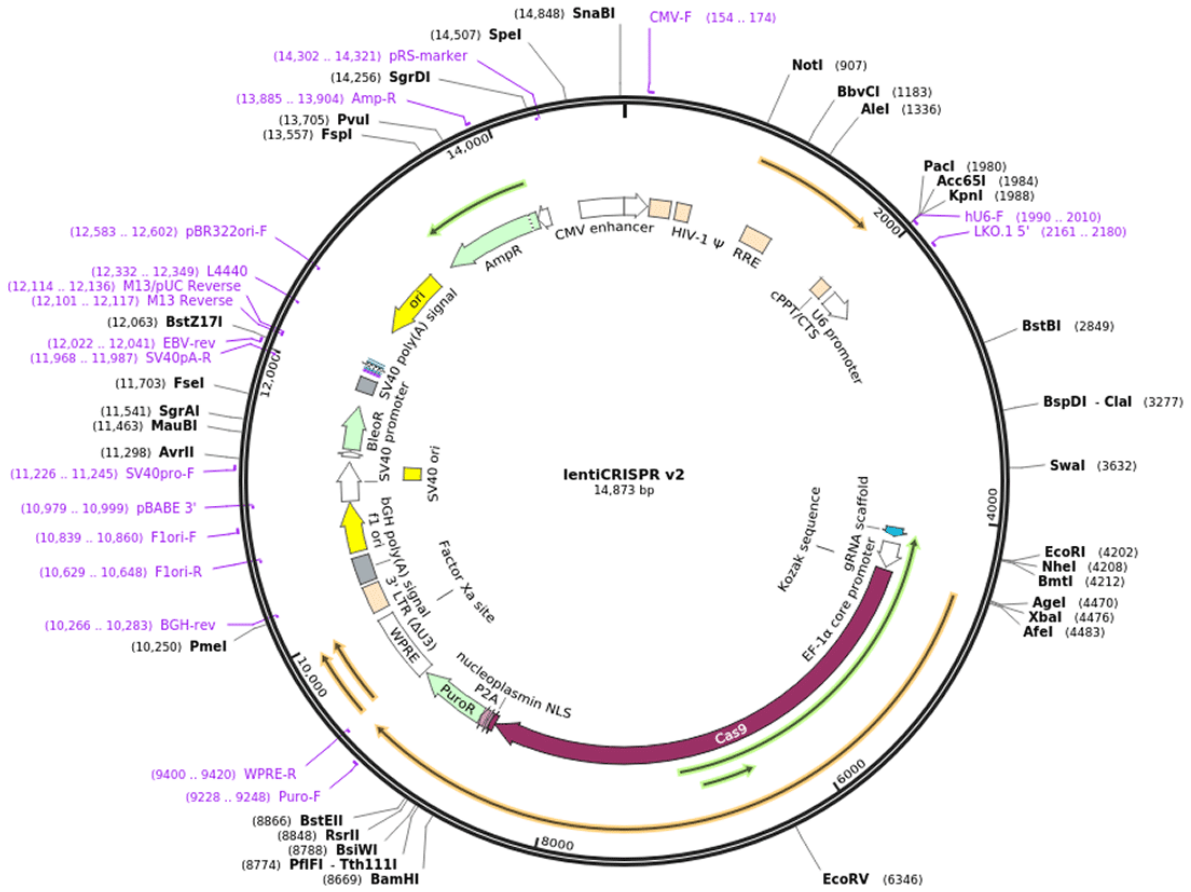

Figure S 4. Plasmid map of lentiCRISPR v2. Plasmid is used as vector backbone for sgRNA cloning and further for lentiviral production (Sanjana, et al., 2014[50]).

Table S 1. List of exons and FASTA sequence of *Homo sapiens* zinc finger FYVE-type containing 27 (ZFYVE27), transcript variant 1, mRNA, used as reference to design sgRNAs. Exon 3 is marked in yellow, exon 4 indicated by red bold font.

Exon No.	Nucleotide positions
Exon 1	1-198
Exon 2	199-269
Exon 3	270-456
Exon 4	457-552
Exon 5	553-665
Exon 6	666-805
Exon 7	806-892
Exon 8	893-913
Exon 9	914-1058
Exon 10	1059-1105
Exon 11	1106-1187
Exon 12	1188-2859
CDS (coding sequence)	2-1252

>NM_001002261.3 Homo sapiens zinc finger FYVE-type containing 27 (ZFYVE27), transcript variant 1, mRNA

GATGCAGACATCAGAACGTGAGGGGAGTGGGCCGGAGCTGAGCCCCAGCGTGATGCCCGAGGCTCCCCTG
GAGTCTCCACCTTTTCCTACCAAGTCCCCAGCGTTTGACCTTTTCAACTTGGTTCTCTCCTACAAGAGGC
TGGAGATCTACCTGGAACCCTTGAAGGATGCAGGTGATGGTGTTCGATACTTGCTCAGGTGGCAGATGCC
TTTGTGTTCCTTGCTGACCTGCCTGGGCCTCAACGTCTTGTTCCTCACTTTGAATGAGGGTGCATGGTAC
TCAGTAGGTGCCCTGATGATTTCAGTGCCCGCCCTGCTGGGCTACCTTCAGGAGGTTTGCCGGGCACGGC
TGCCTGATTCCGAGCTGATGCGGAGGAAGTATCATAGCGTGAGGCAGGAGGACCTGCAGAGAGGTCGCCT
GTCTCGTCCCGAGGCCGTGGCTGAGGTGAAGAGCTT**CTTGATCCAGCTGGAGGCCTTCCTGAGCCGCCTG**
TGCTGCACATGTGAAGCCGCCTACCGCGTGCTGCACTGGGAGAACCCCGTCGTGTCCTCACAGTTCTATG
GGGCTCTTCTGGGCACAGTCTGCATGCTGTATTTGCTGCCACTCTGCTGGGTTCTCACCCTTTTAAACAG
CACGCTCTTTCTGGGGAATGTGGAGTTCTTCCGAGTTGTGTCTGAGTACAGGGCATCTCTGCAGCAGAGG
ATGAACCCAAAGCAGGAAGAGCATGCCTTTGAGAGTCCTCCACCACCAGATGTTGGGGGGAAGGATGGTC
TGATGGACAGCACGCCTGCCCTCACACCCACGGAGAGTCTCTCTTCCCAGGACCTCACACCGGGCAGCGT
GGAGGAGGCTGAGGAGGCTGAGCCAGATGAAGAGTTTAAAGATGCGATTGAGGAGACCCACTTGGTGGTG
CTGGAGGATGATGAGGGCGCCCCGTGCCCAGCAGAGGATGAGCTGGCCCTGCAGGACAACGGGTTCCTGA
GCAAGAATGAGGTGCTGCGCAGCAAGGTGTCTCGGCTCACGGAGCGGCTCCGCAAGCGCTACCCCACCAA
CAACTTCGGGAACTGCACGGGCTGCTCGGCCACCTTCTCAGTGCTGAAGAAGAGGCGGAGCTGCAGTAAT
TGTGGAAACAGCTTCTGCTCTCGATGCTGCTCCTTCAAGGTGCCCAAGTCCTCCATGGGGGCCACAGCCC
CTGAAGCCCAGAGGGAGACTGTGTTTGTGTGTGCCTCGTGTAACCAGACCTTGAGCAAGTGAGAAGAGAG
GCCAGGGTCCAACCAGGCACCCGTCCTTGGGACCAGCAGTAGACCCCCCACTCTCCCCACCCCTGGCCCA
CTGTGGTGTGTGCTGGGCAAATGTGGCCTGAATGCTAGGTAGGCTTCCCCTTCCTTCCTCACTCTCTCCA
GCTGGATTCTGGAGCTGTTCTCCATCCATGAGAGTGGCTGGCAATGGCTGCTCTCAATCCCTTGAGGGAG
AAGAGCCCCTGGAGGGCCTGGCATGTTTGTCCTGCTCTGCCTGGGACTGAGCGAGTGGACTTAGGGCTGG
GCAGGCAGTAGCCACCAGAGGGCAGCAGCGAACTAGGCCAGGCCTGACTGGGGTCTGAAGATCAGGGTCA
GTGTGGCTGTGCCTGGGAATTCCAGACCTGAGGTTGGGAAAAGAGGTTTTTCTCCTGCAGGGTACTGGGC
CAGGCCCTCAGCCTCAGAGAGCCTGCAGAAGGGCTTGGGAGTGCCACACCCCATCTCTGCTGATTGAATG
TCCCTCCAGGCACCAGGATCTCATCATTTCCCCATCAGAGGGTGTGGCCAGGCCTAACAAGACCATGGGT
GCTTCTAGAAACAGGGTTGAAGTTCCCAGATTCCCTGAGAGGAGAATGTGTATAGGAGGGTTTGGCTGAG
TCCTTCAGCGTTAAGTGGAGGAAAGCTTGGGGAAGCCCCAATAGCTGGACAGACCTCGGCCTCCCCTCGA
AGACACCTCAATTCACAGACTCTCAGCCCACACAATGCCCCAGTGTCCCCAGCTCCGCTGGAGCAGCTGC
AGGGCACTTGGATCACAACTTCTGCACCCTCTGTCCAGAGTCTAGGGCAGTCCTCCACTGGCCCAGCACT
CCAGTTTCCTTTCCCTGCCTCTTGTCCAATGGAGTGGGAGGCCAGGTGAGTGGAGCAGAGGTCCTGAAGC
CCTTGACCCCTGGGGGCCTGGGTAGTGTAGGATCTCGCTGGGCTGGGTCCTGGATTCCAGGGCTATTCCC
TGGAGGACAGTCTCAGTTATGGGATAAGGCCCCCTGGGGGTCTCCATTTCTTTCCAACAGTTTCATGTTC
ACTACTGGACTCTTACGGGCTCAGTATCTCTCCCTTAGCCATGAGCTGGCTCAGGCATCCCTTCCCTTCC
CTGGAGCTGCCCTGCCTTTCTCAAGTATTTATTTATTTATTGCATGGTTCCTGGGAACATGTGGCACAAG
TAATGGGATGAGGAGGAATTGGGGGTGGGGGTCTTCTACCTAGGACTCTTCCCTGGAGTCATGGGCTGCC
TGGGACCCAGGACCCATGAGGGGGCTGAGAGGTTTCTACACTCGAGGAGCAGGGGTCCAGAGAGGCAGGC
TGGGGAGGCAAGGGACCCATCCTAGGCCCGCTTTCTTGCCGAGCCAAGCAGCTTAGCTGGGGCTGTGCAG
CCAGGGGCTTACCCAGGCCAGTGGAGGTGCCACAGCCCTGGGGAGCCAGACAGGCTTTGGTATCGTATCG
CCTCTGTGTCCTTTTAAGAGAGGAGAGTTCAGTACCCCGTGCTTTCTTTACACTGGAGAGGAACTAAAAG
GATCTCTGTGTCTATGGAGAATTGTCAATAAAAAGGCCTCAAGCTTCTTGTTTTTGTCAAAAAAAAAAA

Table S 2. List of *ZFYVE27* transcript variants targeted by sgRNAs used to generate verified THP-1 CRISPR/Cas9 *ZFYVE27* KOs. Blastn output of alignments of sgRNA sequences (#3, #5, #6) are shown. Yellow shadowed rows indicate no alignment with the sgRNA sequence #3.

XR_002956957.1	PREDICTED: Homo sapiens zinc finger FYVE-type containing 27 (ZFYVE27), transcript variant X29, misc_RNA
XR_002956956.1	PREDICTED: Homo sapiens zinc finger FYVE-type containing 27 (ZFYVE27), transcript variant X27, misc_RNA
XM_017015653.2	PREDICTED: Homo sapiens zinc finger FYVE-type containing 27 (ZFYVE27), transcript variant X24, mRNA
XM_017015651.2	PREDICTED: Homo sapiens zinc finger FYVE-type containing 27 (ZFYVE27), transcript variant X21, mRNA
XM_005269508.4	PREDICTED: Homo sapiens zinc finger FYVE-type containing 27 (ZFYVE27), transcript variant X19, mRNA
XR_945597.2	PREDICTED: Homo sapiens zinc finger FYVE-type containing 27 (ZFYVE27), transcript variant X28, misc_RNA
XM_017015655.1	PREDICTED: Homo sapiens zinc finger FYVE-type containing 27 (ZFYVE27), transcript variant X26, mRNA
XM_017015654.1	PREDICTED: Homo sapiens zinc finger FYVE-type containing 27 (ZFYVE27), transcript variant X25, mRNA
XM_005269511.3	PREDICTED: Homo sapiens zinc finger FYVE-type containing 27 (ZFYVE27), transcript variant X23, mRNA
XM_017015652.1	PREDICTED: Homo sapiens zinc finger FYVE-type containing 27 (ZFYVE27), transcript variant X22, mRNA
XM_005269509.3	PREDICTED: Homo sapiens zinc finger FYVE-type containing 27 (ZFYVE27), transcript variant X20, mRNA
XM_017015650.1	PREDICTED: Homo sapiens zinc finger FYVE-type containing 27 (ZFYVE27), transcript variant X18, mRNA
XM_011539255.2	PREDICTED: Homo sapiens zinc finger FYVE-type containing 27 (ZFYVE27), transcript variant X17, mRNA
XM_011539254.2	PREDICTED: Homo sapiens zinc finger FYVE-type containing 27 (ZFYVE27), transcript variant X16, mRNA
XM_017015649.1	PREDICTED: Homo sapiens zinc finger FYVE-type containing 27 (ZFYVE27), transcript variant X15, mRNA
XM_017015648.1	PREDICTED: Homo sapiens zinc finger FYVE-type containing 27 (ZFYVE27), transcript variant X14, mRNA
XM_005269510.3	PREDICTED: Homo sapiens zinc finger FYVE-type containing 27 (ZFYVE27), transcript variant X13, mRNA
XM_017015647.1	PREDICTED: Homo sapiens zinc finger FYVE-type containing 27 (ZFYVE27), transcript variant X12, mRNA
XM_005269503.3	PREDICTED: Homo sapiens zinc finger FYVE-type containing 27 (ZFYVE27), transcript variant X11, mRNA
XM_017015646.1	PREDICTED: Homo sapiens zinc finger FYVE-type containing 27 (ZFYVE27), transcript variant X10, mRNA
XM_017015645.1	PREDICTED: Homo sapiens zinc finger FYVE-type containing 27 (ZFYVE27), transcript variant X9, mRNA
XR_945594.2	PREDICTED: Homo sapiens zinc finger FYVE-type containing 27 (ZFYVE27), transcript variant X8, misc_RNA
XM_017015644.1	PREDICTED: Homo sapiens zinc finger FYVE-type containing 27 (ZFYVE27), transcript variant X7, mRNA
XM_011539253.2	PREDICTED: Homo sapiens zinc finger FYVE-type containing 27 (ZFYVE27), transcript variant X6, mRNA

XM_011539252.2	PREDICTED: Homo sapiens zinc finger FYVE-type containing 27 (ZFYVE27), transcript variant X5, mRNA
XM_005269506.3	PREDICTED: Homo sapiens zinc finger FYVE-type containing 27 (ZFYVE27), transcript variant X4, mRNA
XM_005269505.4	PREDICTED: Homo sapiens zinc finger FYVE-type containing 27 (ZFYVE27), transcript variant X3, mRNA
XM_005269504.3	PREDICTED: Homo sapiens zinc finger FYVE-type containing 27 (ZFYVE27), transcript variant X2, mRNA
XM_005269502.3	PREDICTED: Homo sapiens zinc finger FYVE-type containing 27 (ZFYVE27), transcript variant X1, mRNA
NM_001174121.1	Homo sapiens zinc finger FYVE-type containing 27 (ZFYVE27), transcript variant 6, mRNA
NM_001174119.1	Homo sapiens zinc finger FYVE-type containing 27 (ZFYVE27), transcript variant 4, mRNA
NM_001174120.1	Homo sapiens zinc finger FYVE-type containing 27 (ZFYVE27), transcript variant 5, mRNA
NM_001002262.3	Homo sapiens zinc finger FYVE-type containing 27 (ZFYVE27), transcript variant 3, mRNA
NM_001002261.3	Homo sapiens zinc finger FYVE-type containing 27 (ZFYVE27), transcript variant 1, mRNA
NM_144588.6	Homo sapiens zinc finger FYVE-type containing 27 (ZFYVE27), transcript variant 2, mRNA

Table S 3. Topology of ZFYVE27 [Homo sapiens] protein. Table was adapted from UniProt (https://www.uniprot.org/)[61] entry Q5T4F4, which used the Homo sapiens zinc finger FYVE-type containing 27 (ZFYVE27), transcript variant 2, mRNA (NM_144588.6) as reference.

Feature key	Position(s)	Description	Length
topological domain	1-66	cytoplasmic	66
transmembrane	67-87	helical	21
topological domain	88	luminal	1
transmembrane	89-109	helical	21
topological domain	110-187	cytoplasmic	78
intramembrane	188-208	helical	21
topological domain	209-411	cytoplasmic	203

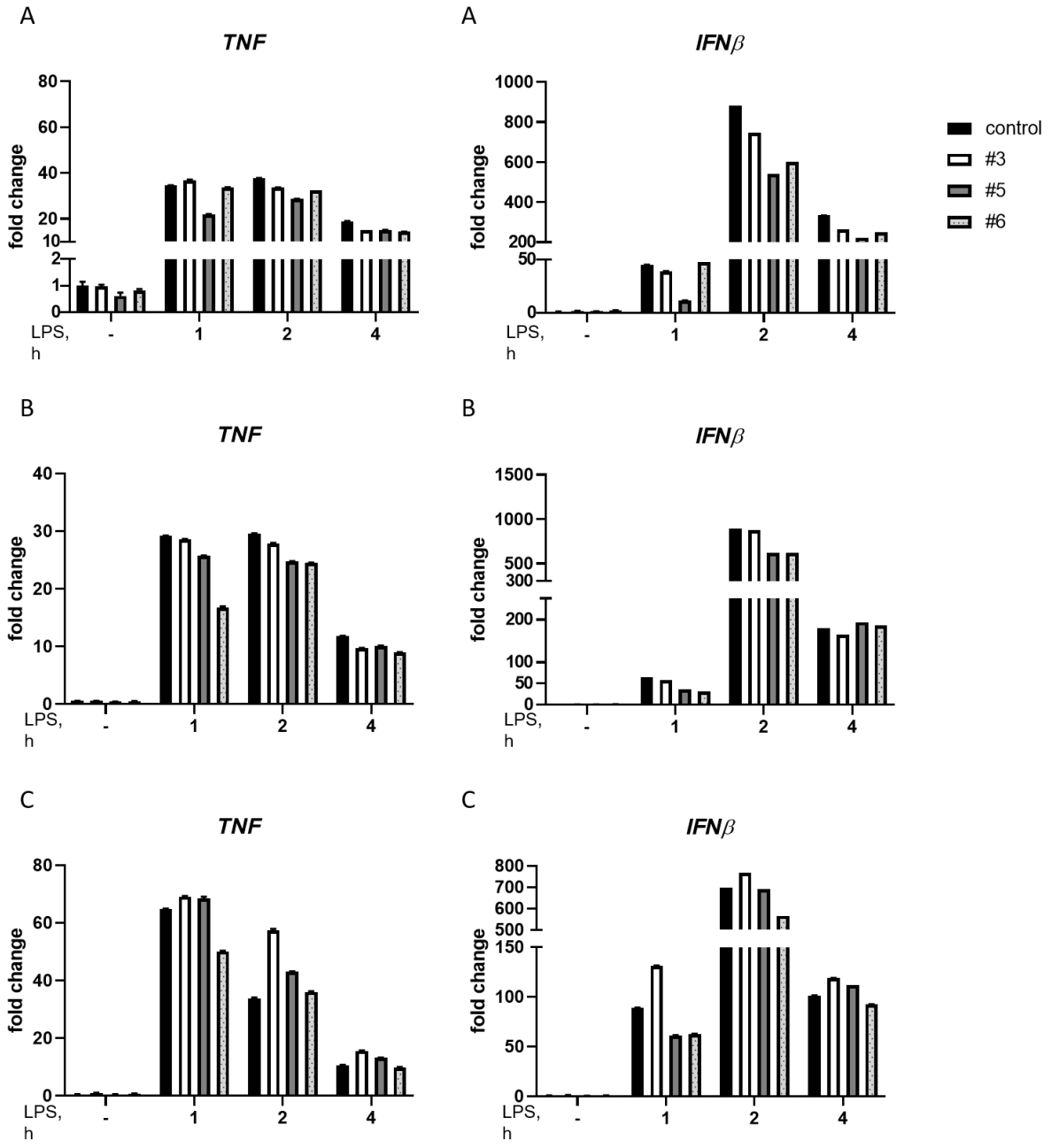

Figure S 5. THP-1 CRISPR/Cas9 *ZFYVE27* KOs show differential TLR4-mediated signaling induced by LPS stimulation. *TNF* and *IFNβ* mRNA expression analyzed by qPCR in differentiated THP-1 CRISPR/Cas9 *ZFYVE27* knockout sublines (#3, #5, #6) and THP-1 CRISPR/Cas9 control subline shown. Bars indicate means from two biological replicates with standard deviations indicated by error bars. Graphs show results from three independent experiments (A, B, C).

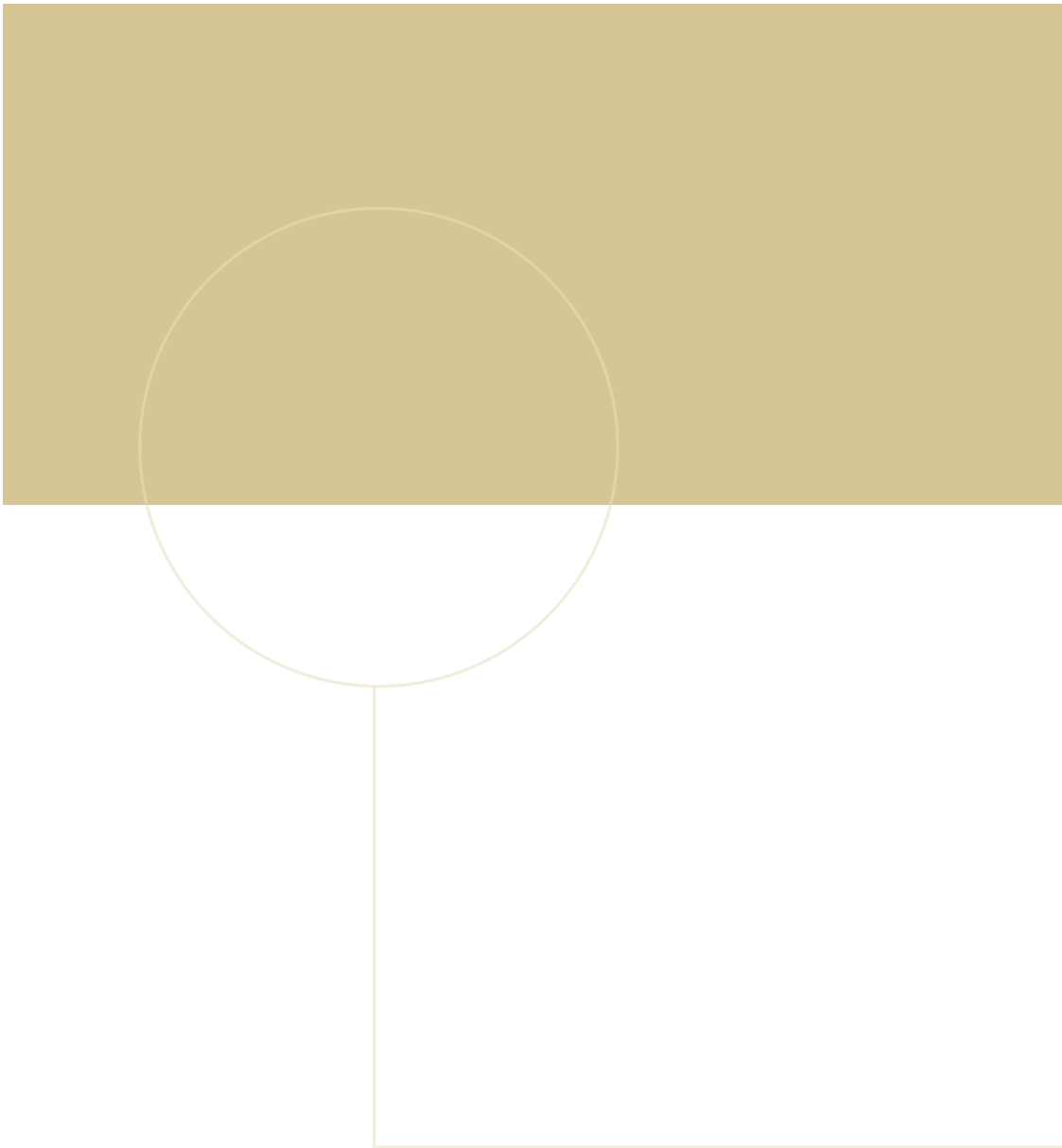

NTNU
Norwegian University of
Science and Technology